~~On the hydrological significance of rock glaciers: A case study from~~ Seasonal ice storage changes and meltwater generation at Murtèl rock glacier (Engadine, eastern Swiss Alps)~~using below-ground energy-flux~~ : Estimates from measurements ~~, ground-ice melt observations~~ and ~~hydrological measurements~~energy budgets in the coarse blocky active layer

Dominik Amschwand[1], Seraina Tschan[1], Martin Scherler[1,†], Martin Hoelzle[1], Bernhard Krummenacher[2], Anna Haberkorn[2], Christian Kienholz[2], Lukas Aschwanden[3], and Hansueli Gubler[4]

[1]Department of Geosciences, University of Fribourg, Fribourg, Switzerland
[2]GEOTEST AG, Zollikofen/Bern, Switzerland
[3]Institute for Geological Sciences, University of Bern, Bern, Switzerland
[4]Alpug GmbH, Davos, Switzerland
[†]deceased, 4 June 2022

Correspondence: Dominik Amschwand (dominik.amschwand@unifr.ch)

Abstract. Intact rock glaciers, a permafrost landform common in high-mountain regions, are often conceptualized as (frozen) water reserves. In a warming climate with slowly degrading permafrost, the large below-ground ice volumes might suggest a buffering effect on summer streamflow that due to the climate resiliency of rock glaciers only increases with rapidly receding glaciers. In this case study, we assess the role and functioning of the active Murtèl rock glacier in the hydrological cycle of its small (30 ha) periglacial and unglacierized watershed located in the Upper Engadine (eastern Swiss Alps). Our unprecedentedly comprehensive hydro-meteorological measurements include below-ground heat flux measurements in the $3-5$ m thick coarse-blocky active layer (AL), direct observations of the seasonal evolution of the ground-ice table, and discharge and isotopic signature of the outflow at the rock-glacier front. The detailed active-layer energy and water/ice balance quantifies precipitation, evaporation, ~~snow melt~~snowmelt, ground ice melt, and catchment surface outflow. ~~Murtèl rock glacier stores and releases water and ice over three different time scales with varying magnitudes and residence times: (1) Liquid water storage on short-term~~ Our single-site, but detailed case study resolves thermo-hydraulic processes in the coarse blocky AL that might enhance the snowmelt–groundwater connectivity in periglacial high-mountain watersheds underlain by discontinuous permafrost. A substantial part of the snowmelt refreezes in the cold AL ($\sim 150-300$ mm w.e. or $\sim 20-30$ % of the snowpack), forming superimposed AL ice that is released during the thaw season at melt rates low enough for the meltwater flow to be routed through the permafrost aquitard to deeper sub-permafrost aquifers. Meltwater fluxes are low ($1-4$ mm w.e. day^{-1}), but sustained throughout the entire thaw season (~~sub-monthly) scale is small in the permafrost-underlain coarse-debris catchment, as shown by~~ ~ 100 days) due to small ground heat fluxes and the ~~'flashy' hydrograph during the thaw season with rapidly varying discharge and little sustained surface baseflow () in the dry summer months. (2) Seasonal ground ice accumulation and~~

melt in the coarse-blocky AL is substantial: Independent direct ground-ice observations and an AL energy budget suggests AL ice melt rates of , amounting to over the thaw season. In the comparatively cool–wet year 2021, ground ice melt represented of the annual precipitation and outflow, but in the hot–dry year 2022. dampening effect of the AL. The superimposed AL ice is sourced by refreezing snowmelt in spring (annually replenished) , protracts the snowmelt into late summer (intermediate-term storage), and cannot increase the total yearly runoff. (3) Meltwater acts as a coupled thermo-hydrological buffer that (to some extent) protects the underlying ice-rich rock glacier core by converting most of the ground heat flux to meltwater during the thaw season. Consequently, meltwater release from the 'old' permafrost ice due to climate-induced permafrost degradation is or ~ 5 – 10 times currently $\sim 10\ \mathrm{mm\ yr^{-1}}$ or an order of magnitude smaller than the AL meltwater contribution contribution of AL meltwater and not more than a few % of the overall water/ice fluxes(long-term storage). Our case study suggests that a hydrologically relevant ice turnover occurs in the active layer in addition to meltwater released from slow degradation of the ice-rich permafrost . The seasonal ice turnover in the AL acts as a coupled thermal and hydrological buffer that to some degree protects the underlying ice-rich rock-glacier core by converting the ground heat flux to meltwater during the thaw season. More measurements of the seasonal ground-ice turnover should tell how generalisable our single-site findings are. . In view of the widespread and long-lasting occurrence of climate-resilient permafrost in high-mountain watersheds and the increasing importance of groundwater-sustained late-summer baseflow relative to vanishing glaciers and diminishing snowpacks, it is important to investigate mechanisms, flow paths, and efficiency of groundwater recharge in mountain permafrost terrain.

1 Introduction

In our rapidly warming Earth, bare-ice changing climate, changing precipitation patterns and enhanced sublimation/evapotranspiration due to warming and greening (vegetation succession) lead to profound hydrological regime shifts in high-mountain regions (Hock et al., 2022). The hydrological buffer capacity of *above-ground* cryospheric components decreases, as glaciers recede and precipitation in form of snow decreases, leading to while evaporative losses to the atmosphere (Fugger et al., 2024) and inter-annual variability in precipitation increase. Droughts and reduced stream flow in the summer months of dry years (Hock et al., 2022). Changing precipitation patterns, a large inter-annual variability in precipitation and with increasing air temperature increasing sublimation/evapotranspiration reduces water security (Haeberli et al., 2017; Schaffer et al., 2019; Hoelzle et al., 20 . In might become more frequent and severe, reducing water security in downstream regions (Haeberli et al., 2017; Schaffer et al., 2019; Ho . Hence, the hydrological buffer capacity of comparatively climate-resilient and robust *below-ground* components will become increasingly important: ice-rich mountain permafrost with rock glaciers as its most conspicuous morphological expression (Barsch, 1996), and groundwater in headwater aquifers (Woo, 2011; Hayashi, 2020).

Intact (i.e., ice-bearing) rock glaciers, a mountain permafrost landform widespread in nearly all mountain ranges worldwide, are distinct bodies of a perennially frozen debris–ice mixture covered by a seasonally thawed debris layer, the active layer (AL) (Haeberli et al., 2006). The perennially frozen interior, the rock glacier core, consists of ice-supersaturated debris whose creep deformation results in the conspicuous lobate or tongue-like form (Barsch, 1996). Intact rock glaciers store and release water in different forms, such as ice, snow, and water, on long-, intermediate- and short-term timescales (Jones et al., 2019).

The insulating and convective cooling effect of the thick AL creates a cool and stable microclimate in the AL that is partially decoupled from the atmosphere (Wakonigg, 1996; Humlum, 1997; Harris and Pedersen, 1998; Hanson and Hoelzle, 2004; Delaloye and L . Controlled by the ground thermal regime rather than by the surface energy balance (SEB) directly (Amschwand et al., 2024a), ground ice melt at depth proceeds slower and delayed compared to snow or glacier melt at the surface on seasonal up to decadal timescales (cf. Reznichenko et al., 2010). On a seasonal time scale, the sustained melt of ground ice is thought to contribute to late-summer streamflow. On decadal time scale, rock glaciers are more resilient (less sensitive) to climate changes compared to (debris-covered) glaciers and expected to outlast them as our mountains shift away from the glacial towards the para- and periglacial realm (Haeberli et al., 2017, 2024; Schaffer and MacDonell, 2022). Especially in semi-arid, already today weakly glaciated and water-stressed high mountain areas such as ~~Central Asia~~ parts of Central Asia, the Himalayas or the Dry Andes, the ~~runoff contribution~~ large below-ground ice volumes and hydrological buffer capacity of ~~comparatively~~ climate-resilient, ice-rich permafrost landforms ~~has gained attention: To what extent can meltwater from rock glaciers compensate decreasing glacier runoff, in particular in the hot-dry summer season after completion of snowmelt? However, different views on the 'hydrological significance' of~~ might become important hydrological elements.

The hydrological significance of rock glaciers primarily relates to (1) the long-term, climate-resilient storage of permafrost ice in the rock glacier core (water in reserve), (2) the seasonal storage and freeze/melt of water/ice in the AL (water/ice in circulation), and (3) water storage in unfrozen fine-grained sediments and interaction with liquid water flowing through or beneath rock glaciers (~~and other ice-rich permafrost landforms) emerged and a consensus is still lacking (Duguay et al., 2015; Schaffer et al.~~ storage–release, routing and chemical alteration/mineralization of water) (Azócar and Brenning, 2010; Corte, 1976; Burger et al., 1999; Jo . An useful concept for their understanding and management is to differentiate between water/ice in circulation (renewable, flow-limited resource) and water/ice in reserve (nonrenewable, stock-limited resource) based on a time scale of one (or a few) hydrological years (Gleick and Palaniappan, 2010).

~~Ice-rich permafrost landforms like rock glaciers or talus slopes are widespread in nearly all mountain ranges. The uppermost layer of these permafrost landforms, the active layer (AL), is subject to annual thawing and freezing. The landform reacts to climate warming~~ Intact rock glaciers have been storing 'old' ice in the permafrost body beneath the AL for centuries up to millennia (Krainer et al., 2015). This permafrost ice at depth has been interpreted to be roughly as old as the rock glacier it is embedded in. Therefore, it is frozen precipitation from past Holocene cold climatic phases and is a nonrenewable resource (Barsch, 1996; Haeberli et al., 2003; Azócar and Brenning, 2010; Krainer et al., 2015; Amschwand et al., 2021; Lehmann et al., 2022; Nic . Protected by the AL, accumulation and melt have been slow and driven by major climatic shifts throughout the Holocene. Driven by the current climate change, permafrost including rock glaciers is found to be degrading widely in high-mountain environments (Beniston et al., 2018; Biskaborn et al., 2019). Intact rock glaciers react by slow AL deepening~~and releases the~~ , releasing meltwater previously bound in the ice-rich permafrost~~. However, due to the strong thermal buffering effect of the AL, ground heat fluxes near the AL base (permafrost table) are small and~~ , and transitioning towards a relict (i.e., ice-free) state over the time scale of centuries (Scherler et al., 2013). As intact rock glaciers are a common periglacial landform and the ice-rich ~~permafrost adjusts slowly to climatic changes. Permafrost landforms have longer response times and will largely outlive bare-ice glaciers.~~

The amount of sub-surface permafrost ice stored core is typically $10-30$ m thick (Cicoira et al., 2021), the amount of below-ground permafrost ice as estimated from remotely sensed (static) rock glacier inventories and empirical area-volume scaling relations is substantial (Rangecroft et al., 2015; Azócar and Brenning, 2010; Brenning and Azócar, 2010; Brenning, 2005; Jones et al., 2018b, a), near-globally (Jones et al., 2018a). At catchment scale in in . In semi-arid, weakly glacierized mountain rangescatchments, water volume equivalent (w.e.) stored in rock glaciers can exceed glacier ice volume (or might do so in the future) (Jones et al., 2018a; Bodin et al., 2010; Janke et al., 2017; Azócar and Brenning, 2010). However, this 'static reservoir view' emphasizes the large ground ice storage capacity and often ignores the question of how much meltwater from thawing ice-rich permafrost is generated *through time* and how this permafrost runoff quantitatively compares to precipitation and evaporation (Arenson et al., 2022). The hydrological cycle and the time dimension are insufficiently addressed because of the hard-to-measure in-situ processes and water flows, the complex structure of rock glaciers, and the scarcity of reliable hydro-meteorological data in remote mountain regions. Quantifying the ground-ice derived meltwater component of the total rock-glacier outflow has proven difficult because of several reasons, including: -3pt The frozen debris–ice mixture is covered by the seasonally thawed AL: The ground ice is rarely accessible, its changes and dynamics not directly visible from afar and the

'Young' ice content varies. Ice volume changes are not straightforward to retrieve from surface deformation measurements because landform creepaccumulates and melts seasonally in the AL ("seasonal AL ice", "superimposed ice" in Bearzot et al. (2023)). This ice is derived from modern precipitation and is a renewable resource. Its accumulation/deformation rates can in cases exceed ice volume changes. Most studies adopt a methodologically involved multi-sensor approach, e.g., combining kinematic remote sensing with geophysics or hydrological investigations to isolate ground ice volume changes from remotely sensed surface elevation changes (Halla et al., 2021; Müller et al., 2014; Bearzot et al., 2023). Melt beneath an insulating AL is slow, and the meltwater in the outflow is diluted by the larger components of snowmelt and rainwater, at least in the comparatively humid European Alps (Krainer and Mostler, 2002). The contribution of ground-ice melt to rock glacier runoff might be so small that hydrological approaches via the water balance are difficult, because uncertainties exceed the ground ice melt rates (Chinellato et al., 2011; Bearzot et al., 2023). The few studies that used radiogenic isotopes (tritium ^{3}H, iodine-129) for relative icerelease is conditioned by freeze/water age dating indicated a pre-modern age of thaw cycles driven by the SEB and short-term weather conditions. AL ice volumes are presumably much smaller compared to that of permafrost ice, but in much faster exchange between the atmo- and hydrosphere. Available studies suggest that a considerable fraction of the annual precipitation can be stored and released from intact rock glaciers. Marchenko et al. (2012) report that the observed accumulation–melt of $40-60$ cm of ground ice seasonally stored a substantial amount ($< 30\%$) of the snowpack in the ground ice (Haeberli, 1990; Cecil et al., 1998), but a modern age of the outflow (Cecil et al., 1998; Munroe, 2018). The chemical and isotopic "fingerprint" of the ground ice (e.g., $\delta^{18}O/\delta^2H$ natural tracer) is only known in few rock glaciers, e.g., drillings in MurtNorthern Tien Shan. Halla et al. (2021) found inter-annual ice storage changes on èDos Lenguas 1 (Haeberli, 1990) and Lazaun (Krainer et al., 2015; Nickus et al., 2023). $\delta^{18}O/\delta^2H$ of rock glacier (Dry Andes of Argentina) of -36 mm yr^{-1} (avalanche) snow, glacier ice, and ground ice is often indistinguishable (Humlum et al., 2007), which is problematic for detecting the water origin in seasonally snow-covered or 'mixed' catchments that contain both glaciers and rock glaciers.

The end-thaw season surface outflow (last sample)is often taken as an end-member for mixing calculations and assumed to represent groundwater baseflow (Williams et al., 2006; Munroe and Handwerger, 2023a, b), but its exact origin is often unclear (Williams et al., 2006). Rock glacier outflow often has a chemical signature distinct from other waters in the catchment. For example, high EC of the late-summer outflow is used as an indicator of ground ice melt$25-80\%$ of the annual precipitation) and $+28\ \mathrm{mm\ yr^{-1}}$ $(17-55\%)$. While the timing of seasonal formation and melt of ground ice has long been inferred from thermal (Hinkel and Outcalt, 1994; Kane et al., 2001; Hanson and Hoelzle, 2003, 2004; Sawada et al., 2003; Rist and Phillips, 2005; Herz, 2006) and geophysical measurements (Hilbich et al., 2009; Schneider et al., 2013), so far few estimates of the magnitude of seasonal to inter-annual ice turnover exist even at plot scale. These estimates are based on rare exposure of ground ice or drillings (Sawada et al., 2003; Yoshikawa et al., 2023; Marchenko et al., 2012, 2024), and petrophysical joint inversions of (most often) geoelectrical and seismic measurements (Mollaret et al., 2019, 2020; Steiner et al., 2021; Bearzot et al., 2023; Bast et al., 2024) , in cases combined with kinematic surveys to relate changes in ground ice content to surface kinematics (heave/subsidence) (Halla et al., 2021). Quantifying changes in ground ice content and AL depth is a progressing research field (e.g. Hauck et al., 2011; Wagner because the closer degrading permafrost approaches $0\ ^{\circ}\mathrm{C}$ and enters the zero curtain, the more its state is reflected by changes in ice content (latent heat) rather than by ground temperatures (sensible heat) (Hauck and Hilbich, 2024). Other approaches include hydro-chemical and water isotope measurements (Blumstengel and Harris, 1988; Harris et al., 1994; Williams et al., 2006; Munroe , AL energy budgets (Scherler et al., 2014), and numerical modelling (Pruessner et al., 2022; Renette et al., 2023; Mendoza López et al., 20 .

The ice-rich permafrost of intact rock glaciers affects the hydrology of a watershed by its semi-impervious layer (aquitard) that controls the lateral flow and limits (but not prevents) the exchange between surface waters and sub-permafrost groundwater (Cheng and Jin, 2012). A perched supra-permafrost aquifer within the AL on top of the ground-ice table is separated from a sub-permafrost aquifer (and unfrozen water in intra-permafrost taliks). Runoff from the shallow, highly permeable supra-permafrost aquifer is rapid and flashy, this quickflow is only weakly chemically altered. However, chemical weathering reactions in the rock-glacier aquifer might alter (mineralize) through-flowing water and mask the original water provenance (Williams et al., 2006; Villarroe . Three different interpretations of how weathersome water can percolate across the permafrost through taliks or ‘warm’, permeable zones. These are characteristic features of the inherently discontinuous mountain permafrost, whose distribution is mosaic-like and controlled by spatially complex topo-climatic conditions like insolation/climate drives solute export from rock glaciers have been proposed (Colombo et al., 2018a): (1) enhanced melting of solute-enriched ‘old’ ground ice in warmperiods (Williams et al., 2006; Nickus et al., 2023); (2) flushing out of solutes by percolating modern precipitation water in wet periods (mobilisation behaviour) (Colombo et al., 2018a; Wanner et al., 2023); or (3) anti-correlating discharge–EC pattern: low EC at high discharge where water has a short residence time (e.g., spring freshet) and rising EC due to falling discharge in dry periods with longer water residence times (dilution behaviour). Hydrological in-situ investigations revealed a complex hydrological behaviour with water/ice storage at different timescales (Krainer and Mostler, 2002; Krainer et al., 2007; Wagner et al., 2016; Winkler et al , water flow at different levels with different residence times (supra, intra- and sub-permafrost) (Trombotto and Borzotta, 2009; Trombotto-L , energy-controlled phase changes, and chemical rock-water interactions (Scapozza et al., 2020; Winkler et al., 2021a; Wanner et al., 2023) . These studies have shown that rock glaciers store–release (redistribute) and chemically alter water . Rock glaciers and other

ice-bearing debris landforms like talus slopes and ice-cored moraines play an important role in high-mountain catchment hydrology by sustaining baseflow (Hayashi, 2020) and by keeping stream temperatures low for cold-adapted species (Millar et al., 2013; Br . However, few studies have examined and quantified the runoff contribution *from melting ground ice* in rock glaciers. Haeberli (1975) roughly estimated that icemelt from shading and snow cover (Arenson et al., 2022). A dynamic sub-permafrost storage of liquid water retains water in fine-grained, unfrozen sediments during months–years and sustains baseflow during summer droughts or in winter (Rogger et al., 2017; Wagner et al., 2021a; Reato et al., 2021; Bearzot et al., 2023). This water is more strongly chemically altered and mineralized, as for example indicated by its higher electrical conductivity (Krainer and Mostler, 2002) . For long-term projections, it is important to appreciate the widely diverging time scales of storage mechanisms (from weeks in the AL to millennia in the seasonally thawing AL contributes to of the annual catchment-wide outflow in a high-alpine catchment in the eastern Swiss Alps. It was intended an order-of-magnitude estimate based on the knowledge available at that time. Halla et al. (2021) relied on the abundant fine-grained material of the pebbly *Dos Lenguas* rock glacier where changes in ground ice content translated to heave/subsidence, i.e., inter-annual volume changes detectable by remote sensing. 50 years after Corte (1976)'s question, it is still unresolved to what extent rock glacier outflow is *sourced* from melting ground icepermafrost core) and the transient state of the mountain permafrost subject to climate change (Jones et al., 2019). As rock glaciers degrade, hydraulic permeability and liquid water storage capacity increases at the expense of the storage of permafrost ice (Winkler et al., 2016a, b; Wagner et al., 2016; Harrington et al., 2018; Colombo et al., 2018b).

Although the conceptual framework of the different rock glacier storage mechanisms is established knowledge, no consensus on the present nor future hydrological role of rock glaciers has been reached to date (Duguay et al., 2015; Schaffer et al., 2019; Jones et al., , not least due to sparse quantitative hydro-meteorological field data from permafrost-underlain high-mountain watersheds.

In this work, we estimate the ground ice melt based on point-wise in-situ observation of the ground-ice table and from the AL energy budget of present quantitative data from a detailed single-site case study on Murtèl rock glacier (Engadine, eastern Swiss Alps) . The idea is that the and compare short-, intermediate and long-term water/ice storage changes for the hydrological years 2021–2023. We estimate the ground ice storage changes based on point-wise in-situ observations of the seasonally moving ground-ice melt rate is determined by the energy available in the coarse-blocky AL . By parametrizing the subsurface energy fluxes towards the ground ice table table and from the AL energy budget. Ground ice storage changes are energy-controlled phase changes, i.e., ice/water and energy turnover in the AL are closely linked. By measuring and parameterizing the ground heat fluxes and accounting for sensible heat storage changes in the thick debris mantle (Amschwand et al., 2024b), the latent storage changes associated with water phase changes ÔÇô- melting and refreezing ÔÇô- can be isolated. The estimates of net heat fluxes and storage changes are derived from our extensive sensor network that we installed above ground as well as below ground in natural cavities in the coarse-blocky AL, including long-wave radiation sensors (pyrgeometer), heat flux plates and wind speed sensors. The sensor array complements the automatic above-ground weather station (AWS) and instrumented boreholes operated by the Swiss permafrost monitoring network (PERMOS). The energy budget-derived melt rates are compared with direct observations of the seasonal ground ice melt (in situ "ablation" measurements) at a ground-ice exposure in a nearby rock-glacier furrow and related to discharge and stable isotope measurements of the rock-glacier outflow. The research questions are: (1) What is the contribution of ground ice melt to the total rock glacier outflow? (2) What are the

~~seasonal patterns of discharge? We provide a comprehensive water and energy budget of the AL from in-situ observations of the seasonally evolving ground-ice table and from heat flux measurements from a comprehensive in-situ sensor array (Amschwand et al., 2024b), and hydro-meteorological measurements~~ We build on a large body of local previous work: The SEB and AL-internal heat fluxes on Murtèl have been measured/estimated by Mittaz et al. (2000); Hoelzle et al. (2001); Stocker-Mittaz et a and Amschwand et al. (2024a, b). Hydro-meteorological measurements (snow, rainfall, outflow discharge) complement the plot-scale water budget. Additionally, we use stable water isotope and ~~continuous EC~~monitoring electrical conductivity (EC) to compare the rock-glacier outflow to the known δ^{18}O–EC signature of the permafrost ice.

~~The intensely researched Murtèl rock glacier (Engadine, eastern Swiss Alps) stores large amounts of subsurface ice, buffered from the atmosphere by a thick, coarse-blocky active layer. The extent and ice content of the ice-rich permafrost body is well known from boreholes (Vonder Mühll and Haeberli, 1990; Vonder Mühll, 1992; Vonder Mühll and Holub, 1992; Vonder Mühll and Klinge and geophysical measurements (Hauck, 2013; Arenson et al., 2010; Mollaret et al., 2019). The Surface energy balance and AL-internal heat fluxes towards the permafrost body have been measured/estimated by a number of studies (Mittaz et al., 2000; Hoelzle et a . Murtèl is one of the worldwide few rock glaciers where the chemical and isotopic signature of the difficult-to-access permafrost ice, the supposed source of the meltwater, is known from analysed drillcores (Haeberli, 1990).~~

This case study contributes to the question of the hydrological significance of rock glaciers by presenting a complete hydro-meteorological data set at the well-studied Murtèl rock glacier ~~. We advance the quantitative process understanding by estimating ice storage–release on different time scales. The plot-scale AL energy and water budgets on the rock glacier itself contributes to characterising the hydrological response of coarse-blocky permafrost and for upscaling to landform and catchment scale.~~ and explores the permafrost–groundwater connectivity.

2 Study site

2.1 ~~Hydro-morphological~~ Rock glacier structure and hydro-morphological setting

The studied Murtèl rock glacier (Murtèl I; WGS 84: 46°25′47″N, 9°49′15″E; CH1903+/LV95: 2'783'080, 1'144'820; 2620–2700 m asl.; Fig. 1, A1), close-by Marmugnun rock glacier (Murtèl II) and the relict Murtèl III rock glacier are located in a north-facing cirque in the Upper Engadine, a slightly continental, rain-shadowed high valley in the southeastern Swiss Alps (Fig. 2a). Mean annual air temperature (MAAT) is $-1.7°C$, mean annual precipitation (MAP) is ~ 900 mm (Scherler et al., 2014). The rock glaciers have an altitude range from 2540 (base of front Murtèl III), 2620 (base of front Murtèl I) to 2720 m asl (transition to talus) (Fig. 2b). The talus slopes (at an elevation 2720–2800 m asl.) connect the active rock glaciers to the headwalls and consist of large, angular debris. The headwalls rise from 2800 to 3165 m asl. (a spur of Piz Murtèl) and are more active above rock glacier Marmugnun (Müller et al., 2014) with massive, long-lasting avalanche deposits in late spring–early summer and a debris cone built by frequent rock falls in summer–autumn. The entire mountain slope is part of the periglacial belt and underlain by permafrost (Müller et al., 2014). Perennial snow patches reported by Haeberli (1990) and Tenthorey and Gerber (1991) disappeared by the early 2000s (M. Hoelzle, pers. comm.), but were exceptionally present in the cool-wet summer 2021. Soils are absent–thin and vegetation is sparse. The catchment is small (30 ha) and not glacierized.

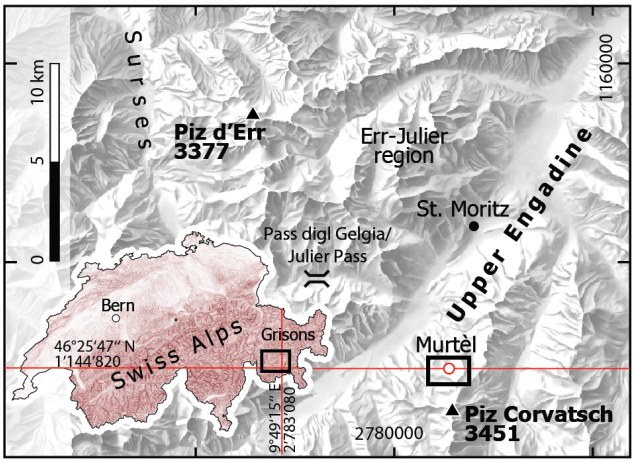

Figure 1. Location of Murtèl rock glacier in the Upper Engadine, a high valley in the eastern Swiss Alps. Inset map: Location and extent (black rectangle) of regional map within Switzerland (source: Swiss Federal Office of Topography swisstopo).

The lobate Murtèl rock glacier is ca. 300 m long, 180 m wide, and covered by a 2–5 m thick coarse-blocky AL (debris mantle). Geophysical investigations revealed that its thickness varies according to the surface micro-topography, from 2 m in the furrows to 5 m beneath the ridges (Vonder Mühll and Klingelé, 1994; Vonder Mühll et al., 2000). Thus, the permafrost table shares the surface furrow-and-ridge micro-topography, although attenuated (water ponding or channelling?). Fine material increases towards the AL base, but is overall sparse. The permeable coarse-blocky AL does not inhibit water flow and has a very low water retention capacity (Springman et al., 2012). The Murtèl permafrost body between the seasonally thawed coarse-blocky AL (0–3 m) and bedrock (at 50 m) is comprised of three distinct layers (Vonder Mühll and Haeberli, 1990; Haeberli, 1990; Arenson et al., 2002): (1) massive ice, sparsely sand- and silt-bearing (3–28 m, supersaturated with over 90% ice ~~by volume~~content); (2) a layer of ice-saturated frozen sand (28–32 m) accommodating ca. 60% of the total/surface displacement (shear horizon); and (3) ice-saturated debris (32–50 m; 40% ice). The three deep boreholes (Fig. 2), all located within 30 m distance, share this three-part stratigraphy, but also reveal lateral small-scale material differences (e.g., laterally variable ice/sand content, lenses) and thermal anomalies (e.g., pointing at non-diffusive heat transfer and intra-permafrost water flow (Vonder Mühll, 1992; Arenson et al., 2010)). ~~Geophysical soundings (ERT profiles) indicated~~ The extent and ice content of the ice-rich permafrost body is well known from boreholes (Vonder Mühll and Haeberli, 1990; Vonder Mühll, 1992; Vonder Mühll and Holub, 1992; V and geophysical measurements (electrical resistivity tomography (ERT) and seismic refraction tomography) (Hauck, 2013; Arenson et al., 2 . These data indicate that the ice-rich permafrost core has an extent of 150×300 m^2 [C. Hauck, pers. comm.], amounting to a water volume equivalent (WVEQ) of $\sim 1.5 \times 10^6$ m^3. Observations at the surface and during drilling operations, borehole temperature and ERT found evidence for supra-permafrost, (artesian) intra-permafrost, and sub-permafrost water flow (Arenson et al., 2002; Springman et al., 2012). Intra- and sub-permafrost conduits were revealed by water leakage into all drilled boreholes at several depths (Arenson et al., 2002), audible water flow, strong air inflow at the surface, and voids photographed by the borehole camera. Overall, even though Murtèl has a relatively massive, 'clean' ice core compared to other permafrost

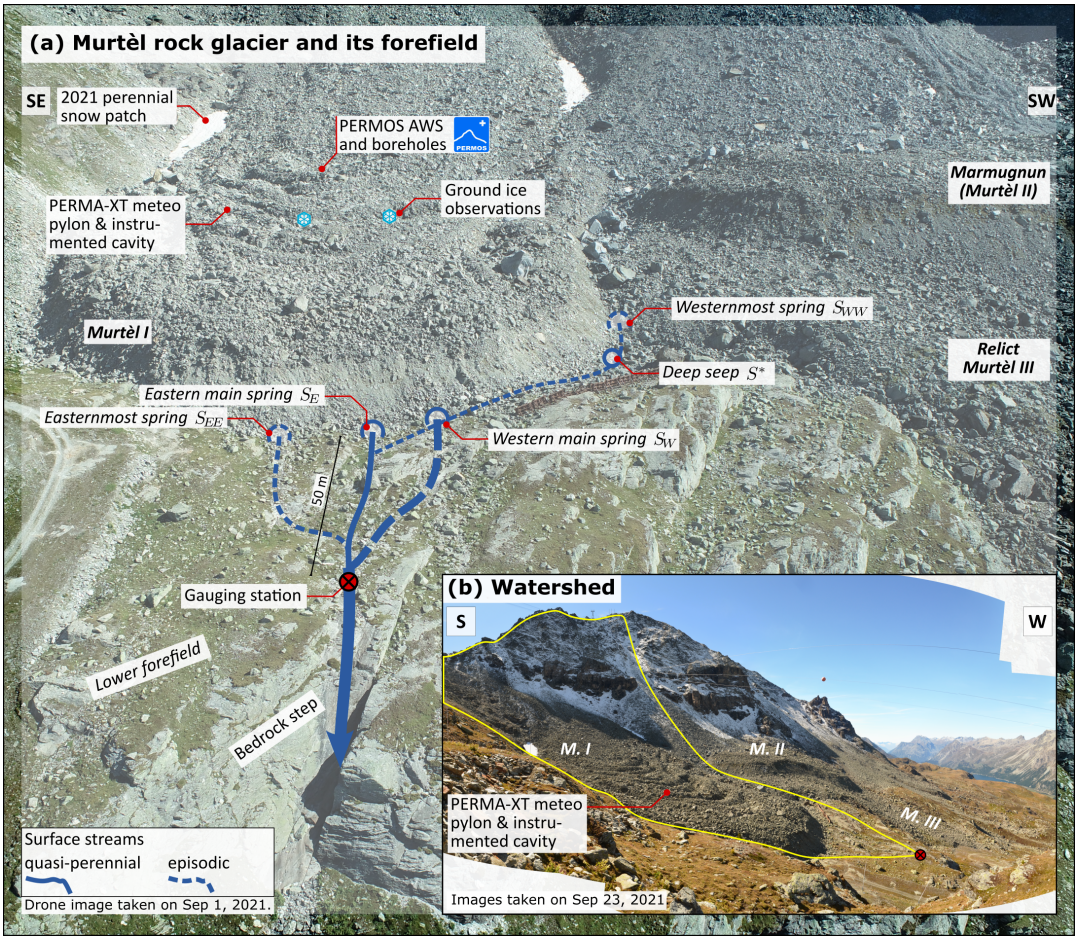

Figure 2. (a) Oblique aerial view of the Murtèl rock glacier and its forefield showing location of the rock glacier springs S_{EE}, S_E, S_W, S_{WW} and S^*. ~~In the exceptionally cool–wet summer 2021,~~ Parallel rock ledges show a ~~few snow patches survived in the Murtèl catchment, which has rarely been occurring in the last years~~set of N-S running fractures. ~~The main springs are already reported by Tenthorey and Gerber (1991).~~ **(b) Inset** The Murtèl periglacial catchment.

drill cores (Lazaun, Krainer et al. (2015); Nickus et al. (2023)), the permafrost body is far from being ~~completely impermeable.~~ impermeable.

The Murtèl rock glacier sits in a bowl-shaped, glacially overdeepened bedrock depression as shown by boreholes and geophysical soundings/gravimetry (Vonder Mühll and Klingelé, 1994). The rock glacier front has advanced beyond the cirque lip (bedrock sill) onto the forefield that slightly dips away to NNW. Four rock-glacier springs and one seep emerge between coarse blocks at the base of the rock-glacier front (Fig. 2). The forefield is thinly covered by glacial sediments (till veneer, few large boulders), not perennially frozen (from ERT), and vegetated by grasses (Schneider et al., 2013). There are no surface waters upslope of the rock-glacier springs, and no surface water bodies are impounded in the catchment (except episodically during

snowmelt or rainstorms). The bedrock appears fractured. For a few days after strong precipitation, water flows out of bedrock cracks/fissures fractures in the steep rock face below the forefield (Fig. 2). The bedrock of the Murtèl cirque predominantly consists of granodiorite, whose blocks make up the bulk of the talus slopes and rock glacier coarse-blocky AL. This *Corvatsch granodiorite* unit is separated by a tectonic thrust from a westward-thickening seam/wedge of meta-sedimentary units of the *Rusenna formation* and *Blais radiolarite* consisting of weakly metamorphosed limestone, mica schists, and radiolarite.

2.2 Past "Gray" hydrological and hydro-chemical investigations

Water-related observations made in the field and from borehole drilling published in Haeberli et al. (1988); Vonder Mühll (1992); Arenson e are summarized in Sect. 2.1. The few studies with We summarize three site-specific past hydrological or water (isotope-)chemical focus on studies which are not easily accessible, namely Haeberli (1990), Tenthorey and Gerber (1991), and Stucki (1995) .

Murtèl are Haeberli (1990); Tenthorey and Gerber (1991); Stucki (1995), a hydrological modelling work by Speck (1994), and permafrost melt modelling by Pruessner et al. (2018, 2021, 2022). The ground thermal modelling study by Scherler et al. (2014) has hydrological relevance by providing indirect estimates of the ground-ice melt from the non-closure of the AL energy budget.

Haeberli (1990) is one of the worldwide few rock glaciers where the chemical and isotopic signature of the difficult-to-access permafrost ice, the supposed source of the meltwater, is known from analysed drillcores (Haeberli, 1990). This report provides a concise overview of the isotope (δ^2H, δ^{18}O, tritium) and major ion chemistry of the 2/1987 drillcore at depths between 3.34 and 20.92 m. The δ^{18}O values of the permafrost ice is in the range of -16 to -13‰, the deuterium excess in the range of 13 to 15‰, and the δ^{18}O–δ^2H relationship is $\delta^2\mathrm{H} = 7.97\,\delta^{18}\mathrm{O} + 12.67$‰. The electrical conductivity estimated from the major ion concentration is in the range of $5-30$ µS cm^{-1}. They interpreted the ground ice as refrozen "diluted groundwater" (non-closed ion balance/cation surplus, pH in the range of $6.3-8.6$) likely derived from winter precipitation/snowmelt (syngenetic permafrost formation).

Tenthorey and Gerber (1991) carried out tracer tests in summer 1989 (napthionate and sodium chloride) and found evidence of two types of water flow, a rapid–channelised (supra-permafrost; > 120 m h^{-1}) and a slow–diffuse (intra-permafrost?; < 25 m h^{-1}) flow . (Figs. A1, A1). The Murtèl supra-permafrost water drains predominantly to the main springs S_E and S_W; a hydrological connection to the deep seep S^* and even to the relict Murtèl III rock glacier (Fig. 2b) exists but is inefficient. The tracer tests revealed that minor amounts of water leave the catchment via slow groundwater pathways.

Stucki (1995) attempted to establish the provenance of the water that flows in the intra-permafrost bedrock talik at $52-55$ m (Sect. 2.1) using stable isotopes as tracers of possible water sources: glacier ice from nearby *Vadret da Corvatsch*, permafrost ice from the same 2/1987 drillcore sampled near the ground-ice table, precipitation, and nine springs in the catchment (among them S_{EE}, S_E, S_W, and S_{WW}). The δ^{18}O of the ground ice was with -15.3‰ identical to that of the snow sample, the δ^{18}O of the outflow S_E became seasonally depleted from -11‰ (July 30, 1994) to -14‰ (Oct 7) at overall decreasing discharge, and their δ^{18}O–δ^2H relationship is $\delta^2\mathrm{H} = 8.4\,\delta^{18}\mathrm{O} + 18.7$‰ ($n = 30$, $R^2 = 0.99$).

Speck (1994) did numerical coupled thermo-hydrological modelling of heat transfer and groundwater flow in Murtèl rock glacier accounting for ice–water phase changes and changing material parameters. Valuable for this work are his estimates of the hydraulic conductivity: (rather low) for the highly permeable coarse-blocky AL, for the ice-rich rock-glacier core, and for strongly fractured bedrock.

The modelling studies by Pruessner et al. (2018, 2021, 2022) expanded the Glacier Evolution and Runoff Model (GERM) with a module accounting for wind-forced convection and ice loss/subsidence to simulate the evolution of the ground thermal regime, ground ice content, and permafrost runoff of coarse-blocky permafrost under different climate scenarios.

Finally, Scherler et al. (2014) estimated the Murtèl AL energy budget using two approaches, a process-based soil heat transfer model (the COUP 'Coupled heat and mass transfer model') and heat exchange calculations that integrate thermal radiation between adjacent blocks, turbulent heat flux, and sensible heat storage changes in the coarse-blocky AL. The energy-budget deviations are hypothesized to approximately equal unmeasured freezing and thawing processes within the blocky surface layer.

3 Measurements and data processing

A comprehensive hydro-meteorological data set is obtained from hydrological sensors (Table 1, Sect. 3.1), from the PERMA-XT and PERMOS automatic weather stations (AWS) on the rock glacier (Amschwand et al., 2024a) (Sect. 3.2), from active-layer sensors complemented with PERMOS borehole temperature data to estimate the AL energy budget (Amschwand et al., 2024b) (Sect. 3.3), and direct observation of the ground ice table (Sect. 3.4). Throughout this publication, the term 'meltwater' denotes melt from various types of ground ice, but neither from snow (explicitly denoted as 'snowmelt'), nor from glacier ice (the catchment is not glacierized).

3.1 Hydrological measurements

Hydrological measurements (salt dilution gauging with sodium chloride, bucket method) for discharge estimates, hydrochemical characterization of precipitation and spring water with electrical conductivity (EC), and stable isotope chemistry (δ^2H, δ^{18}O).

3.1.1 Discharge measurement

The water level gauge is located in the lower forefield after the confluence of all four rock-glacier springs and captured the catchment-integrated surface outflow (Fig. 2, Table 1). The discharge Q_w is expressed as a power-law relation of water level h_w (stage) with empirically fitted coefficients c_1 and c_2,

$$Q_w = c_1(h_w - h_0)^{c_2}, \tag{1}$$

where h_0 is the stage at zero discharge (standing water in logger pool). The coefficients for the stage–discharge (h_w–Q_w) relation (Eq. 1) were constrained by dilution gaugings with sodium chloride as a chemical tracer or the volumetric method ("bucket method") if discharge was too low for dilution gaugings. The water level is obtained from the total pressure P_{tot}

Table 1. PERMA-XT sensor specifications. The below-ground sensors were operational from Sep 2020 to Sep 2023 (destroyed by rockfall).

Quantity [unit]	Manufacturer	Sensor type	Accuracy
Sensors above ground (details in Amschwand et al. (2024a))			
Air temperature T_a [°C]	CSI[a]	107 temperature probe[b]	±0.01 °C
Relative humidity (rH for q_a) [%]	CSI	HygroVUE10 hygrometer[b]	±3%; ±0.1°C
Barometric pressure P [Pa]	CSI/SETRA	CS100 barometer	±1.5 hPa
Liquid precipitation r [mm h^{-1}]	CSI	SBS500 tipping bucket rain gauge (unheated)	±30% (undercatch)
Snow temperature [°C]	TE Connectivity[d]	44031RC NTC thermistors (0, 25, 50, 100 cm a.g.l., unshielded)	±0.1°C
Snow height h_S [cm]	CSI	SR50A sonic ranging sensor	max{±1 cm, ±0.4%}
Automatic time-lapse camera	MOBOTIX	M16B IP camera (RGB)	
Sensors below ground (active-layer sensors in instrumented main cavity, details in Amschwand et al. (2024b))			
AL air temperature $T_{al}(z)$ [°C]	TE Connectivity[a]	44031RC NTC thermistor chain TK1/1	±0.1°C
AL net long-wave radiation Q^{rad}_{CGR3} [W m^{-2}]	Kipp & Zonen	CGR3 pyrgeometer (4.5−42 µm, FoV 150°)	< 4 W m^{-2}
Heat flux Q_{HFP} [W m^{-2}]	Hukseflux	HFP01 heat flux plate	site-specific
Hydrological sensors (on Murtèl forefield)			
Water level[c] (pressure P_{tot}) [Pa]	Onset	HOBO U20-001-04 water level logger	±0.43 kPa (±3 mm)
Water electrical conductivity[c] $\varkappa$ [µS cm^{-1}]	Onset	HOBO U24-001 conductivity logger	max{3%, ±5 µS cm^{-1}}
	Driesen+Kern	D+K μS-Log3040	2% FS

Measurement range and accuracy by manufacturer/vendor. The specifications of the PERMOS sensor are given in Scherler et al. (2014) and Hoelzle et al. (2022).
[a]Thermistor strings manufactured by Waljag GmbH. [b]CSI: Campbell Scientific, Inc. Sampling interval: 30 minutes (or shorter). [c]All water sensors additionally measure temperature.

measured by the submerged logger (pressure compensation) via the *hypsometric equation* that corrects the barometric pressure measured on the rock glacier to the elevation of the gauging station,

$$h_w = \frac{P_{tot} - P'_{atm}}{\rho_w\, g}, \quad P'_{atm} = P_{atm} \cdot \exp\left\{\frac{\Delta z\, g}{R \bar{T}_v}\right\}. \tag{2}$$

$\Delta z = 42$ m is the elevation difference, $\bar{T}_v$ [K] the layer-averaged virtual temperature (approximated by the actual temperature T_a), P'_{atm} the elevation-corrected air pressure, $\rho_w = 10^3$ kg m^{-3} the water density, g the gravitational acceleration [9.81 m s^{-2}], and R the specific gas constant [287 J kg^{-1} K^{-1}].

3.1.2 ~~Electrical~~ Water electrical conductivity ~~measurements~~monitoring

The electrical conductivity (EC) of the water is monitored at the two main springs at the rock-glacier front and of the total outflow in the bedrock step downstream of the confluence (Fig. 2). We report water EC referenced to 25°C, $\varkappa$ [µS cm^{-1}],

calculated from the measured conductivity $\varkappa_\vartheta$ [µS cm^{-1}] at water temperature ϑ_w [°C] via

$$\varkappa = \frac{\varkappa_\vartheta}{1 + \alpha(\vartheta_w - 25°\mathrm{C})}, \tag{3}$$

with ~~the~~ a linear temperature compensation factor ~~α (Hayashi, 2004; McCleskey et al., 2011). We use a linear correction with a constant~~ $\alpha = 0.019°\mathrm{C}^{-1}$ ~~–OR– non-linear temperature compensation for natural water according to EN 27888 (DIN 38404). CHECK!!~~ (Hayashi, 2004; McCleskey et al., 2011). Additionally, we measured EC manually using a WTW LF 320 with a TetraCon 325 probe as a reference for the two quasi-continuously measuring conductivity logger models (Table 1) and when the water loggers were found dry (~~too low water level~~ water level too low).

3.1.3 Stable isotope composition

We took grab samples of the spring snowpack before onset of snowmelt (coring with a plastic tube), of the rock-glacier outflow, cumulative rainwater, and supra-permafrost water in a rock glacier furrow where the ground ice is accessible (next to the 'ablation stake'; Sect. 3.4, Fig 2). The water samples were stored in PP bottles with little head space and tightly sealed parafilm in order to minimize evaporation effects.

Water stable isotope composition (δ^2H, δ^{18}O) was analysed by Cavity Ring Down Spectroscopy at the Institute of Geology of the University of Bern using a Picarro L2120-i analyzer attached to a V1102-i vaporizer.

We report the water stable isotope composition as a δ ratio [‰] of the sample to the Vienna Standard Mean Ocean Water (VSMOW), where δ is the ratio of ^{18}O/^{16}O and ^{2}H/^{1}H. Analytical precision is $\pm$1.0‰ for δ^2H and $\pm$0.1‰ for δ^{18}O. The altitudinal gradient in $\delta^{18}O$ does not exceed -0.2‰ per 100 m (annual average) (IAEA/WMO, 2015; Bowen, 2017; Kern et al., 2014), i.e. the isotopic differences over the catchment elevation range (2600–3100 m asl.) is within 1‰.

3.2 Surface fluxes: Precipitation and evaporation

3.2.1 Snow

The PERMA-XT point-wise snow depth measurements h_S (sonic ranger data, Table 1) located on a wind-swept rock-glacier ridge are converted to snow water equivalent (SWE) [kg m^{-2} = mm w.e.] with the semi-empirical parsimonious ΔSNOW model (Winkler et al., 2021b). Additionally, to harness the larger footprint of the SEB ~~calculations~~ for a spatially averaged snow depth estimate on the rugged rock-glacier surface, the deviation of the ~~surface energy balance~~ SEB $\mathrm{dev}_{\mathrm{SEB}}$ during the snow melt months is back-calculated to SWE,

$$\mathrm{SWE} \approx \mathrm{dev}_{\mathrm{SEB}} \Delta t / L_m, \tag{4}$$

where $\mathrm{dev}_{\mathrm{SEB}} := Q^* - Q_H - Q_{LE} - Q_G$ (Amschwand et al., 2024a): The SEB deviation is the remainder of the turbulent fluxes $Q_H + Q_{LE}$ and ground heat flux Q_G subtracted from the surface net radiation Q^*. Δt refers here to the duration of the snowmelt period as estimated from temperature measurements in the snowpack (0°C) and using time-lapse imagery from an on-site camera (Table 1).

3.2.2 Rain

Liquid precipitation data is taken from the on-site rain gauge, assuming that precipitation is liquid based on a threshold air temperature of $T_{wb} = 2°\mathrm{C}$. The rainfall heat flux Q_{Pr} was estimated via (Sakai et al., 2004; Reid and Brock, 2010)

$$Q_{Pr} = C_w r\,(T_P - 0°\mathrm{C}), \tag{5}$$

where $C_w = \rho_w c_w$ [4.18 MJ m^{-3} K^{-1}] is the water volumetric heat capacity and r [m^3 m^{-2} s^{-1}] is the rainfall rate intercepted at the surface as measured by our on-site rain gauge or from MeteoSuisse data (Sect. 4.3). Precipitation temperature T_P was approximated using the wet-bulb temperature T_{wb}, calculated from air temperature and relative humidity (Amschwand et al., 2024a).

3.2.3 Evaporation/sublimation

The evaporative water flux (including sublimation if $T_s < 0$ °C) is derived from the ~~sensible~~ latent turbulent flux Q_{LE} of the Amschwand et al. (2024a) SEB that is estimated with the the bulk aerodynamic method (Mittaz et al., 2000; Hoelzle et al., 2022). The flux–gradient relation is expressed as

$$Q_{LE} = \rho_a L_v \frac{q_a - q_s}{r_q}. \tag{6}$$

Q_{LE} is driven by the specific humidity difference between the atmospheric air q_a and the snow (if snow-covered) or debris surface (if snow free) q_s. q_s under snow-free conditions is taken from humidity measurements in the near-surface AL (q_a at 0.7 m depth; Table 1), otherwise the surface is considered saturated at the radiometrically determined surface temperature. The bulk aerodynamic resistance for vapour transport in the near-surface atmosphere r_q [s m^{-1}] decreases with the strength of turbulence: a thermally unstable atmosphere or strong winds enhance turbulent transport. r_q is estimated using the Monin–Obukhov similarity theory (MOST) and the parameterisations detailed in Rigon et al. (2006); Endrizzi et al. (2014).

3.3 AL heat ~~and water~~ fluxes

~~The~~

3.3.1 The AL energy budget

During the thaw season, the ground heat flux Q_g [W m^{-2}] downwards into the coarse-blocky AL is spent on warming the debris ΔH^{θ}_{al} (sensible heat storage changes), melting ground ice in the AL ΔH^{i}_{al} (latent heat storage change or ground ice storage change), and conducted into the permafrost body beneath Q_{PF} ('permafrost heat flux') (cf. Woo and Xia, 1996; Hayashi et al., 2007; Boike et al., 2003; Zhu et al., 2024) (Fig. 3),

$$\underbrace{\frac{\partial}{\partial t}\int_0^{\zeta(t)} C_v\,(T_{al}(z,t) - 0°\mathrm{C})\,\mathrm{d}z}_{\Delta H^{\theta}_{al}} + \underbrace{L_m \rho_i \frac{\partial}{\partial t}\int_0^{\zeta(t)} f_i(z)\mathrm{d}z}_{\Delta H^{i}_{al},\ \mathrm{dev}_{al},\ Q_m} = \underbrace{Q_g - Q_{\mathrm{PF}}}_{Q^{\mathrm{net}}}\ [\mathrm{W\ m^{-2}}]. \tag{7}$$

where ζ is the depth of the ground-ice table (AL thickness) [m], C_v the volumetric heat capacity of of the debris [J m^{-3} K^{-1}], and T_{al} AL temperatures [°C]. f_i [−], L_m [3.35×10^5 J kg^{-1}], and ρ_i [kg m^{-3}] are the volumetric ice content, latent heat of melting, and ice density, respectively. The AL energy budget Eq. 7, derived from the conservation of energy principle, is estimated based on data from the instrumented main cavity (Fig. 2) as outlined below. We compare two independent estimates of the ground ice melt ΔH^i_{al}, one from the deviation of the AL energy budget denoted by dev_{al} (Sect. 3.3.3), and one from the Stefan model based on direct observations of $\zeta(t)$ in a nearby rock-glacier furrow ('ablation measurements') denoted by Q_m (Fig. 2, Sect. 3.4). Details on the measurement set-up and data processing are in Amschwand et al. (2024a, b).

3.3.2 Ground heat flux Q_g

We estimate the thaw-season ground heat flux from two measurements, from the AL net long-wave radiation Q^{rad}_{CGR3} and the heat flux plate Q_{HFP} (Table 1). These two measurements are correlated and represent the ~~*downward* heat transfer~~ downward heat flux Q_g in the absence of buoyancy-driven convection, i.e. in conditions of stably stratified AL air column which prevails during the thaw season. These Q_g measurements are at $1.5{-}2.0$ m depth in the AL, not at the surface. Details about data pre-processing are in Amschwand et al. (2024b).

3.3.3 Sensible and latent heat storage changes ΔH^{θ}_{al}, dev_{al}

The sensible heat ΔH^{θ}_{al} stored/released by temperature changes of the blocks in the coarse-blocky AL beneath the Q_g ~~-measurement~~ measurement depth are estimated by

$$\Delta H^{\theta}_{al} \approx C_v h \frac{\partial \langle T_{al} - 0\,^{\circ}\mathrm{C} \rangle}{\partial t} \tag{8}$$

where $C_v = (1-\phi_{al})\rho_r c_r$ is the volumetric heat capacity [$0.6{\times}2690$ kg m$^{-3}{\times}780$ J kg^{-1} K^{-1}] (porosity $\phi_{al} = 0.4$), h the distance from the Q_g–measurement level to the AL base [2 m], and $\langle T_{al} \rangle$ spatially averaged AL temperatures [°C].

The deviation dev_{al} to closure of the AL energy budget (Eq. 7), after assessment of the uncertainties, corresponds to the ~~heat~~ latent heat storage changes, i.e. heat spent on melting ground ice,

$$\mathrm{dev}_{al} := (Q_g - Q_{\mathrm{PF}}) - \Delta H^{\theta}_{al}. \tag{9}$$

3.3.4 AL base flux through permafrost body Q_{PF}

The heat flux across the permafrost table Q_{PF} is estimated with the gradient method from PERMOS borehole temperature data via Fourier's heat conduction equation

$$Q_{\mathrm{PF}} \approx -k_{\mathrm{PF}} \frac{\Delta T_{\mathrm{PF}}}{\Delta z}, \tag{10}$$

where the borehole temperatures are measured at 4 and 5 m depth in the permafrost body beneath the AL. We take a thermal conductivity k_{PF} value of 2.5 W m^{-1} K^{-1} (Vonder Mühll and Haeberli, 1990; Scherler et al., 2014).

3.4 'Ablation measurements' at ground-ice table

3.4.1 Observations of seasonal evolution of the ground-ice table

The ground ice is accessible at a few spots, all located in furrows where the AL is thinner ($1-2$ m). In one spot, a plastic tube was drilled ca. 120 cm into the ice in August 2009 but subsequently abandoned (C. Hilbich, pers. comm.). We made serendipitous use of it as an 'ablation stake', manually measuring the depth of the ground-ice table $\zeta(t)$ [m] at each field visit in summer 2022 and 2023 (Amschwand et al., 2024b). ~~Since~~ Assuming that changes in ice content f_i only occur at the phase change boundary $\zeta(t)$ ~~, the~~ coinciding with the $0°$C isotherm (negligible melting point depression in the coarse material), the ice melt heat flux ~~$Q_m = \Delta H^i_{al}$ (Eq. 7)~~ Q_m can be expressed as

$$Q_m = f_i L_m \rho_i \frac{\mathrm{d}\zeta}{\mathrm{d}t}. \tag{11}$$

3.4.2 ~~Parameterisation~~ Stefan parameterisation of ground-ice melt

Given the sparse and point-wise ablation observations, we use a Monte Carlo simulation and a Stefan model (Eq. 12) to assess a plausible range of ground-ice melt for a range of input parameter values as expected on landform scale (probabilistic uncertainty estimate, Sect. 4.4.2). The Stefan model has been widely used to ~~estimate the active layer thickness in polar permafrost settings (e.g., Hayashi et al., 2007; Riseborough et al., 2008; Hrbáček and Uxa, 2019)~~simulate the freezing and thawing fronts in permafrost (e.g., Hayashi et al., 2007; Riseborough et al., 2008; Bonnaventure and Lamoureux, 2013; Hrbáček and Uxa, 2019), including the Cold Regions Hydrological Model (Pomeroy et al., 2022). We parameterise the cumulative heat flux from ground ice melt on Murtèl ~~$H^i_{al} = \int_0^t Q_m \mathrm{d}t' = f_i L_m \rho_i \zeta(t)$~~ $H^i_{al}(t) = \int_0^t Q_m \mathrm{d}t' = f_i L_m \rho_i \zeta(t)$ as a function of the depth of the ground ice table $\zeta(t)$ ~~(Fig. 3) using Aldrich and Paynter (1953)'s equation~~ using a modified Stefan equation by Aldrich and Paynter (1953) that is appropriate for a two-layered stratigraphy (Fig. 3) (Kurylyk, 2015; Kurylyk and Hayashi, 2016),

$$\int_0^t Q_m(t')\mathrm{d}t' := \Sigma_t Q_m = f_i L_m \rho_i \sqrt{h_1^2 + \frac{2k_{\mathrm{eff}}(I(t) - I_1)}{L_m f_2 \rho_i}}, \tag{12}$$

where the surface thawing index $I(t)$ is defined as

$$I(t) := \int_0^t \lambda_5^2 T_s \mathrm{d}t' \approx 86400 \sum_i \bar{\lambda}_5^2 \bar{T}_s \tag{13}$$

and the thaw index of the ice-poor AL overburden I_1 as

$$I_1 := \frac{h_1^2 L_m f_1 \rho_i}{2k_{\mathrm{eff}}}. \tag{14}$$

The factor $\lambda_5 \leq 1$ corrects for the sensible heat storage in the thawed layer and is a polynomial of the Stefan number Ste, $\lambda_5 = 1 - 0.16\,\mathrm{Ste} + 0.038\,\mathrm{Ste}^2$ (Kurylyk and Hayashi, 2016). The depth-averaged dimensionless Stefan number Ste is proportional to the ratio of sensible heat to latent heat absorbed during thawing,

$$\mathrm{Ste} := \frac{C_v \bar{T}_s}{L_m \langle f \rangle \rho_i}, \tag{15}$$

with the bulk volumetric heat capacity C_v [J m^{-3} °C^{-1}] of the (unfrozen, ice-free) AL (identical for both layers), the average surface temperature $\bar{T}_s$ for the time t elapsed since onset of the thaw season, and the latent heat consumed by the melting of the ground ice $L_m \langle f \rangle \rho_i$ (different in each layer and depth-averaged denoted by $\langle \cdot \rangle$; details in Kurylyk and Hayashi (2016)).

~~We use Eq. 12 (i) to compare Q_m with the AL energy budget deviation dev_{al}, (ii) to estimate the ground ice melt in thaw season 2021, where no systematic ablation measurements were carried out, and, given the sparse and point-wise observations, (iii) to assess a plausible range of ground-ice melt for a range of input parameter values as expected on landform scale (probabilistic uncertainty estimate, Sect. 4.4.2).~~

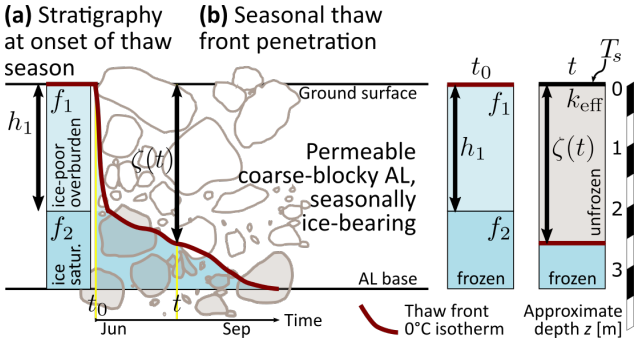

Figure 3. Ground-ice thaw and the Stefan equation of a two-layered stratigraphy. **(a)** Initial stratigraphy at the onset of the thaw season with ice-poor overburden ~~(h_1, f_1)~~ (thickness h_1 and ice content f_1) and ice-saturated layer ~~(f_2)~~(ice content $f_2 = \phi_{al}$). **(b)** Seasonal thaw front penetration, $\zeta(t)$, driven by the ground surface temperature T_s. Maximum thaw depth is denoted by ζ_{max}.

4 Results

4.1 Meteorological conditions

The weather in each season differed markedly in the two years 2020–2022. Figs. 4a and 5a show temperature and precipitation during the summers 2021 and 2022, respectively. The winter 2020–2021 was colder than the 2021–2022 one (November–April: average temperature: -6.2°C vs. -5.3°C; minimum daily average temperature: -16.5°C vs. -15.1°C) and richer in terms of snow amount (November–April: average snow height measured on a wind-swept ridge: 76 cm vs. 54 cm) and duration (early onset of snow cover: 5 October vs. 3 November; later melt-out: mid-June vs. mid-May). Summer 2021 was cool-wet compared with the hot-dry summer 2022; temperatures were lower (July–August: average: 6.9°C vs. 9.3°C) with frequent passage of synoptic fronts, often bringing cold air (≤ 3°C; minimum daily average temperature: 0.7°C vs. 5.6°C) and mixed precipitation (sleet). Snowfall occurred in a few days throughout the summer and melted within hours. A few snow patches survived over the summer after melt-out of the winter snowpack in mid-June (Fig. 2), which has rarely been occurring in the last ~ 15 years. A thermistor installed above the ground-ice table in August 2020 became embedded into newly formed ground ice and was only released in August 2022. In contrast, the hot-dry summer 2022 was marked by three

heat waves (in June, July and August) and daily minimum temperatures not below $5°C$. Several dry spells occurred during this season; the longest one was an 11-day long dry spell within the 5–19 July heat wave. Almost no precipitation was recorded between 20 June and 1 August, despite strong convective precipitation events recorded on by the nearby MeteoSuisse station *Piz Corvatsch* (3294.31 m asl., 1.2 km away). Discharge data of the rock glacier outflow (Fig. 5b), camera images and post-event field observations (fresh debris flow deposits, flooding of furrows) revealed rainwater funnelled onto the rock glacier. We augment the PERMA-XT precipitation measurements with MeteoSuisse precipitation data from the station *Piz Corvatsch*. Immediate on-site inspection of the PERMA-XT rain gauge did not suggest any technical malfunctioning, speaking for a spatially heterogeneous precipitation pattern (Sect. 4.3).

4.2 Hydrological results

4.2.1 ~~Field observations~~

Frequent field visits were indispensable to obtain the in-situ measurements, to obtain grab samples of water between the coarse-blocky material, and to adapt the logger placement to the strongly variable discharge. Suitable places for the EC loggers at the two main springs were found only in late summer 2021. Still, data gaps due to incompletely submerged loggers at extremely low outflow during hot–dry periods (precisely when meltwater signal can be expected to be clearest) could not be avoided. Six snapshots of the strongly variable discharge in the Murtèl ~~rock glacier~~ rock glacier forefield are drawn in Fig. A2. All springs are mentioned in previous investigations (Tenthorey and Gerber, 1991; Stucki, 1995).

4.2.1 Discharge and water temperature

The empirical stage–discharge (h_w–Q) relation (Eq. 1) based on eight gaugings (Fig. 6, Table 2) yields ~~with~~ the fitted coefficients $h_0 = 780$ mm (stage of the standing water), $c_1 = 7429$, and $c_2 = 5.15 \pm 0.753$ (1σ uncertainties; h_w in m, Q_w in $m^3\ s^{-1}$). Because of the wide channel (plane-bed type stream morphology) in the slightly dipping forefield, the water level covered by gaugings varies by merely 9 cm that covers a discharge range from 3 L min^{-1} (detection threshold) to 27.7 L sec^{-1} (Fig. 6). The channel remained stable during the study period August 2020–September 2022. Discharge estimates in the wet summer 2021 relies on extrapolated stage–discharge relation (often exceeding 27.7 L sec^{-1}), while discharge in the dry summer 2022 is mostly interpolated and better constrained (except early snow melt period and peak discharge of event water). ~~Additionally~~Importantly, no stage measurements could be made beneath a snow cover, hence snowmelt discharge before complete melt-out of the forefield is not ~~captured~~gauged. We consider our stage–discharge relation and discharge estimate sufficient for our purpose of season-cumulative water balances and emphasize that our focus is on the low-discharge summer periods where the contribution from ground-ice melt is potentially largest. In the context of the hydrological significance of Murtèl rock glacier, the (reliably measured) zero-discharge estimates will be important.

Discharge in the small catchment is variable and shows a seasonal trend and decreases as snowmelt progresses (Figs. 4, 5), superimposed by regular diurnal fluctuations related to radiative forcing/snowmelt. Total measured discharge was 160×10^3 m^3 in summer 2021 (snowmelt and thaw season), and 97×10^3 m^3 in summer 2022. After completion of the snowmelt, outflow is

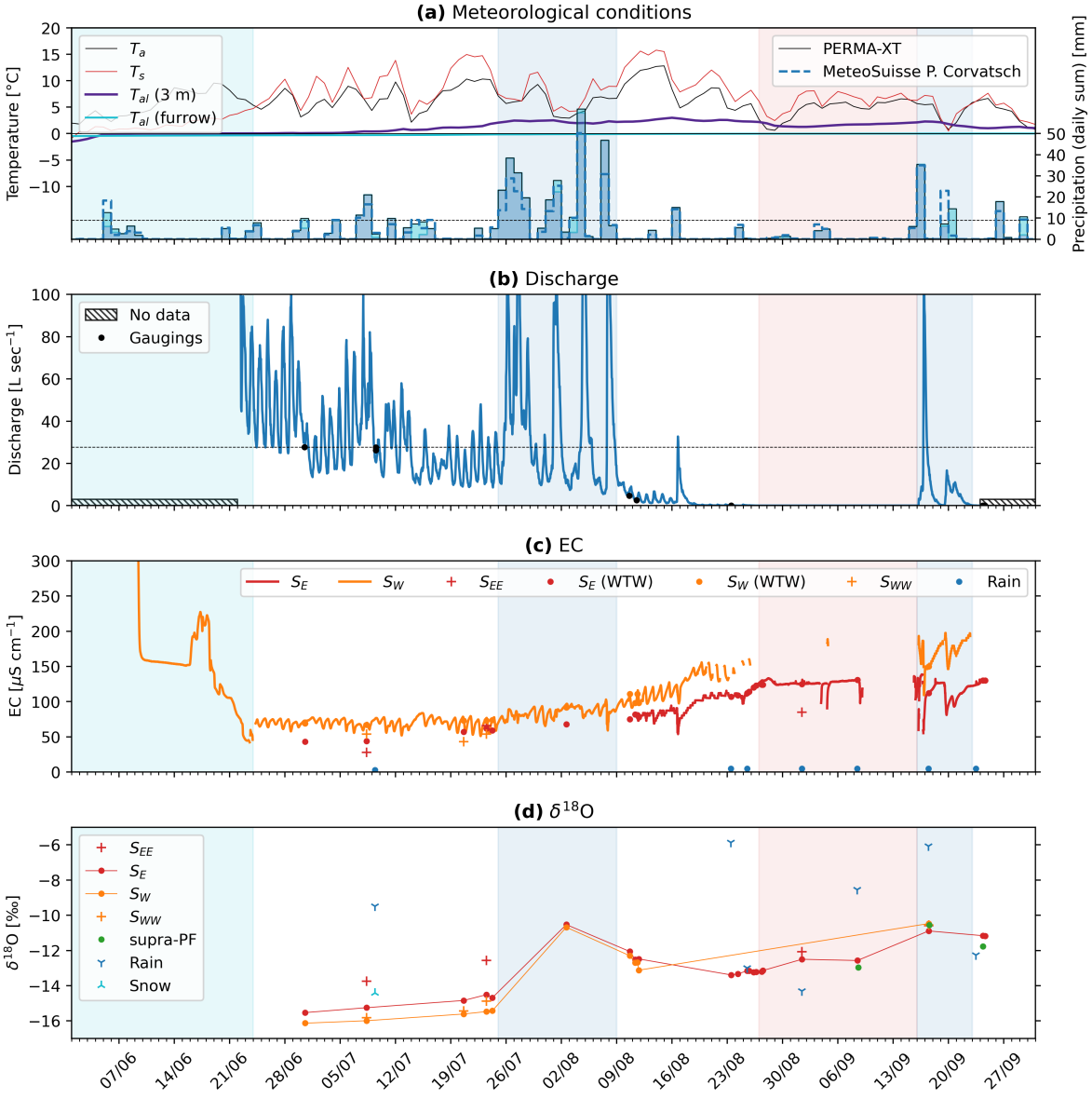

Figure 4. Hydro-meteorologial data for summer 2021. **(a)** Temperature and precipitation (daily averages~~; note the frozen thermistor~~). Thermistor TK4/5 $T_{al} = 0°\mathrm{C}$ in the furrow remained frozen. 9 mm w.e. day^{-1} is the infiltration capacity (horizontal dashed line, Fig. 7). **(b)** Discharge. Maximum gauged discharge is 27.7 L s^{-1} (horizontal dashed line). **(c)** Water electrical conductivity (EC). **(d)** δ^{18}O.

'flashy' where dry phases without measurable baseflow ($\lessapprox 3$ L min^{-1}) ~~is~~ are interrupted by precipitation-fed discharge spikes (event water). The qualitative discharge pattern is similar in both summers. Field observations and additional EC measurements

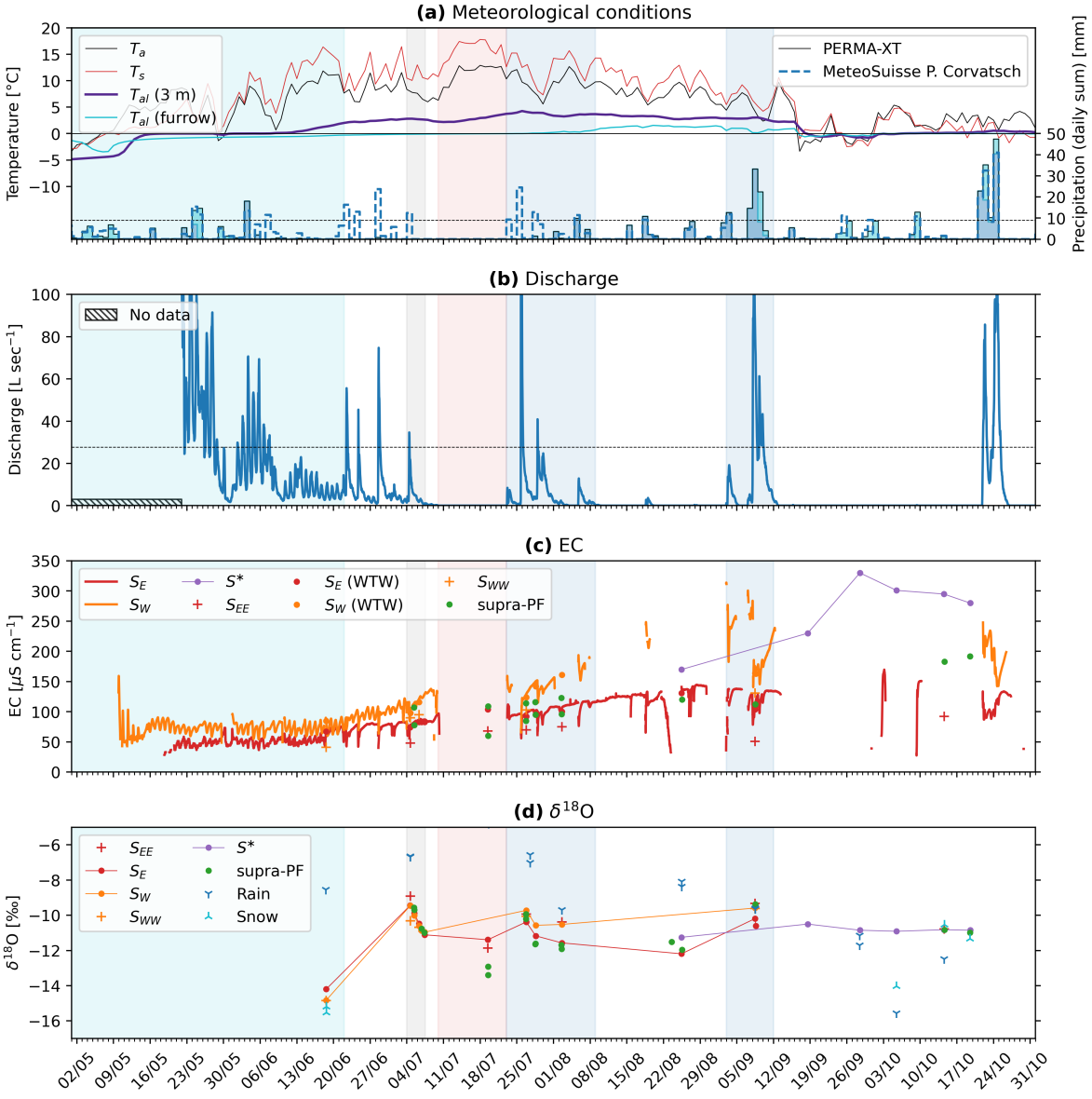

Figure 5. Hydro-meteorologial data for summer 2022.

at the bedrock step downstream of the confluence (mixing calculations) suggest that the discharge of S_W exceeds that of S_E, if S_W is active. Water temperature of the outflow and the deep seep are stable and always at $0-1°C$.

~~The rainfall–runoff~~ The rainfall–streamflow relation from the *threshold analysis* (Wagner et al., 2020; Harrington et al., 2018) (Fig. 7) is calculated for the late-summer discharge after completion of the snowmelt in the entire catchment. For our purpose, only one observation is relevant: Rainfall less than $9\ \mathrm{mm\ day^{-1}}$ in most cases (8/10) does not generate measurable

Table 2. Discharge measurements and observations in summer 2021.

Date (CEST time)	Stage[a] [mm]	Discharge[b] [L s^{-1}]	Method
Jun 30 (15:00–15:42)	89	27.7 ± 1.3	dilution gauging
Jul 9 (08:45–09:41)	88	27.6±1.6	dilution gauging
Jul 9 (09:46–10:33)	85	26.1±1.9	dilution gauging
Aug 10 (14:07–16:14)	67	4.7±0.05	dilution gauging
Aug 11 (10:37–13:45)	56	2.6±0.3	dilution gauging
Aug 23 (14:30)	22	3.6±0.4 L min^{-1}	volumetric method
Aug 24 (09:00)	17	3.1±0.3 L min^{-1}	volumetric method
Aug 24 (15:00)[c]	0.0	$\lessapprox 3$ L min^{-1}	field observation

[a] Stage relative to stage h_0. Analytical stage uncertainty of stage measurement: ±3 mm (Table 1). [b] Analytical discharge uncertainty: standard deviation from three simultaneous EC measurements; 10% of bucket measurement. [c] Spring discharge of $\lessapprox 3$ L min^{-1} seeps away between the spring and the gauging station (detection threshold), the logger pond falls dry (Fig. A2c).

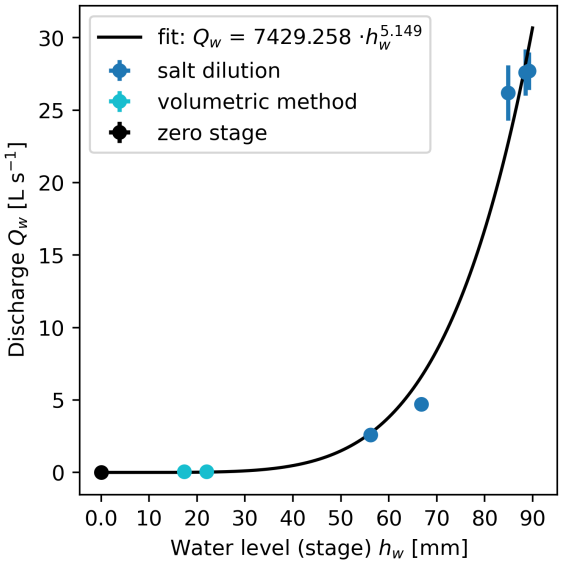

Figure 6. Stage-discharge relation as established with dilution gaugings and bucket measurements in summer 2021 (Table 2).

outflow at the gauging station (and this finding is independent of the quality of the stage–discharge relation). This agrees with field observations: Total spring discharge below the detection threshold of ~ 3 L min^{-1} seeps into the ground along its way from the rock-glacier springs to the gauging station located ∼50 m below the rock-glacier front ("not measurable baseflow" refers to maximal discharge of ~ 3 L min^{-1}). We observed rapid recession and drying out of the stilling pool at the gauging

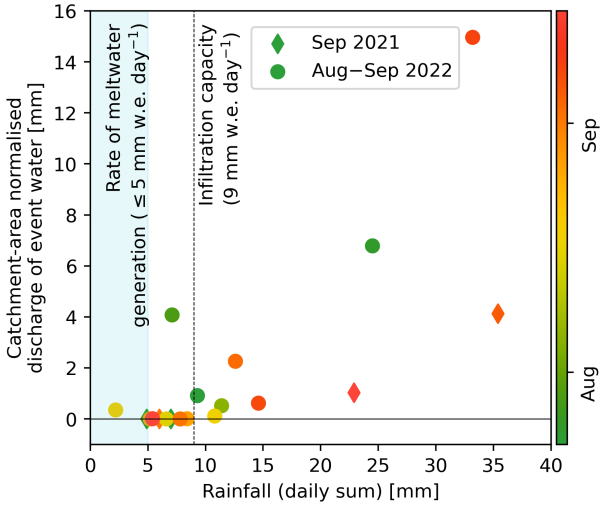

Figure 7. ~~Threshold analysis: Rainfall–runoff~~ Rainfall–streamflow relation (threshold analysis). Rainfall less than $9\ \mathrm{mm\ day^{-1}}$ ~~generally~~ does not ~~generate measurable~~ trigger surface outflow (infiltration capacity).

station after the discharge estimate in the morning of Aug 24, 2021 (Fig. A2c, Table 2). We so constrained the detection limit of $\sim 3\ \mathrm{L\ min^{-1}}$ using the bucket method (discharge too small for dilution gaugings).

4.2.2 Water electrical conductivity

EC of the outflow seasonally increases from $\sim 50\ \mu\mathrm{S\ cm^{-1}}$ to $\sim 150\ \mu\mathrm{S\ cm^{-1}}$ (Figs. 4, 5). Both main springs S_E and S_W show a qualitatively similar behaviour in both summers, despite different weather conditions: They transition from a snowmelt-regime (daily oscillations) to a rain-regime (rapid EC drop after onset of event discharge that stabilises). The lower-lying main spring S_E (2624 m asl.) has a lower EC than S_W (2626 m asl.) and appears more strongly buffered in terms of smaller daily oscillations and smaller seasonal shift. Still, the different weather conditions might show up in the late-season EC: The S_E–S_W EC difference is largest in autumn 2022 after the dry hydrological year 2021–2022 (SWE and summer rainfalls below average; Fig. 9), where the EC of S_W reaches $> 250\ \mu\mathrm{S\ cm^{-1}}$. EC is in general anti-correlated with discharge from seasonal down to hourly timescales suggesting dilution behaviour or longer water residence times: High EC at low discharge which is best seen during snowmelt, although the hourly EC evolution during late-summer rainfalls can be complex with a high-EC peak at the onset of event-water discharge (a timescale beyond the scope of this study). Point-measurements of the seep S^* show a strong enrichment up to $250{-}350\ \mu\mathrm{S\ cm^{-1}}$ of the autumn seep water. The supra-permafrost water co-evolves with the outflow. Notable are the persistent EC difference between two nearby sampling spots in the same rock-glacier furrow, one next to the 'ablation stake', the other next to thermistor TK4/5 (Fig. 2). Spatially varying EC speaks for channelised supra-permafrost flow as interpreted ~~by (Tenthorey and Gerber, 1991)'s tracer tests~~ from tracer tests by Tenthorey and Gerber (1991).

4.2.3 Stable isotope signature

We collected a total of 145 samples from different rock glacier springs and seeps (referred to as outflow), supra-permafrost water, snowpack, and rainwater: 2 samples in 2020, 57 samples collected in 2021, and 86 in 2022 (Tables B1–B5). All but a few rainfall samples are aligned on our local meteoric water line (LMWL) given by $\delta^2\mathrm{H} = 8.19\,\delta^{18}\mathrm{O} + 15.35‰$ ($R^2 = 0.9919$) (Fig. 8). The δ^{18}O–δ^2H relationship of the outflow samples is $\delta^2\mathrm{H} = 8.06\,\delta^{18}\mathrm{O} + 13.78‰$ ($R^2 = 0.9969$), with its slope of 8.1 similar to the local (LMWL, 8.2) and global meteoric water line (GMWL, 8.0), suggests that the source waters of the outflow have undergone little if any evaporation. This finding is consistent with a sparsely vegetated coarse-blocky landform with rapid infiltration (Williams et al., 2006; Krainer et al., 2007), and it is consistent with the measured specific humidity gradients in the Murtèl AL (Amschwand et al., 2024a, b): Moisture for evaporation is (generally) drawn from a rain-fed reservoir in the shallow AL, not from the supra-permafrost water in the deep AL. Moisture transport in the AL is generally downwards leading to condensation; upwards transport and evaporation from the deep AL occurs only episodically during droughts.

δ^{18}O of the outflow and supra-permafrost water showed an enrichment during the thaw season from $-16‰$, also measured in the spring snowpack, to $-10‰$, levelling off in late summer–autumn, and repeatedly interrupted by short excursions towards isotopically 'heavier' values of $-10‰$ that co-occur with the isotopically enriched rainfall (typically -10 to $-6‰$). δ^{18}O was overall higher in summer 2022 and reached the plateau phase sooner (by July), likely reflecting a proportionally smaller amount of snowmelt in the catchment after the snow-poor winter 2021–2022 (consistent with the EC pattern discused above). We do not observe the seasonal late-summer isotopic depletion reported by Stucki (1995). The two main springs S_E and S_W showed overall the same pattern, although S_W showed seasonally somewhat more extreme values, i.e. isotopically 'lighter' than S_E during snowmelt and 'heavier' in late summer. Discrepancies were smallest at high discharge during major rainfall periods. δ^{18}O of the supra-permafrost water was always close to the outflow δ^{18}O. Analogous to its EC, δ^{18}O value of the supra-permafrost water in the eastern stretch of the furrow is closer to the eastern main spring S_E, while the one in the western stretch of the furrow (next to the 'ablation stake') is often closer to spring S_W (if active). δ^{18}O of the rainwater varied considerably between $-13‰$ and $-6‰$, but were generally 'heavier' than all other sampled waters. The denser 2022 data set shows the well-known seasonal pattern with maximum enrichment in July–August. The pattern agreed with 1994–2022 long-term measurements from the nearby Global Network for Isotopes in Precipitation (GNIP) station in Pontresina (1724 m asl.) with $\delta^2\mathrm{H} = 8.095\,\delta^{18}\mathrm{O} + 9.53‰$ ($n = 321$, $R^2 = 0.9943$) (accessible via https://nucleus.iaea.org/wiser/ (IAEA/WMO, 2023)). δ^{18}O of the snowpack were from $-15‰$ to $-19‰$. Although snow δ^{18}O is sensitive to the sampling timing (Beria et al., 2018), its δ^{18}O does not exceed outflow δ^{18}O and is meaningful as a qualitative end member. The deuterium excess, in cases used as in indicator of multiple freeze-thaw cycles (Williams et al., 2006; Steig et al., 1998; Liaudat Trombotto et al., 2020; Munroe and Handwerger, 2023a, b), shows no clear seasonal trend (Fig. A4).

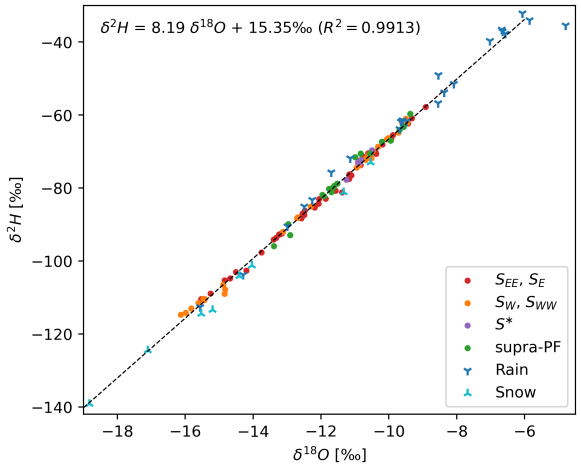

Figure 8. Dual isotope plot: δ^{18}O–δ^2H relationship of the outflow, supra-permafrost water, rainfall and snowpack.

4.3 Precipitation (snow and rain) and evaporation/sublimation

The plot-scale water balance (Fig. 9) refers to the point-wise (not areal) ablation observations, precipitation measurements and measurements for the AL energy budget. For the precipitation, we compare different measurements to obtain a spatially representative value (Sect. 4.1):

- We augment the on-site PERMA-XT rainfall data with MeteoSuisse data from the nearby station *Piz Corvatsch*. Rainfall from these stations reasonably agree (Fig. A3) except during a "dry window" in July 2022 where no on-site precipitation was recorded, but rock glacier outflow occurred whose timing coincides with the MeteoSuisse measurements (Fig. 5a, b). Rain-on-snow events are not considered. The two thaw season differed in terms of cumulative precipitation: $460-500$ mm in the cool-moist 2021, and ~ 320 mm in the hot–dry 2022.
- We use the SEB deviation during the snow melt period to obtain a representative SWE estimate ('SWE $\mathrm{dev_{SEB}}$' in Fig. 9). Comparison with the PERMOS snow height data and time-lapse images shows that the PERMA-XT snow depth measurement located on a wind-swept ridge grossly underestimates the average SWE on the rugged terrain (at least by a factor of 2.3). Total SWE was 915 mm in winter 2020–2021 (average), but only 600 mm in the snow-poor winter 2021–2022.

The evaporative water flux (Fig. 9) during the thaw season is ≤ 3 mm day^{-1}, amounting to 90 mm in the thaw season 2021 and 120 mm in 2022. Two remarks: First, we consider these values as upper bounds, since the SEB parameterisation in Amschwand et al. (2024a) likely tends to overestimate Q_{LE}. The additional aerodynamic resistance arising from the vapour transport within the coarse-blocky AL is unknown and ignored in Eq. 6, the more so, the deeper the moisture is drawn from, i.e. the most during dry spells. Second, thaw-season vapour transport in the coarse-blocky AL is generally downwards, the specific humidity gradient is aligned with the temperature gradient. It is not the supra-permafrost water that evaporates but meteoric

water from the uppermost AL, except during dry spells when the rain-fed moisture store in the shallow AL is exhausted ~~.~~ and the specific humidity gradient reverses (Amschwand et al., 2024a). In contrast to fine-grained material (or blocky material containing a fine-grained matrix), there is no upward transport of liquid water by capillary suction (Pérez, 1998).

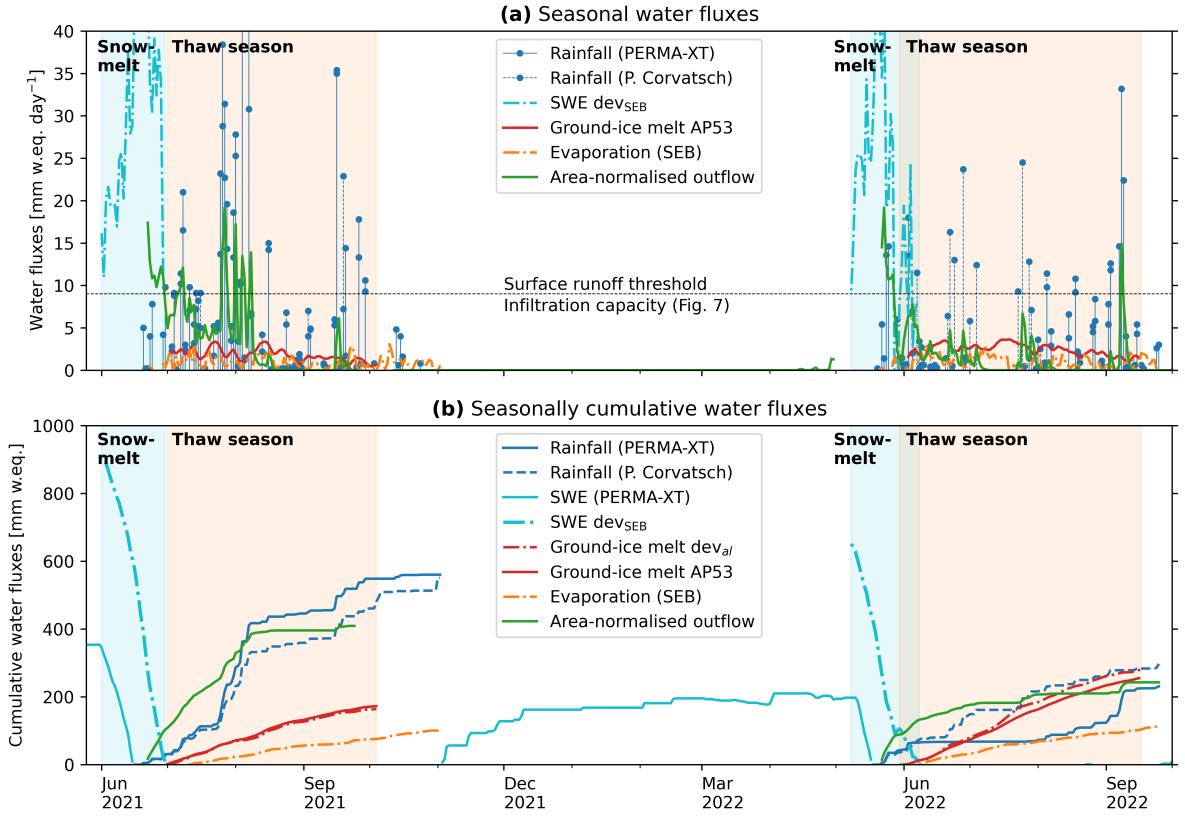

Figure 9. Murtèl water balance on a plot scale (daily average water fluxes in L m^{-2} or mm w.e.). **(a)** Seasonal water fluxes~~(surface runoff threshold in Fig. 7).~~ **(b)** Seasonally cumulative water fluxes.

4.4 ~~Ground-ice observations~~Ground ice storage changes from in-situ measurements

4.4.1 ~~Observations~~Point-scale observations in the AL

The ground ice is rarely accessible in coarse-blocky landforms. Here, we present one of the worldwide few (to the best of our knowledge) direct observations of the seasonal evolution of superimposed AL ice in rock glaciers, ice that forms each spring from refreezing of percolating melt water. The ground ice table as observed in a rock glacier furrow in the thaw seasons 2022 and 2023 underwent seasonal accumulation and melt of ~ 70 cm within the coarse-blocky AL, showing the seasonal build-up and melt of superimposed AL ice (Fig. 10). The seasonal release of water from melting ground ice in the coarse-blocky AL

is $200-300$ L m^{-2} over a thaw period of ~ 100 days, corresponding to 250 mm water equivalent (w.e.) or a melt rate of $1-4$ mm w.e. day^{-1} ($1-4$ kg m^{-2} day^{-1}).

Our observations indicate two different mechanism of ground ice accumulation: (1) refreezing of snowmelt onto cold blocks (analogous to the formation of basal ice at the ground–snow interface), and (2) blowing in of snow with subsequent metamorphosis to ice. The 'warming spikes', the AL energy budget and ice coatings/icicles (Herz, 2006) in sheltered cavities indicate the former, while the observation of ripe snow on top of the fresh ground ice in exposed cavities indicate the latter mechanism.

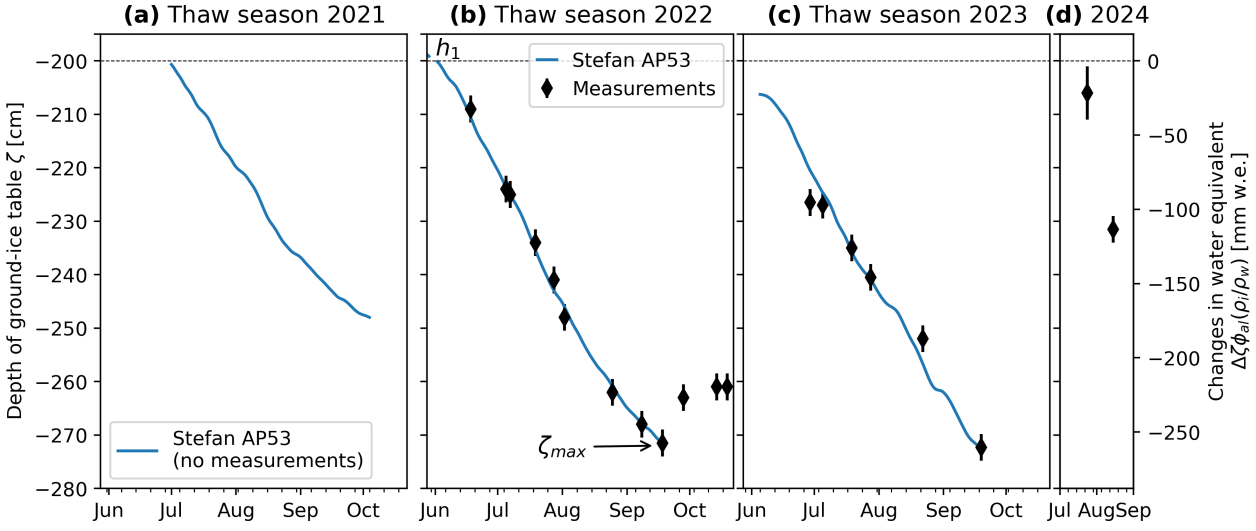

Figure 10. Observed and modelled vertical changes in the ground-ice table in thaw season **(a)** 2021 (modelled only), **(b)** 2022, **(c)** 2023, and **(d)** 2024 with seasonal accumulation and melt. Ice melt is simulated with the Stefan model (Eq. 12).

4.4.2 Stefan model and probabilistic uncertainty estimate

The Stefan model (Eq. 12) describes the observed lowering of the ground-ice table ('Stefan AP53' in Fig. 10) and relates it to a modelled ground ice melt Q_m. The effective thermal conductivity $k_{\text{eff}} = 3$ W m^{-1} K^{-1} is derived from the heat flux measurements (Amschwand et al., 2024b), the ice-poor AL overburden thickness $h_1 = 3$ m and ice content $f_1 = 0.01$ is calibrated with the 2022 ablation measurements. This 2022 parameter set also describes the 2023 ablation (Fig. 10c). The ablation observation-derived ground ice melt Q_m is shown in Fig. 9 ("Ground-ice melt AP53") alongside the AL energy-budget estimate (dev_{al}, Sect. 4.5).

Systematic ablation observations were not performed in summer 2021. The modelled 2021 ablation qualitatively agrees with observations insofar as a nearby thermistor (TK4/5) remained ice-embedded in summer 2021 and was only released in July 2022 (T_{al} in furrow shown in Figs. 4, 5).

~~Observed and modelled vertical changes in the ground-ice table in thaw season **(a)** 2021 (modelled only), **(b)** 2022, and **(c)** 2023 with seasonal accretion and ablation. Ablation is simulated with the Stefan model (Aldrich and Paynter (1953), Eq. 12).~~

4.4.3 ~~Probabilistic uncertainty estimate~~

Given the sparse and point-wise observations ~~and the only~~ on Murtèl and the few other published observations of seasonal ground ice melt in coarse-blocky landforms, we estimate the uncertainty with a probabilistic Monte Carlo approach. We make an educated guess of the value range of ~~those parameters that~~ the input parameters the Stefan melt parameterisation is most sensitive to (Eq. 12)~~is most sensitive on, ~~, namely the effective thermal conductivity k_{eff} ~~and the AL overburden thickness~~ ($2.0-3.5$ W m^{-1} K^{-1}, Fig. 11c, Amschwand et al. (2024b)), the AL overburden thickness h_1 ~~. Then, we estimate the range of expected depth of AL thaw ζ_{max} and total amount of generated meltwater for a given forcing $I(T_s)$, i.e. $Q_m := f\{I(T_s); k_{\text{eff}}, h_1\}$ with the function f given by Eq. 12. Based on Amschwand et al. (2024b)~~($1.5-4.0$ m, ~~k_{eff} is in the range of , and h_1 plausibly is (the prior distributions shown in~~ Fig. 11~~c, d). We assume that the ice content in the coarse-blocky AL beneath the ground-ice table is at saturation (neither air-filled voids nor excess ice), i.e. $f_2 = \phi_{al}$. Ten~~ d), and ice content f_2 ($0.2-0.8$, Fig. 11e), assuming that these parameters are independent from each other and to the ground surface temperature T_s. Fifty thousand model runs with the 2021 and 2022 T_s forcing to represent two contrasting thaw seasons yield the ~~posterior~~ outcome distribution of maximum thaw depth ζ_{max} and the total amount of ground ice melt (Fig. 11~~a, b~~, a). The expected amount of meltwater released in summer 2021 is ~~, and~~ $100-200$ mm w.e., and $150-350$ mm w.e. in summer 2022, with a large range of overlapping values of $150-250$ mm w.e.

4.5 Ground ~~heat fluxes~~ice storage changes from the AL energy budget

The ground heat flux estimates were gained in the instrumented cavity (Fig. 2). Downward heat flux during the thaw season is typically $10-15$ W m^{-2} as measured by the pyrgeometer Q_{CGR3} and the heat flux plate Q_{HFP} (Fig. 12a), amounting to $40-60$ MJ m^{-2} in cool–wet thaw season 2021, and $75-95$ MJ m^{-2} in hot–dry thaw season 2022 (Fig. 12b, c). The rain heat flux Q_{Pr} adds another $5-15$ MJ m^{-2}. The thaw-season cumulative heat uptake corresponds to less than 10% of the net surface radiation Q^* and is spent on warming the coarse-blocky AL (H_{al}^{θ} of $10-20$ MJ m^{-2}) and transmitted into the permafrost body beneath (Q_{PF} of $5-15$ MJ m^{-2}). The remaining energy dev_{al} of $52-94$ MJ m^{-2} corresponds to a potential ice melt of dev_{al}/L_m of $160-280$ mm w.e.. The date of snow melt-out and onset of thaw-season primarily explains the $\sim 40\%$ larger cumulative heat uptake in 2022 compared to 2021, and the heat uptake scales with the positive degree day sum (PDD). The direct ground-ice melt estimate Q_m from the ablation measurements (Fig. 10), here converted to a heat flux via Eq. 11, tends to be larger than dev_{al} ('AP53' in Fig. 12), but agrees well at the end of the thaw season, i.e., the estimates of the total ice melt during the thaw season are consistent. Conspicuous 'warming spikes', i.e. rapid AL warming and downward heat fluxes, occurred in winter–spring and are caused by non-conductive heat transfer. Certainly during the spring snowmelt beneath a thick, closed/insulating snow cover (Amschwand et al., 2024a), but possibly also during intra-winter melt events under a thin, discontinuous snow cover, these 'warming spikes' are caused by latent heat effects from refreezing of infiltrated snowmelt rather than air convection ('wind pumping', Humlum (1997); Juliussen and Humlum (2008)).

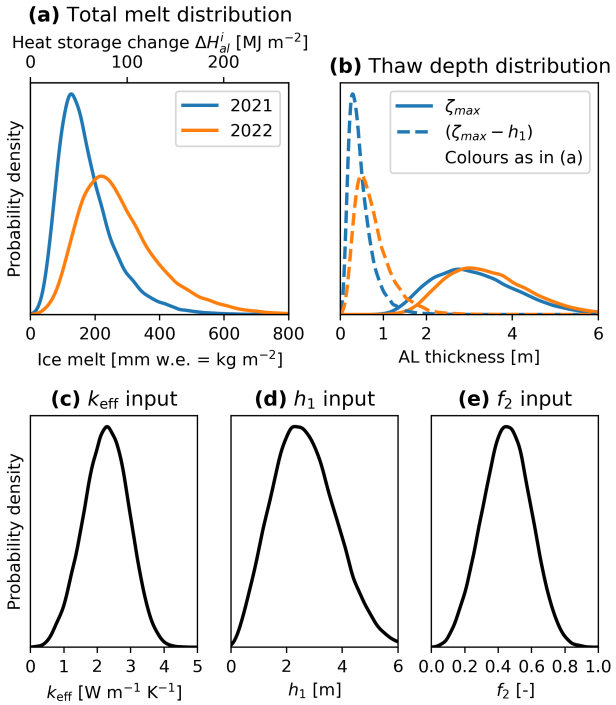

Figure 11. Probabilistic uncertainty estimate: Distribution of the thaw-season cumulative **(a)** ground-ice melt ~~Q_m~~ and **(b)** maximum thaw depth ~~$(\zeta_{max} - h_1)$ for~~ ζ_{max} calculated with the 2021 (wet-moist summer) and 2022 (hot–dry summer) T_s forcing (Eq. 12) ~~. The prior distribution~~ and a range of AL properties (k_{eff}, h_1, f_2) expressed by their input distributions **(c)** k_{eff} ~~and~~ , **(d)** h_1, and **(e)** f_2. Variables as in Fig. 3.

The impact of advective heat transfer by the rainwater increases with depth. In the AL, the warming effect of the rain heat flux is limited compared to the other heat fluxes (radiation, air convection) and overcompensated by the evaporative cooling effect and decreased insolation from the cloud cover during precipitation (Amschwand et al., 2024a). Also, the water content in the coarse material remains low and does not affect thermal properties. The effect of drip water on the heat flux plate measurement were not significant for daily to monthly energy budgets as shown by the good correlation to the pyrgeometer measurements (Amschwand et al., 2024b). However, in the permafrost body beneath the active layer, heat fluxes are smaller and the effects of rainwater (heat advection, changing thermal and mechanical properties) are not negligible, but hard to quantify with our measurements located in the uppermost 3 m.

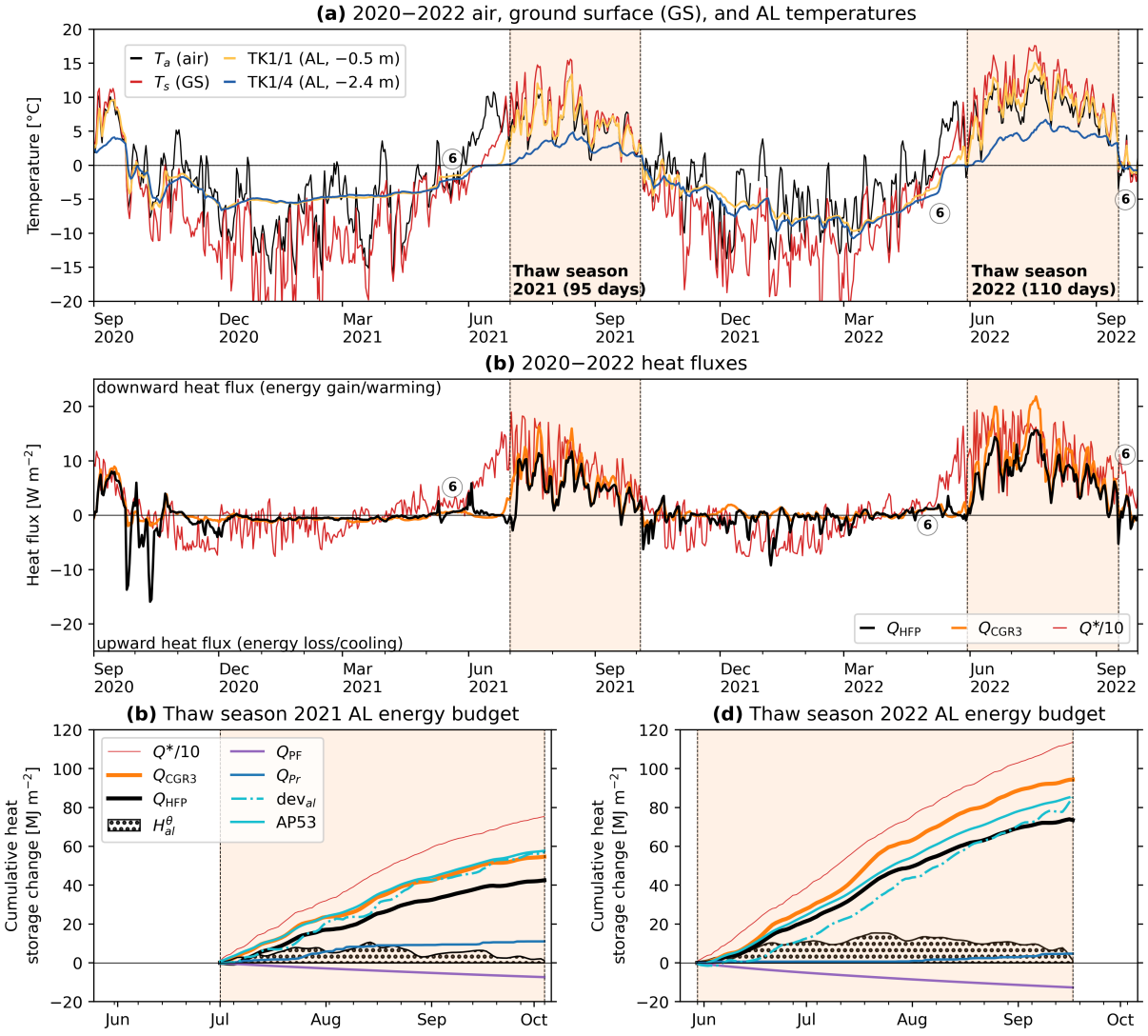

Figure 12. ~~(a)~~ Measured (a) temperatures and (b) heat fluxes in the coarse-blocky Murtèl AL. ~~(b–c)~~ 'Warming spikes' ⑥ indicate refreezing events. (c–d) Cumulative heat fluxes in the thaw season ~~(b)~~ (c) 2021 and ~~(c)~~ (d) 2022.

5 Discussion

5.1 Summary of hydro-chemical findings

Many of the hydrological and isotope results on Murtèl rock glacier are along the lines of past studies and are briefly summarised here. A consistent finding are ~~the~~ seasonal trends of discharge (decreasing), EC (increasing), and δ^{18}O (increasing) interrupted by precipitation-related excursions (spikes of high discharge, low EC, and 'heavier' δ^{18}O). This pattern is observed

in both summers 2021 and 2022, despite different weather conditions. The synthesis plot EC–δ^{18}O–Q–t (Fig. 13) plots the water samples of the Murtèl outflow as a function of EC, δ^{18}O, discharge Q, and timing t. The plot suggests three end-member components whose contribution varies throughout the summer, namely: (1) ~~Snow melt~~ Snowmelt (depleted isotopic composition, low EC, discharge high during weeks) dominant in early summer, (2) rainwater (enriched δ^{18}O, low EC, discharge episodically high after rainfall) dominant after snowmelt, and (3) groundwater baseflow ('reacted groundwater' of intermediate δ^{18}O, moderate–high EC, very low discharge) to which the system tends to in late summer–autumn (Aug–Oct; S_E then stagnant with discharge beneath the detection threshold of 3 L min^{-1}). The plot is based on samples from spring S_E, which is the last to fall dry and provided the most complete data set, extended into autumn 2022 by the ~~then-discovered~~ then discovered seep Q^*. The other main spring S_W is different enough from nearby S_E to hint at different water flow paths (a level of detail beyond the scope of this study), yet similar enough to provide a comparable picture. The Y-shape with three end members based on the three-component model using dual chemical (EC) and isotopic (δ^{18}O) tracers agrees with previous studies on intact rock glaciers (Krainer and Mostler, 2002; Harrington et al., 2018; Winkler et al., 2021a). Snowmelt and rock glacier core/permafrost ice (Haeberli, 1990) have a similar isotopic fingerprint ($\delta^{18}O$ of $-13‰$ to $-17‰$), i.e. using isotopes alone, the ground-ice meltwater is likely indistinguishable from snowmelt. Evidence for ground-ice melt is potentially available during dry phases after snowmelt is completed and its meltwater largely flushed out of the supra-permafrost aquifer, otherwise the signal is masked by snowmelt or diluted by rainwater. We suspect that the two strikingly depleted mid-July 2022 supra-permafrost samples collected during a dry spell–heat wave might most closely represent ground-ice melt (-12.9 and $-13.5‰$, Fig. 5). S_E surface outflow at that moment was so small that the carefully placed EC logger was not submerged (data gap), the outflow infiltrated on the spot. Also, the S_E outflow was diluted with enriched rainwater, as shown by the $\delta^{18}O$ of the manually sampled S_E water ($-11.4‰$). The presumed signal of ground-ice melt recorded in the active layer is already lost ~~at~~ in the rock-glacier spring, and associated surface outflow is very small ($\ll 3$ L min^{-1}).

~~The Murtèl hydrographs are 'flashy', responding rapidly (little delay) and strongly (high peak discharge) to daily oscillating snowmelt and rainfall events (Figs. 4, 5). The permafrost table is an aquitard that restricts (but not completely prevents) vertical water flow, the coarse-blocky AL has little water retention capacity (Geiger et al., 2014). Once snowmelt is completed, most rock glacier springs fall dry a few days after the last rainfalls. The outflow is primarily derived from snowmelt and precipitation. The~~

5.2 The Murtèl plot-scale water balance

With our comprehensive hydro-meteorological data set, we resolve the water fluxes and ice storage changes on Murtèl rock glacier ~~yields so little baseflow that it is hardly quantifiable () because the little water that emerges at the springs immediately infiltrates. How much meltwater is generated during hot–dry summer phases (Sect. **??**), how much is it compared to other water fluxes, and where does it flow to (~~on plot scale for the hydrological years 2021–2022 (Table 3; Fig. 9), except for groundwater (discussed in Sect. ~~**??**)?~~

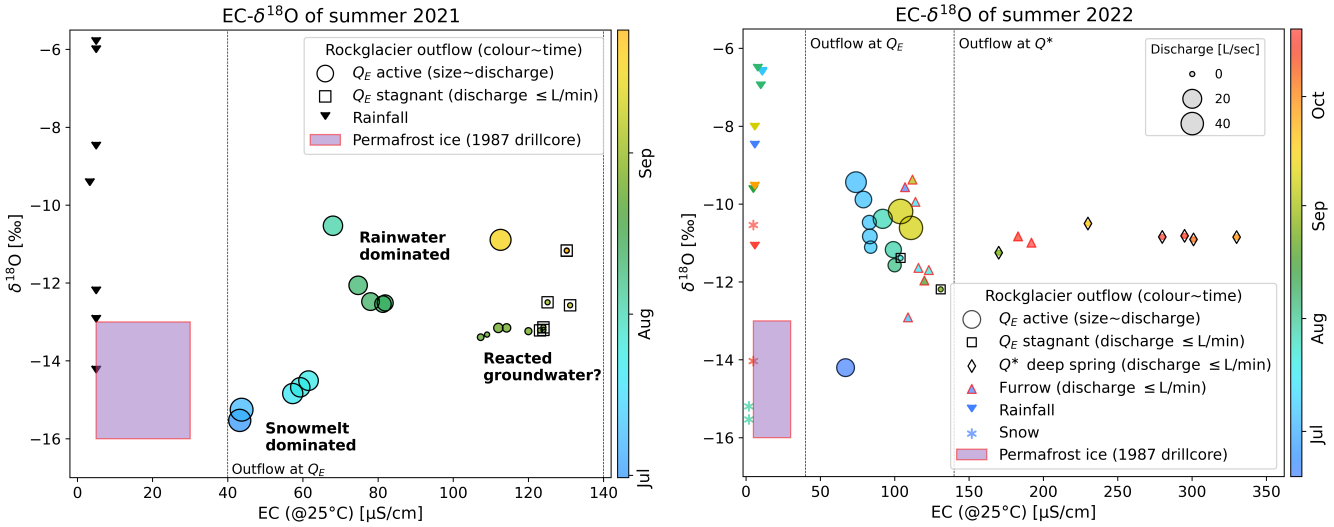

Figure 13. Synthesis: EC–δ^{18}O–Q–t plot showing the inter-annual variability of the two summers 2021 and 2022 with different weather (main spring S_E and seep S^*). Since EC increases throughout the summer, the EC axis can be roughly read as time axis (time/season is shown by the colours).~~Summer 2021: comparatively cool-wet. Surface snow patches in the talus remained all summer long, net accumulation of ground ice (freezing in of sensors; only liberated again in Aug 2022). Summer 2022: hot–dry, net loss of ground ice. No clear isotopic signal from ground ice recorded in the outflow, except perhaps in the supra-permafrost water sampled in the furrow in July.~~

5.3 ~~Ground-ice melt at two time scales~~

5.2.1 ~~In-situ observations of seasonal ground ice melt~~

~~The ground ice is rarely accessible in coarse-blocky landforms. Here, we present one of the worldwide few (to the best of our knowledge) direct observationsof the seasonal evolution of superimposed AL ice in rock glaciers, ice that forms each spring from refreezing of percolating melt water. Importantly, the ground ice melt inferred from the~~ 5.4). The plot scale refers to the point-wise (not areal) ablation observations, precipitation gauging and measurements for the AL energy budget ~~deviation dev_{al} reasonably agrees with the (also point-wise) ablation observation Q_m, at least towards the end of the thaw season. Reasons for the discrepancy likely arise from the differences in the micro-topographic setting, debris texture, and AL thickness of the two measurement points: heat flux estimates dev_{al} beneath a ridge, ablation observations Q_m in a furrow. This implies a different SEB, different temperature gradients, and different sensible heat storage H^{θ}_{al}.~~

~~The superimposed AL ice constitutes a hydrological buffer that protracts the snowmelt into summer, since the AL ice is refrozen winter precipitation temporarily immobilised as ground ice. The seasonal water storage as superimposed ice is one mechanism that makes rock glaciers "*streamflow regulators*" (Hayashi, 2020; Halla et al., 2021; Reato et al., 2022; Del Siro et al., 2023) , in addition to the storage of liquid water ('dynamic storage') (Winkler et al., 2016b; Wagner et al., 2021b, a; Bearzot et al., 2023)~~ .

Seasonal ice accumulation has been observed in other landforms such as a permafrost-underlain scree slope (Rist and Phillips, 2005; Rist, or block fields (Sawada et al., 2003; Yoshikawa et al., 2023; Marchenko et al., 2012). Our observations agrees with Marchenko et al. (2012 's observation in the Northern Tien Shan, where the observed accumulation–melt of ground ice seasonally stored a substantial amount ()of the snowpack in that dry mountain region. Our measurements also agree with Haeberli (1975)'s winter-time AL ice content estimate of . The formation of seasonal ground ice within the AL has long been inferred from ground thermal measurements (Hanson and Hoelzle, 2003, 2004), AL energy budgets (Scherler et al., 2014), on the rock glacier. The rock glacier outflow is normalised by the catchment area (30 ha) inferred from the topography, i.e. the rock glacier and the surrounding talus and rock faces. The thaw-season water budgets are closed, but annual water budgets are not. During the thaw season after near-completion of the snowmelt (Jul–Sep 2021 and geophysical measurements (Schneider et al., 2013) on Murtèl and elsewhere (Haeberli, 1975; Rist and Phillips, 2005; Bearzot et al., 2023). The release of latent heat leads to a sudden, rapid AL warming into the zero curtain (Hanson and Hoelzle, 2004). Finally, unstable water isotopes (tritium ^{3}H) can provide evidence for modern ice accumulation ('young ice'): Blumstengel and Harris (1988) found elevated tritium contents in the uppermost of the Slims River lobate rock glacier (Yukon, Canada) . Jun–Sep 2022), surface stream discharge equals available precipitation (i.e., precipitation minus evaporation) and there is no sustained baseflow, suggesting that liquid water storage changes are negligible (within the precision of the water budget) and that little rainwater infiltrates (Eq. 1) in Arnoux et al., 2020) (these assumptions are revisited in Sect. 5.4). Discharge during the snowmelt period (Apr–Jun 2021 and Apr–May 2022) and consequently the annual discharge are strongly underestimated because discharge before snow melt-out of the forefield is not gauged.

In our warming climate, the seasonal AL ice turnover is superimposed on the melt of permafrost ice. The Murtèl rock glacier is slowly degrading (AL thickening (Noetzli et al., 2019)) and also releasing meltwater from the 'old' permafrost core. Neither our ablation observations nor our energy balance measurements that span only two years can separate melt from superimposed 'young' AL ice from melt of 'old' permafrost ice. Satellite or terrestrial multi-sensoral surveys (TLS data, photogrammetric imagery and geodetic measurements) on Murtèl revealed small volume losses that were attributed to ground ice melt in over-saturated permafrost (Kääb et al., 1998; Müller et al., 2014).Kääb et al. (1998) reported or roughly 5 – 10 times less than the seasonal AL ice melt (massive ice beneath permafrost table, i.e. volume loss ≈ ice loss).

5.2.1 Kinematic/geodetic mass balances

Only few kinematic remote sensing studies achieved the temporal resolution and accuracy needed to resolve inter-annual/seasonal ground ice storage changes. An example is Halla et al. (2021) who used airborne UAV photogrammetry jointly with geophysical investigations (ERT, SRT) to relate the surface changes to changes in material composition. They found inter-annual ice storage changes on the pebbly (not coarse-blocky) *Dos Lenguas* rock glacier (Dry Andes of Argentina) of (of the annual precipitation) and () , i.e. releasing and buffering a substantial fraction of the annual precipitation.

The (surface) mass balance (SMB) of a rock glacier fundamentally differs to that of glaciers (Arenson et al., 2022): accumulation/ablation is within the AL (rather than at the surface), separated temporally rather than spatially (there are no accumulation or ablation areas), and there are no short-term feedbacks between SMB and landform dynamics (creep rates). The seasonal ice turnover in

the AL ('internal accumulation/ablation' in glaciological terms) is missed by long-term (decadal) studies like Cusicanqui et al. (2021) that estimated the geodetic mass balanceof the *Laurichard* rock glacier. It is unclear for such coarse-blocky material as on MurtEC and stable isotope signature of the Murtèl whether seasonal ice accumulation/melt results in heave/subsidence large enough to be separated from dynamic effects (compressive/extensional creep or water-related seasonal acceleration/deceleration (Cicoira et al., 2019; Müller et al., 2016)) l surface outflow suggest that there must be some liquid water storage in the catchment which is however too small to sustain surface baseflow over more than a few days and is not resolved by the water balance. Evidence for aquifers come from the seasonal increase in in EC (a proxy for mineralisation) and the δ^{18}O of the outflow which is buffered to the rainfall δ^{18}O (Figs. 4 the pore space offers ample storage possibly without forming excess ice and without deforming the debris matrix.

5.2.1 Energy flux-derived ground ice melt estimates

Our measurement results agree with Scherler et al. (2014) who hypothesized a seasonal ice melt of in the period June–September or melt rates corresponding to on Murtèl. These are modelling results based on the deviation of an AL energy budget conceptually similar to our work (Amschwand et al., 2024b), but run with sparser input measurements (PERMOS data only, namely no pyrgeometer and heat flux plate measurements in the AL).

Pruessner et al. (2022) modelled a monthly average permafrost runoff of up to which agrees with our estimates (converted to rock-glacier underlain area to make their numbers comparable with ours).They defined permafrost runoff as the amount of ground ice lost, i.e. they neither differentiate between AL ice and ground ice in the permafrost rock-glacier core, nor do they show the amount of refreezing in the AL.

5.3 Book-keeping of water fluxes and ice stores

5.2.1 Plot scale

The water fluxes and ice stores on Murtèl rock glacier on a plot scale (fluxes per) are summarised in Table 3 (cf. 5, 13). In particular, the late-summer water sampled in the 'deep seep' S^* (Fig. 2) which shows a stable δ^{18}O value of -10.9 ± 0.2 ‰ (Fig. 5d), intermediate between depleted snowmelt (around -15‰) and enriched summer rainfall (around -8‰), might hint at a sub-permafrost aquifer in the overdeepened bedrock depression (Fig. 9) . As already mentioned, the plot scale refers to the point-wise (not areal) ablation observations, precipitation measurements and measurements for the AL energy budget. The rock-glacier outflow is normalised by the catchment area. 14b) (Arenson et al., 2010) recharged from both snowmelt (or icemelt) and rainfall and a water residence time of several months.

We The single largest contribution comes from the snowmelt which amounts to 65 % of the total annual precipitation released in a few weeks during spring freshet (Table 3; Figs. 4, 5). This is typical for seasonally snow-covered mountain sites. Here, we focus on the contribution of the ground-ice melt compared to precipitation and outflow of the plot-scale water balance (Table 3, Fig. 9). Meltwater from ground ice constituted of the seasonal precipitation and of the surface outflow First, in the hot–dry summer year 2022 , and roughly of the 2022 annual outflow and precipitation. On the one hand, these seasonal meltwater

Table 3. Murtèl rock glacier plot-scale water balance in terms of cumulative water fluxes for the respective seasons: winter (Oct–Mar), spring snow melt until end surface zero curtain (May–Jun/Jul), thaw season/summer–autumn (Jun/Jul–Sep), and annual.

Cumulative water flux [~~, mm w.e.~~mm w.e.]	Hydrological year 2020–2021 Oct–Mar	Apr–Jun	Jul–Sep	*annual*	Hydrological year 2 Oct–Mar	Apr–M
SWE ($\mathrm{dev_{SEB}}$)	—	915	~ 0[e] [f]	*915*	—	596
Rainfall (on-site/corrected)	23[g]	0[f] [g]	462/502	*485/525*	0[g]	0[f] [g]
Evaporation and sublimation (SEB)	33	24	<89[g] [h]	*<146*	74	17
Available precipitation[a]			373/413	*1254/1294*		
Watershed area-normalised outflow[b]	39	>140[i]	415	*>595*	0	>129[i]
Ground-ice melt[b] [c]			167	*167*		
~~energy~~ Energy budget dev_{al}/'ablation stake' Q_m	0	0	167/167		0	0
~~Watershed area-normalised outflow[c]~~ *Ratios*						
Water balance closure[d]	~~67~~	~~239[h]~~	~~706~~ 100 %	*~~1012~~ 46 %*	~~0~~	~~220[h]~~
~~*Ratios*Surface outflow / available precipitation[d]~~ Snowpack retention ratio[e]				*~~78~~18%*		
Ground ice melt / ~~rainfall + SWE~~ total precipitation			33%	*~~13~~12%*		
Ground ice melt / ~~surface outflow~~ available precipitation			~~24~~40%	*~~17~~13%*		
Ground ice melt / surface outflow			40%			

[a] Available precipitation is rainfall and snowmelt (winter precipitation) minus evaporation/sublimation. [b] Total surface outflow measured at gauging station (Fig. 2), normalized by catchment area of average of two independent estimates of ground ice storage changes (cf. Table 3 in Amschwand et al. (2024b)). [d] Surface outflow / available precipitation. Deviation arising from infiltration and mea gauged snowmelt, water level–discharge relation, and uncertain catchment delineation/area). [e] Amount of accreted ground ice (that is derived from the snowpack) divided by the SWE. [f] Surviving s sustained some snowmelt throughout summer 2021, but it was too small to produce measurable surface outflow. [g] Rain-on-snow events not quantifiable by our measurement setup. [h] Evaporation lik when water-level sensor beneath snow cover; i.e. no measurable discharge as long as the rock glacier field is snow covered.

~~contributions are substantial. Freezing and thawing in the~~ with a snow-poor winter, accumulation and melt in coarse-blocky AL seasonally ~~stores and releases up to of the yearly precipitation in~~ stored and released up to 44% of the winter precipitation (SWE; "snowpack retention ratio" in Table 3) and 28% of the annual precipitation (37 % of the available precipitation if evaporation/sublimation is subtracted) in form of temporarily fixed ground ice. ~~On the other hand, of the surface outflow is precipitation–derived even in a~~ In the cool–moist year 2021 and a winter with average snowfall, the relative importance of the ground-ice melt was smaller: 18 % of SWE, 12 % of the yearly precipitation (13 % of the available precipitation). All these components show a strong, weather-sensitive inter-annual variability. Second, negative ground ice storage changes amount to 127% of the surface outflow during the hot–dry ~~summer as 2022 with strong ground ice melt and little rainfall, and that on~~

~~the rock glacier itself (plot scale). These are rough estimates limited by the accuracy of the stage–discharge relation (Fig. 6). Nonetheless, with increasing catchment scale where the relative permafrost-underlain area decreases, the contribution from ground-ice melt becomes smaller. Importantly, most of the melting AL iceis refrozen winter precipitation , and not derived~~ summer 2022 (40 % in the cool, rainy summer 2021), but the meltwater does not appear as surface outflow: The streambed dries out in phases without precipitation (Sect. 5.4). However, even if all of the icemelt reached the surface springs (if the permafrost body were impervious), meltwater exposed to the atmosphere outside of the protecting AL would have a local importance only. Evaporation rates are similarly high as ice melt rates, the meltwater would practically evaporate on the spot (Fig. 9).

5.3 Substantial ground ice turnover in the AL, little meltwater from degrading permafrost

Most (90−100 %) of the generated (ice) meltwater is derived from winter precipitation accumulated in the AL (active-layer thaw), not from the ice-rich, but quasi-inert permafrost body (~~rock-glacier core) .~~ rock glacier core) beneath.

~~A conundrum emerged: The~~

5.3.1 Seasonal ice turnover in the AL

We obtained consistent estimates of seasonal ground ice melt from the AL energy budget (dev_{al}, Fig. 12) and ablation observations (Q_m, Figs. 9, 10), although we estimated the AL energy budget dev_{al} beneath a broad ridge and made ablation observations Q_m in a narrow furrow. End-of-thaw season values (cumulative ice melt) are 160 mm w.e. in the thaw season 2021, and 260 mm w.e. in 2022 (Table 3). Although our point-wise observations cannot exclude some differential accumulation/ablation in furrows and ridges (a micro-topographic variability mentioned by Kääb et al. (1998) and Halla et al. (2021)), the agreement suggests that our estimates of end-of-thaw season ice storage changes are fairly representative over the landform and within an uncertainty of ±50 % (Fig. 11). Smaller discrepancies in the sub-seasonal evolution of Q_m and ~~ground-ice meltobservations on the one hand, and the hydro-chemical measurements on the other hand gave seemingly contradicting ideas about the ground-ice melt. As noted above, we neither observed streamflow during hot–dry weather spells (insignificant baseflow of , Figs. 5b, 9)~~dev_{al} (Fig. 12) likely arise from differences in the micro-topographic setting, duration of snow cover, debris texture, and AL thickness at the two measurement points. Our estimates of the icemelt agree with prior studies on Murtèl by Scherler et al. (2014) and Pruessner et al. (2022).

The 'ablation stake' measurements show no local AL thickening for the years 2021–2023 (Fig. 10). The ground ice that melted during the thaw season was regenerated by refreezing and accumulation in the following winter and spring. In the exceptionally cool–wet summer 2021 with late snow melt-out (begin of thaw season in July), even net accumulation occurred at least locally in the rock-glacier furrow (frozen thermistor TK4/5; Fig. 4a). The surviving snow patches (Fig. 2) tentatively support the net positive mass balance observed in 2021, but cannot provide conclusive evidence on a landform scale.

A net increase in below-ground ice content during snowmelt, i.e. the conversion of snowmelt to ground ice, as observed on Murtèl is arguably most efficient on well-drained coarse-blocky permafrost landforms. Such terrain, abundant in periglacial high-mountain areas, features a distinct seasonal chain of coupled heat and water–ice transformations co-controlled by the snow

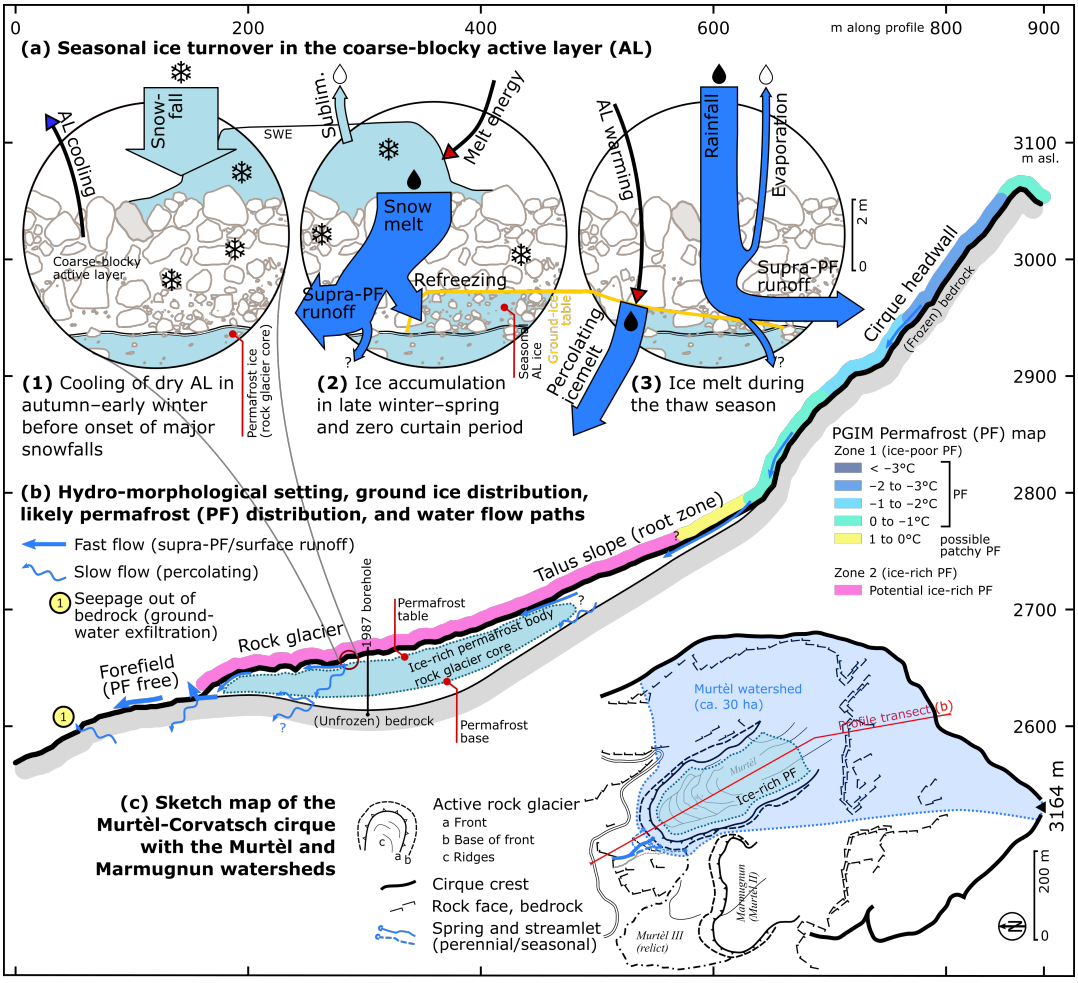

Figure 14. Conceptual model of the near-surface hydrogeology of the periglacial Murtèl watershed. **(a)** Seasonal thermo-hydrological processes in the Murtèl coarse-blocky AL. Water fluxes (thick arrows) for the 2021/22 hydrological year (arrows to scale, Table 3). **(b)** Profile through the Murtèl watershed. Rock glacier structure drawn after Vonder Mühll (1993); PGIM permafrost distribution after Kenner et al. (2019). **(c)** Sketch map of the Murtèl watershed in its cirque.

cover (illustrated in Fig. 14a (1)–(3)). In autumn–early winter, the permeable AL contains little water to freeze, enabling a rapid and pervasive ground cooling to large depths before the onset of an insulating snowcover (Renette et al., 2023; Luetschg et al., 2008) (Fig. 14a (1)). In late winter and during spring snowmelt, whenever a warm and melting snowpack releases water into the subfreezing AL, the large cold content (sensible heat) is partly transformed into the build-up of new ground ice (latent heat) (Fig. 14a (2); 'warming spikes' in Fig. 12). The timing of ground ice build-up, ~~nor retrieved a clear isotopic signal from the ground-ice melt (Figs. 5d, 13b) . The observed surface outflow of~~ *from snowmelt in spring* rather than by freezing soil water in autumn–early winter (Mendoza López et al., 2024), is distinct from fine-grained material with a larger water retention capacity

(Renette et al., 2023) and is observed in other coarse-blocky permafrost landforms (e.g., Sawada et al., 2003; Rist and Phillips, 2005; Marc
. From a hydraulic perspective, the large and permeable pores provide ample storage space for the infiltrating snowmelt to
refreeze and in-blown snow to be trapped *at depth* without blocking the water infiltration/percolation pathways by the newly
formed ground ice (Woo, 2012) or basal ice at the ground–snow interface (Phillips et al., 2017) (but see also Scherler et al. (2010)
). During the thaw season, the melting AL ice largely (~ 80 %) absorbs the ground heat flux (Fig. 14a (3); Amschwand et al. (2024b)
). Numerical simulations by Renette et al. (2023) of the coupled heat and water/ice balance apply to Murtèl~~, whose ice-underlain
area is , was not more than a few in hot–dry periods, at least $10\times$ less than expected by extrapolating the melt rates over the
ice-underlain rock-glacier area. Where does the meltwater go? Because we obtained consistent estimates of~~ . They showed that
alone this interplay between the subsurface water/ice balance and ground freezing/thawing leads to negative ground thermal
anomalies (up to $2.2\ ^{\circ}\mathrm{C}$ in their modelling scenarios), i.e. even without air convection which is an additional efficient cooling
mechanism common for such terrain (Amschwand et al., 2024b; Wicky and Hauck, 2020; Wicky et al., 2024; Amschwand et al., 2024b)
. The regeneration of ground ice in the AL partly explains the climate resilience of coarse-blocky landforms (Scherler et al., 2013; Amschwa
. If the lost ground ice is not regenerated, the permafrost landform is preconditioned towards irreversible degradation (Hilbich et al., 2008; H
. Finally, permafrost conditions might be required in seasonally snow-covered terrain to keep winter ground temperatures
well below the freezing point until the spring snowmelt, depending on the timing and insulation of the snow cover. This
is shown by the ~~ground ice melt from the AL energy budget (dev_{at},~~ 'bottom temperature of snow cover' (BTS temperatures)
(Haeberli, 1973, 1975; Haeberli and Patzelt, 1982), a winter-equilibrium ground surface temperature attained beneath a closed/insulating
snow cover, that are near or above the freezing point in permafrost-free (seasonally frozen) Alpine terrain. To sum up, ground
ice accumulation by snowmelt refreezing relies on strong (preferentially convective) ground cooling and water supply into the
subfreezing AL, in turn sensitive to debris texture, thermo-hydraulic properties, and weather/snow conditions.

5.3.2 Melt of permafrost ice in the rock glacier core

In our warming climate, net accumulation as possibly in 2021 is the exception. Murtèl rock glacier is slowly degrading (AL
thickening (Noetzli et al., 2019)) and must be on multi-year average releasing meltwater from the 'old' permafrost core. Neither
our ablation observations nor our energy balance measurements that span only two years can reliably separate melt from
superimposed 'young' AL ice from melt of 'old' permafrost ice (and a possible 'transient layer' in between, Mendoza López et al. (2024)
). Inter-annual to decadal surface subsidence estimates from kinematic surveys (Barsch and Hell, 1975; Kääb et al., 1998; Müller et al., 201
and vertical borehole deformation (Arenson et al., 2002) revealed slow subsidence attributed to ground ice melt in the over-saturated
permafrost body. Kääb et al. (1998) report $2{-}5\ \mathrm{cm\ yr^{-1}}$ for the period 1987–1996. The most recent 2022–2023 geodetic
measurements (I. Gärtner-Roer, pers. comm.) yield $1\ \mathrm{cm\ yr^{-1}}$ in the mid–frontal parts of the rock glacier (no significant
net change in the surface elevation: the ice melt compensates compressive thickening; subsidence $\approx$ ice loss in massive ice).
The amount of meltwater released from the permafrost core is an order of magnitude smaller than the seasonal ice turnover
in the AL and negligible compared to precipitation, surface outflow, and even evaporation, agreeing with previous studies
(Bearzot et al., 2023).

5.4 Near-surface hydrology of the periglacial Murtèl watershed: Meteoric water runs off, icemelt infiltrates

The periglacial Murtèl watershed underlain by either ice-rich permafrost (active rock glacier and talus slope) or steep bedrock (Fig. ~~12) and the ablation observations (Q_m,~~ 14b, c) has a small storage and retention capacity for liquid water (cf. Geiger et al., 2014; Rogg
. The thaw-season hydrograph is flashy, responding rapidly (little delay) and strongly (high peak discharge) to daily oscillating snowmelt and rainfall events (Figs. ~~9, Fig. 10)within (~~4, 5). There is no sustained baseflow during winter and summer droughts ($\lessapprox 3$ L min^{-1} for a 30 ha watershed). Once snowmelt is completed, the rock glacier springs fall dry a few days after the last rainfalls. Surface outflow is derived from snowmelt and precipitation (meteoric water, Fig. ~~11), we hypothesize that the ground ice meltwater preferentially infiltrates and does not generate surface runoff . This hypothesis is supported by the rainfall-runoff relation (~~14a (2)–(3)), as shown by the isotopic signature and the thaw-season water balance (Table 3). Importantly, we could neither observe surface runoff from ground-ice melt nor retrieve a clear isotopic signal in the rock-glacier springs during hot–dry weather spells (Figs. 5d, 13b), although extrapolating the melt rates over the ice-underlain rock-glacier area ($\sim 150 \times 300$ m^2 à 3 mm w.e. day^{-1}) would yield ~ 100 L min^{-1}. Whereas snowmelt and rainwater leave the watershed largely as supra-permafrost runoff (some unknown fraction does infiltrate; Fig. ~~7) that suggests a rainfall threshold of required to trigger measurable surface outflow: *Slowly generated ice melt preferentially infiltrates, whereas comparatively intense rainfall mostly exceeds the infiltration capacity and runs off as streamflow.*~~ 14a (2)–(3)), no traces of the ice melt are visible (except perhaps on the rock glacier itself, Fig. 13b).

Whereas comparatively intense rainfall that exceeds the infiltration capacity largely runs off as supra-permafrost water and generates surface streamflow, slowly generated ice melt (limited by the small ground heat flux Q_G) fully infiltrates into the permafrost body. In fact, ~~the~~ observed and calculated ground-ice melt rates of $1-4$ mm w.e. day^{-1} ~~or is (~~$\sim 10^{-8}$ m s^{-1}; Fig. 9) are beneath the surface runoff threshold or infiltration capacity of 9 mm day^{-1} indicated by the rainfall–streamflow relation (Fig. ~~9). The meltwater might be evacuated via subsurface pathways as shown by the 'deep seep' S^* or the tracer~~ 7). Tracer tests by Tenthorey and Gerber (1991) ~~that~~ proved a sub-surface hydraulic connection ~~in the fractured bedrock~~ to the front of the relict Murtèl III rock glacier (~~Fig~~Figs. 2~~). Furthermore,~~ , A1). Also the Murtèl drilling campaigns showed that neither the permafrost body nor the unfrozen bedrock beneath are impermeable: ~~Intra-~~ Supra-, intra- and sub-permafrost water flow ~~is reported in Vonder Mühll and Haeberli (1990); Vonder Mühll (1992); Arenson et al. (2002, 2010) and Springman et al. (2012) . Speck (1994) estimated a hydraulic conductivity of for the ice-rich rock-glacier core and for the fractured crystalline bedrock as outcropping in the study area; i.e. also the least permeable material of the rock-glacier stratigraphy could accommodate the meltwater flow. Seasonal groundwater circulation in a talik in bedrock at beneath the rock glacier was inferred from seasonally fluctuating borehole temperatures at around (Vonder Mühll and Haeberli, 1990; Vonder Mühll, 1992). Note that the terrain in front of the Murtèl rock glacier (forefield) is permafrost-free (Vonder Mühll and Haeberli, 1990). Finally, poor recovery of dye tracer as reported by Mari et al. (2013); Bearzot et al. (2023) (on other rock glaciers) also supports this hypothesis, and~~ in conduit-like taliks, water inflow, and air loss during drilling operations are reported in Vonder Mühll and Haeberli (1990); Vonder Mühll (19 and Arenson et al. (2002, 2010). Also Halla et al. (2021) estimated that $58-89\%$ of the seasonal meltwater left the *Dos Lenguas*

rock glacier hydrologic system via groundwater pathways. ~~The cold groundwater might sustain 'icy seeps' that are climate refugia for cold-adapted species (Hotaling et al., 2019; Tronstad et al., 2020; Brighenti et al., 2021).~~

5.4.1 ~~Landform scale and ground-ice accumulation~~

~~On landform scale, the probabilistic uncertainty estimate (Fig. 11) gives an idea of the expected variability of meltwater generation Q_m over a coarse-blocky permafrost landform with spatially varying debris texture and initial depth to the ground-ice table h_1 (assuming that the two prior distributions are uncorrelated), $Q_m := f\{I(T_s); k_{\text{eff}}, h_1\}$ (Eq. 12). The two parameters (k_{eff}, h_1) control the ground ice melt as much as the thaw-season weather forcing via $I(T_s)$. The k_{eff} uncertainty reflects debris texture and the AL heat transfer processes (discussed in Amschwand et al. (2024b)) . Here, we discuss the uncertainty of the ice-poor ALoverburden h_1.~~

~~h_1, the initial depth of the ground-ice table~~ Cicoira et al. (2019) and Kenner et al. (2020) inferred rapid percolation of snowmelt through the permafrost body to the basal shear zone based on the widely observed spring-time rock glacier acceleration immediately after onset of the snowmelt.

The Murtèl periglacial watershed is not a 'teflon basin' (cf. Williams et al., 2015). In mountain permafrost, the ground ice table (permafrost table) is a semi-impervious aquitard that restricts (but not completely prevents) vertical water flow. Mountain permafrost is inherently discontinuous and characterized by a mosaic distribution of perennially and seasonally cryotic ground with varying ground temperatures and water/ice content that reflects the variable micro-climatic conditions in the complex terrain (illustrated in Fig. 14b). Zones of "warm" permafrost (containing unfrozen water) and taliks enhance the hydraulic permeability (connectivity) of discontinuous permafrost and allow for water movement and groundwater recharge/discharge (Cheng and Jin, 2012; Luethi et al., 2017; Wagner et al., 2020; Arenson et al., 2022; Bearzot et al., 2023). We propose that icemelt in the abundant coarse-blocky permafrost landforms – intact rock glaciers, frozen talus slopes, block fields – contribute to groundwater recharge despite low melt rates, because melt rates are steadily sustained over the entire thaw season (insulating effect of the AL), the infiltration efficiency is high, and the infiltrating icemelt is additional to the infiltrating snowmelt and rainwater (Fig. ~~3), reflects to what extent the coarse-blocky AL is refilled with ice in winter and spring. Coarse-blocky permafrost landforms can potentially refreeze a lot of water in the AL and offer favourable conditions for a substantial seasonal ground-ice turnover. First, strong winter-time heat extraction from the AL is favoured by convective heat transfer (air ventilation) within the AL and through a semi-closed snow cover, which in turn relies on a permeable, coarse-blocky AL and a snow cover that is 'thin' compared to the terrain roughness. Second, the pore space is large enough to accommodate the ground ice while preventing the formation of impermeable ice lenses that would block further infiltration/percolation (Woo, 2012). The potential storage space $\phi_{al} h_{al}$ is large in a porous and thick AL. Coarse-blocky AL can *potentially* refreeze a lot of water — but water drains rapidly within hours–days~~14a). ~~In a sloped and well-drained~~ As glaciers retreat, permafrost thaws and snowpacks diminish in the rapidly deglacierizing mountains, groundwater as the most climatically resilient freshwater resource will be increasingly important to sustain baseflow in the headwaters of rivers originating in mountain ranges (Hayashi, 2020) . Additionally, the cold groundwater might sustain 'icy seeps' that are climate refugia for cold-adapted aquatic organisms (Hotaling et al., 2019; Tronstad et al., 2020; Brighenti et al., 2019a, b, 2021; Bearzot et al., 2023). Since coarse-blocky ~~landform,~~

only as much ground ice is accumulated as infiltrating water is rapidly "fixed" by refreezing onto the already cooled blocks, otherwise the water runs off. Water supply needs to be well-timed and "ò la minute", unlike in water-holding fine-grained material that can slowly freeze the soil water over weeks. Refreezing only occurs when precipitation or snowmelt released from a "warm" snowpack infiltrates into the ground that is already at subfreezing conditions (however at the cost of the liberated latent heat that warms the AL and the permafrost beneath). Such a specific weather situation occurs every year in spring, but might occur increasingly frequent as winters become milder. *Spring-time refreezing is energy-limited, but the total winter–spring AL ice accumulation is controlled both by the weather-sensitive water supply and ground cooling.* permafrost landforms are abundant in periglacial high-mountain areas, understanding their climate-controlled future changes, quantifying subsurface water/ice storage and pathways in mountain permafrost-underlain catchments (Woo, 2011; Louis et al., 2024), and assessing the cryosphere–groundwater connectivity are policy-relevant research topics (cf. van Tiel et al., 2024).

6 Conclusions

We assess the role of the active Rock glaciers store and release water and ice on different time scales with varying magnitudes and residence times: (1) Liquid water on short-term (sub-monthly) scale, (2) ground ice in the coarse-blocky AL on intermediate term (seasonal), and (3) 'old' permafrost ice on long-term (over millennia). We quantify supra-permafrost ice storage changes, precipitation, evaporation and snowmelt on the intact Murtèl rock glacier in the hydrological cycle of its small periglacial and unglacierized watershed located in the Upper Engadine ((Engadine, eastern Swiss Alps) and the surface outflow of its periglacial, permafrost-underlain watershed. The single-lobe rock glacier (4 ha) and its watershed (30 ha) are small, unglacierized, and sparsely vegetated. Boreholes revealed a rock glacier stratigraphy of $2-5$ m thick coarse-blocky AL over ~ 30 m of nearly massive ice (perennially frozen rock-glacier rock glacier core). Our unprecedentedly comprehensive hydro-meteorological measurements include heat flux measurements resolve the water balance and snow/ice storage changes between ground surface and permafrost table at plot scale, i.e. isolated on the rock glacier itself. We estimated ice storage changes (melt and accumulation) in the coarse-blocky active layer (AL) , from direct observations of the seasonal evolution of the ground-ice table , and discharge and isotopic signature of the outflow at the rock-glacier front. The detailed active-layer energy and water/ice balance quantifies precipitation, evaporation, snow melt, ground ice melt, and catchment surface outflow.

The intact Murtèl rock glacier stores and releases water and ice over different time scales with varying magnitudes and residence times: (1) Liquid water on short-term (sub-monthly) scale, (2) ground ice in the coarse-blocky AL on intermediate term (seasonal), and (3) 'old' permafrost ice on long-term (over millennia) . Our main findings are: -3pt Short-term storage: The Murtèl surface outflow is dominated by snowmelt and rainwater. The hydrograph during the thaw season 'ablation stake' measurements) and an AL energy budget derived from in-situ heat flux measurements.

The thaw-season hydrograph at the rock-glacier front is flashy with rapidly varying discharge typical for a small, permafrost-underlain catchment with limited water storage capacity: Precipitation peaks are followed by dry phases with little sustained baseflow (, below gauging limit), and without baseflow when the rock glacier springs temporarily fall dryin the absence of precipitation. The small, coarse-debris dominated and sparsely vegetated periglacial catchment is weakly buffered, and storage capacity

for liquid water is small. Nonetheless, the seep water sampled in autumn is likely groundwater-derived. Intermediate-term storage: Seasonal ground ice accumulation and melt in the AL is substantial. Independent direct observations and an The isotopic signature and electrical conductivity of the outflow suggests that the Murtèl surface outflow is largely derived from snowmelt and rainwater. No clear hydro-chemical evidence (δ^{18}O natural tracer) of permafrost meltwater could be found in the surface outflow. In contrast, the in-situ ablation measurements and AL energy budget suggests AL ice melt rates of , amounting to concurrently suggested substantial seasonal ground ice turnover in coarse blocky AL with accumulation and melt of 150−300 mm w.e. over the thaw season. In the comparatively cool–wet year (160 mm w.e. in 2021, ground ice melt represented of the annual precipitation and outflow, and in the hot–dry year 2022. The superimposed AL ice is sourced by refreezing snowmelt in winter and spring (i.e. annually replenished) and acts as a hydrological and thermal buffer by protracting 260 mm w.e. in 2022). 20−40 % of the snowpack is accumulated directly (in-blown snow) or refreezes onto the convectively cooled blocks as snowmelt infiltrates into the coarse blocky AL during winter warm spells and the spring snowmelt, forming annually replenished superimposed ground ice. This freeze/thaw storage protracts the snowmelt into late summer and protecting the underlying permafrost. Despite non-negligible contribution to runoff that the water balance suggests, we could not track the ground-ice melt in absorbs ∼ 80 % of the thaw-season ground heat flux, i.e. is a coupled thermo-hydrological buffer that releases meltwater in late summer and protects the underlying permafrost body, contributing to the surface outflow using δ^{18}O natural tracer. The ground-ice meltwater preferentially infiltrates. The rainfall–discharge relation suggests that of rainfall triggers surface outflow, hence ground ice melt rates of are likely too low to generate surface outflow (baseflow). Long-term storage: Nonetheless, subsidence measurements and AL thickening suggests that the Murtèl rock glacier is slowly degrading, hence releases meltwater rock glaciers' climate resilience. Consequently, the amount of meltwater released from the 'old' permafrost ice (long-term storage in the rock glacier core) . This contribution, what might be referred to as 'permafrost runoff' in the strict sense, is or ∼ 5 − 10× is currently ∼ 10 mm w.e. yr^{-1}, an order of magnitude smaller than the AL meltwater contribution and not more than a few of the precipitation and runoff in the catchment. negligible compared to the inter-annual variations of precipitation. Melting superimposed ice sourced from winter precipitation cannot increase the total annual runoff. We hypothesize that the generated meltwater (which we could not track in the surface outflow) largely percolates deeper and recharges the sub-permafrost groundwater. Ground ice melt rates are limited by the ground heat flux to 1−4 mm w.e. day^{-1}, which is below the 9 mm day^{-1} infiltration capacity inferred from the local rainfall–streamflow relation. Sub-surface water pathways have been identified by tracer tests (Tenthorey and Gerber, 1991).

Concerning the debate on the hydrological significance of rock glaciers, our finding of ice melt at two scales points out the loose definition of 'permafrost runoff' that often either ignores the substantial AL ice turnover or subsumes AL ice melt under 'permafrost runoff'. On the one hand, the seasonal ice accumulation/melt Our case study supports the concept that intact rock glacier sustain baseflow by recharging groundwater with meltwater from the seasonal AL thaw, in addition to the large, climate-resilient sub-surface permafrost ice reserves they hold (Jones et al., 2019; Hayashi, 2020; Wagner et al., 2021a; Arenson et al., 202 . Specific to permeable, coarse blocky landforms with a small water retention capacity as Murtèl rock glacier, little water is stored in liquid form. Instead, the water is immobilized by forming ice in the ALis larger than previously assumed, hinting at the role of rock glaciers as 'streamflow regulators' regardless of their permafrost ice volumes. On the other hand, the : Snowmelt is

rapidly fixed as AL ice in winter–spring, but slowly released during the thaw season, routing a small, but sustained meltwater flow through the low-permeability permafrost aquitard to deeper aquifers. The superimposed AL ice is refrozen winter precipitation and cannot increase the total ~~yearly runoffwhile melt of the insulated 'old' permafrost body (rock-glacier core) is negligibly slow compared to the water cycle. Our water balance refers to point-scale on the rock glacier itself. Substantial AL ice accumulation relies on strong convective winter cooling and an efficient conversion of the sensible cold content to snowmelt refreezing and is sensitive to debris texture, thermo-hydraulic properties, and weather/snow conditions.~~

~~Observing ground-ice accumulation and melt in the inaccessible AL is challenging and few data sets exist. Still insufficiently understood is the ground ice accumulation in winter–spring that relies on strong ground cooling and well-timed meltwater supply into the subfreezing AL. More data from rock glaciers and other (permafrost) landforms (talus slopes, moraines) should tell how generalizable the~~ annual runoff. While our isolated energy and water balance investigations provided detailed and quantitative insights into hydro-thermal processes in the Murtèl ~~point-wise observations are with respect to other debris textures and arid climatic settings facing water scarcity. Given the difficult accessibility of the ground ice, indirect methods of jointly deployed geophysical, hydrological, and kinematic approaches are most promising.~~ AL, integrated hydrogeological studies are needed to address rock glaciers as embedded in their watersheds, namely the connectivity to adjoining landforms and the groundwater, sub-surface groundwater pathways, and their capacity to sustain baseflow compared to other high-mountain landforms such as relict rock glaciers, moraines, meadows, and wetlands.

Data availability. The PERMOS data can be obtained from the PERMOS network (http://www.permos.ch), and the PERMA-XT measurement data from https://www.permos.ch//doi/permos-spec-2023-1 (doi:10.13093/permos-spec-2023-01).

Appendix A: Additional figures

A1 Hydro-morphological sketch map

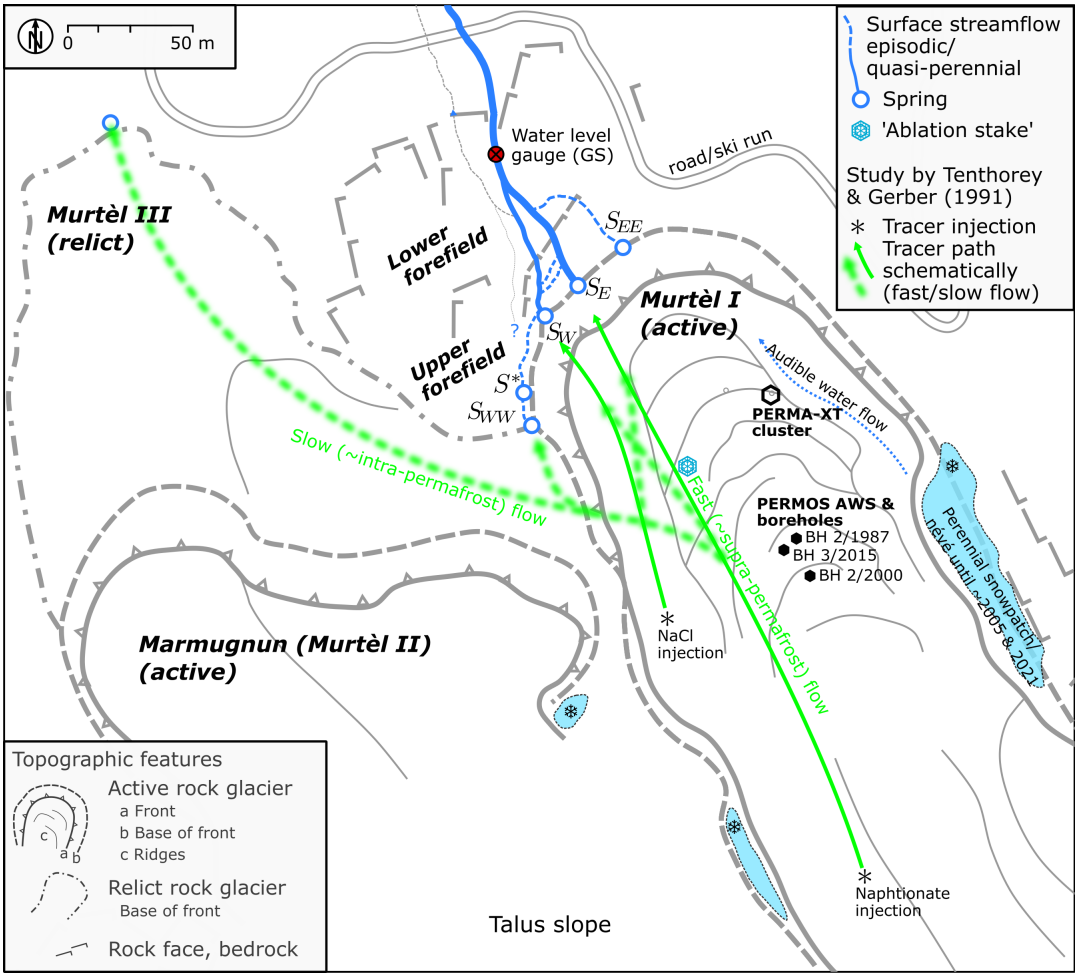

Figure A1. Hydro-morphological setting. Sketch map of the active rock glaciers Murtèl I and Marmugnun (Murtèl II), and the relict rock glacier Murtèl III.

A2 Field observation: Six snapshots of the strongly variable discharge

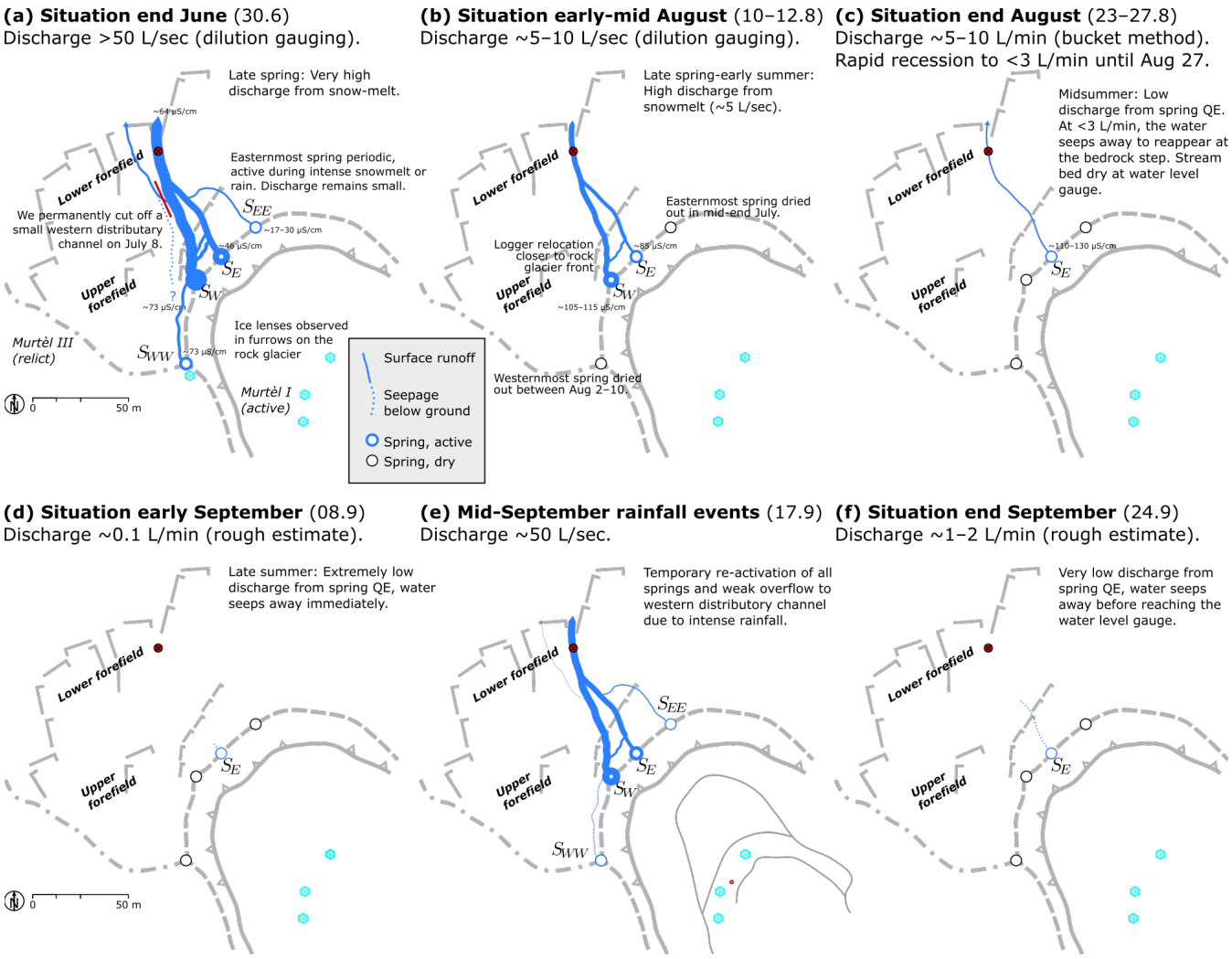

Figure A2. Six snapshots of the strongly variable discharge on the ~~rock glacier~~ rock glacier forefield in summer 2021 as observed on the regular field visits. **(a)–(c)**: Spring–early summer (end June until end August) with declining discharge as snowmelt progressed; **(d)–(f)**: Late summer–autumn (end August until end September) with strong discharge changes within days as a response to rainfall events. The baseflow in dry periods seeps into the ground before reaching the gauging station in the lower forefield.

A3 Rainfall MeteoSuisse station *Piz Corvatsch* (COV)

Rainfall at the PERMA-XT station on Murtèl and on MeteoSuisse station *Piz Corvatsch* (actually located on a promontory of *Piz Murtèl*) is shown in Fig. A3.

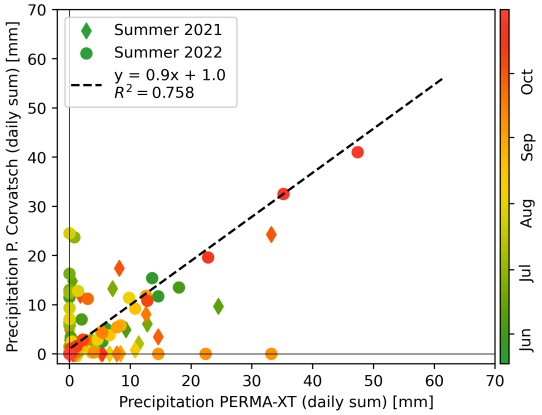

Figure A3.

A4 Deuterium excess d_{excess}

Deuterium excess [‰] is defined as (Williams et al., 2006)

$$d_{excess} := \delta^2\mathrm{H} - 8 \cdot \delta^{18}\mathrm{O}. \tag{A1}$$

Results for the thaw season 2021 and 2022 are shown in Fig. A4.

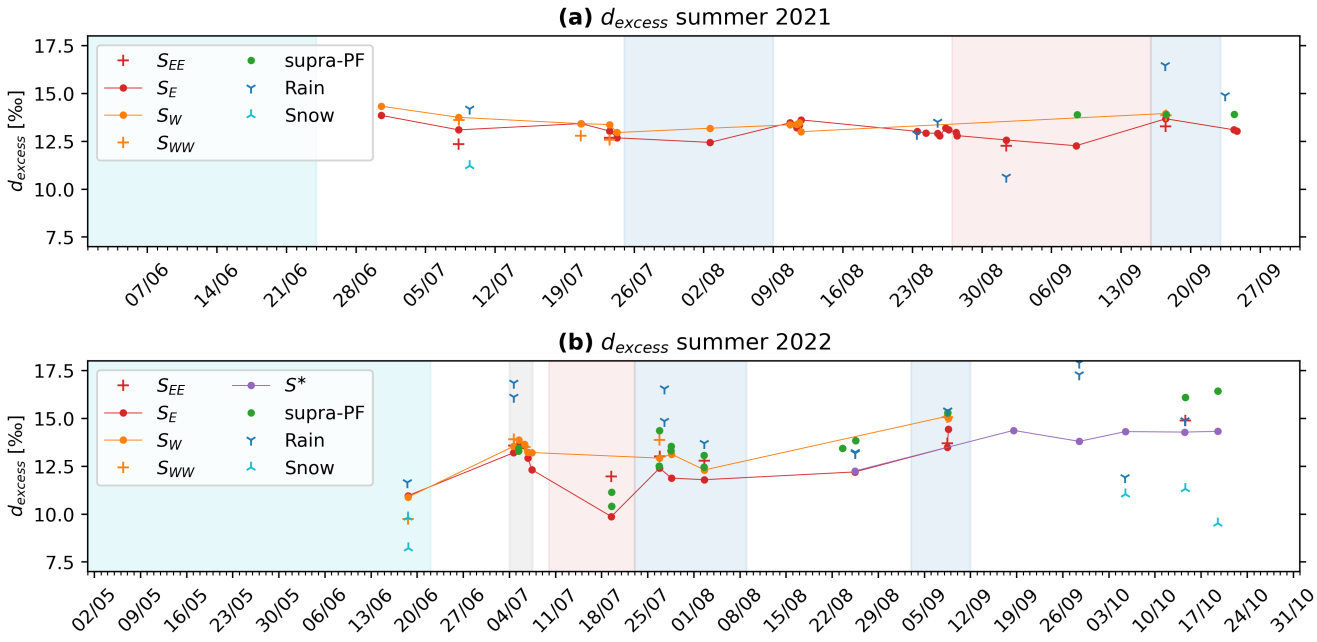

Figure A4. Deuterium excess d_{excess} (Eq. A1) for the summers **(a)** 2021 and **(b)** 2022.

Appendix B: Stable isotope data

The isotope data are listed in Tables B1–B5.

Table B1. Isotope data (1/5). Water temperature and EC measured in the field with WTW probe.

ID	Job	Sampling date	Location	T_w [°C]	EC [µS cm^{-1}]	δ^{18}O [‰]	δ^{2}H [‰]	d_{excess} [‰]
ISO01	21-233	2020-08-27, 13:50	SE	1.2	122	-13.37	-95.67	11.29
ISO02	21-233	2020-08-27, 14:00	SW	0.5	214	-12.79	-89.95	12.37
ISO03	21-233	2021-06-30, 13:04	SE	-0.1	43	-15.53	-110.38	13.86
ISO04	21-233	2021-06-30, 13:07	SW	0.2	69	-16.13	-114.74	14.33
ISO05	21-233	2021-07-08, 08:00	SEE	4.5	28	-13.75	-97.66	12.35
ISO06	21-233	2021-07-08, 08:00	SE	-0.2	44	-15.25	-108.93	13.10
ISO07	21-233	2021-07-08, 08:00	SW	-0.1	67	-15.99	-114.16	13.75
ISO08	21-233	2021-07-08, 08:25	SWW	-0.2	54	-15.82	-112.98	13.62
ISO09	21-233	2021-07-08, 10:00	rSE	1.7	86	-15.50	-110.42	13.59
ISO10	21-233	2021-07-09, 10:00	RW	3.8	3	-9.48	-61.68	14.20
ISO11	21-233	2021-07-09, 10:00	SS	0.0	5	-14.41	-104.04	11.21
ISO12	21-233	2021-07-20, 15:15	SE	0.1	57	-14.84	-105.29	13.43
ISO13	21-233	2021-07-20, 15:05	SW	0.0	73	-15.61	-111.45	13.42
ISO14	21-233	2021-07-20, 14:55	SWW	0.1	43	-15.44	-110.72	12.80
ISO15	21-233	2021-07-23, 12:30	SEE	1.5	66	-12.57	-87.84	12.68
ISO16	21-233	2021-07-23, 12:30	SE	0.1	62	-14.51	-103.03	13.04
ISO17	21-233	2021-07-23, 12:30	SW	-0.1	73	-15.47	-110.37	13.38
ISO18	21-233	2021-07-23, 12:30	SWW	0.1	54	-14.88	-106.46	12.57
ISO19	21-233	2021-07-23, 12:30	rSE	4.5	91	-15.06	-107.81	12.68
ISO20	21-233	2021-07-24, 06:30	SE	0.1	59	-14.68	-104.75	12.68
ISO21	21-233	2021-07-24, 06:30	SW	-0.1	74	-15.42	-110.44	12.96
ISO22	21-233	2021-08-02, 15:00	SE	0.1	68	-10.53	-71.80	12.44
ISO23	21-233	2021-08-02, 14:50	SW	0.0	92	-10.68	-72.28	13.18
ISO24	21-233	2021-08-10, 15:56	SE	0.2	75	-12.06	-83.01	13.47
ISO25	21-233	2021-08-10, 15:56	SW	0.0	111	-12.30	-85.02	13.36
ISO26	21-233	2021-08-11, 08:00	SE	0.0	82	-12.51	-86.89	13.20
ISO27	21-233	2021-08-11, 08:05	SW	0.0	98	-12.70	-88.25	13.38
ISO28	21-233	2021-08-11, 15:03	SE	0.4	81	-12.54	-87	13.35
ISO29	21-233	2021-08-11, 15:11	SW	0.3	111	-12.68	-87.99	13.47
ISO30	21-233	2021-08-11, 11:37	BR	15.5	33	-9.51	-67.29	8.76
ISO31	21-233	2021-08-11, 18:48	SE	0.0	78	-12.48	-86.20	13.62
ISO32	21-233	2021-08-11, 18:54	SW	0.0	98	-13.12	-91.96	13.00

Analytical uncertainty: 0.1‰ for δ^{18}O, 1.5‰ for δ^{2}H (1σ). Cf. Fig. 2 for sampling locations. Sample location abbreviated as follows: RW rainwater (RWe event, sampled at every field visit; RWi ca. monthly integrated). SS snow sample. SEE easternmost main spring S_{EE}. SE eastern main spring S_E. SW Murtèl western main spring S_W. SWW westernmost main spring S_{WW}. SD deep seep S^*. rSE seep in front of relict Murtèl III rock glacier. sPF supra-permafrost water sampled in rock-glacier furrow (sPFc next to ablation stake, sPFt next to thermistor TK4/5). BR bedrock seepage (Fig. 2).

Table B2. Isotope data (2/5). Water temperature and EC measured in the field with WTW probe.

ID	Job	Sampling date	Location	T_w [°C]	EC [µS cm^{-1}]	δ^{18}O [‰]	δ^{2}H [‰]	d_{excess} [‰]
ISO33	21-258	2021-08-23, 11:00	RW		5	-5.86	-33.97	12.89
ISO34	21-258	2021-08-23, 11:40	SE	0.5	107	-13.39	-94.12	13.02
ISO35	21-258	2021-08-24, 08:33	SE	0.5	109	-13.33	-93.67	12.93
ISO36	21-258	2021-08-25, 12:35	SE		112	-13.15	-92.32	12.92
ISO37	21-258	2021-08-25, 17:55	SE		114	-13.15	-92.43	12.80
ISO38	21-258	2021-08-25, 12:30	RW		5	-12.99	-90.45	13.51
ISO39	21-258	2021-08-26, 08:10	SE		120	-13.24	-92.72	13.19
ISO40	21-258	2021-08-26, 15:40	SE		123	-13.22	-92.63	13.11
ISO41	21-258	2021-08-27, 09:00	SE	0.3	124	-13.21	-92.69	12.96
ISO42	21-258	2021-08-27, 12:01	SE	0.5	124	-13.14	-92.33	12.80
ISO43	21-258	2021-09-01, 11:00	SEE	3.0	85	-12.07	-84.32	12.27
ISO44	21-258	2021-09-01, 11:00	SE	2.0	125	-12.50	-87.40	12.57
ISO45	21-258	2021-09-01, 11:00	RW		5	-14.30	-103.74	10.64
ISO46	21-258	2021-09-08, 11:13	SE		131	-12.57	-88.32	12.27
ISO47	21-258	2021-09-08, 11:00	RW		5	-8.55	-49.03	19.34
ISO48	21-258	2021-09-08, 13:45	sPFc	0.0		-12.97	-89.86	13.89
ISO49	21-258	2021-09-17, 11:40	SEE			-10.58	-71.37	13.28
ISO50	21-258	2021-09-17, 11:43	SE		112	-10.89	-73.46	13.68
ISO51	21-258	2021-09-17, 11:45	SW		150	-10.47	-69.79	13.95
ISO52	21-258	2021-09-17, 12:03	SWW			-10.56	-70.61	13.86
ISO53	21-258	2021-09-17, 13:30	sPFc			-10.56	-70.55	13.90
ISO55	21-258	2021-09-24, 08:20	SE		130	-11.16	-76.22	13.10
ISO56	21-258	2021-09-24, 15:24	SE		130	-11.17	-76.33	13.04
ISO57	21-258	2021-09-24, 09:00	sPFc			-11.77	-80.22	13.91
ISO58	21-258	2021-09-23, 11:35	RW		5	-12.26	-83.21	14.89
ISO59	21-258	2021-09-17, 11:00	RW		5	-6.07	-32.10	16.46

Cf. Table B1 for abbreviations of sample locations.

Table B3. Isotope data (3/5). Water temperature and EC measured in the field with WTW probe.

ID	Job	Sampling date	Location	T_w [°C]	EC [µS cm^{-1}]	δ^{18}O [‰]	δ^{2}H [‰]	d_{excess} [‰]
ISO2201	22-139	2022-04-20, 12:00	SS	-2.0	3	-18.83	-139.12	11.51
ISO2202	22-139	2022-04-20, 12:20	SS	-2.0	2	-20.32	-151.27	11.32
ISO2203	22-139	2022-05-20, 12:30	GS	-0.2	68	-17.10	-124.43	12.39
ISO2204	22-139	2022-06-18, 14:09	SE	0.0	67	-14.20	-102.66	10.96
ISO2205	22-136	2022-06-18, 14:13	SW	-0.2	85	-14.83	-107.75	10.88
ISO2206	22-139	2022-06-18, 14:20	SWW	0.0	41	-14.84	-109.01	9.75
ISO2207	22-136	2022-06-18, 12:40	RWe	22.7	6	-8.55	-56.73	11.65
ISO2208	22-139	2022-06-18, 15:30	SS	0.0	2	-15.20	-113.35	8.23
ISO2209	22-139	2022-06-18, 15:20	SS	0.0	2	-15.53	-114.43	9.83
ISO2210	22-139	2022-07-04, 15:55	SEE	7.9	48	-8.92	-57.75	13.57
ISO2211	22-136	2022-07-04, 15:25	SE	-0.1	74	-9.44	-62.30	13.21
ISO2212	22-136	2022-07-04, 15:30	SW	0.1	98	-9.46	-62.15	13.55
ISO2213	22-139	2022-07-04, 15:35	SWW	-0.1	90	-10.32	-68.63	13.92
ISO2214	22-139	2022-07-04, 16:30	RWe	16.6	11	-6.65	-37.09	16.12
ISO2215	22-139	2022-07-04, 16:30	RWi	16.6	11	-6.68	-36.56	16.86
ISO2216	22-136	2022-07-05, 10:00	SE	-0.2	79	-9.88	-65.49	13.58
ISO2217	22-136	2022-07-05, 10:05	SW	-0.1	110	-10.02	-66.32	13.87
ISO2218	22-136	2022-07-05, 09:30	sPFt	0.2	78	-9.69	-64.03	13.45
ISO2219	22-136	2022-07-05, 09:00	sPFc	0.0	107	-9.57	-63.22	13.31
ISO2220	22-139	2022-07-06, 07:35	SE	-0.1	83	-10.47	-70.19	13.57
ISO2221	22-139	2022-07-06, 07:40	SW	-0.1	116	-10.61	-71.24	13.66
ISO2222	22-139	2022-07-06, 07:50	SWW	0.1	95	-10.68	-71.89	13.51
ISO2223	22-139	2022-07-06, 19:30	SE		83	-10.83	-73.72	12.93
ISO2224	22-139	2022-07-06, 19:35	SW			-10.87	-73.72	13.22
ISO2225	22-139	2022-07-06, 19:10	sPFc			-10.77	-73.21	12.95
ISO2226	22-139	2022-07-07, 09:25	SE		83	-11.11	-76.53	12.33
ISO2227	22-139	2022-07-07, 09:35	SW			-10.96	-74.43	13.22
ISO2228	22-139	2022-07-07, 08:40	sPFc			-10.99	-75.13	12.76
ISO2229	22-139	2022-07-19, 11:30	SEE	12.0	68	-11.86	-82.91	11.97
ISO2230	22-136	2022-07-19, 11:20	SE	4.2	104	-11.39	-81.21	9.87
ISO2231	22-136	2022-07-19, 15:00	RWe			-4.79	-35.41	2.93
ISO2232	22-139	2022-07-19, 12:25	sPFt	1.9	60	-13.39	-95.94	11.14
ISO2233	22-136	2022-07-19, 12:40	sPFc	0.0	109	-12.91	-92.87	10.41

Cf. Table B1 for abbreviations of sample locations.

Table B4. Isotope data (4/5). Water temperature and EC measured in the field with WTW probe.

ID	Job	Sampling date	Location	T_w [°C]	EC [µS cm^{-1}]	δ^{18}O [‰]	δ^{2}H [‰]	d_{excess} [‰]
ISO2234	22-139	2022-07-26, 19:30	SEE	5.1	70	-9.93	-66.41	13.03
ISO2235	22-136	2022-07-26, 19:10	SE	-0.1	92	-10.38	-70.63	12.40
ISO2236	22-136	2022-07-26, 19:05	SW	0.0	124	-9.72	-64.80	12.93
ISO2237	22-139	2022-07-26, 18:55	SWW	-0.1	103	-10.06	-66.64	13.87
ISO2238	22-139	2022-07-26, 18:30	sPFt	0.0	85	-10.21	-67.29	14.37
ISO2239	22-136	2022-07-26, 18:00	sPFc	0.0	114	-9.94	-67.02	12.52
ISO2240	22-139	2022-07-27, 12:50	RWe		10	-7.02	-39.64	16.55
ISO2241	22-136	2022-07-27, 12:50	RWi		8	-6.57	-37.73	14.85
ISO2242	22-136	2022-07-28, 14:30	SE		99	-11.17	-77.49	11.88
ISO2243	22-136	2022-07-28, 14:30	SW	5.0	142	-10.57	-71.39	13.13
ISO2244	22-139	2022-07-28, 13:45	sPFt	0.0	95	-11.61	-79.36	13.54
ISO2245	22-139	2022-07-28, 12:36	sPFc	0.0	116	-11.64	-79.81	13.31
ISO2246	22-139	2022-08-02, 14:10	SEE	6.3	75	-10.38	-70.28	12.79
ISO2247	22-136	2022-08-02, 14:20	SE	0.4	100	-11.57	-80.77	11.80
ISO2248	22-136	2022-08-02, 14:25	SW	6.4	161	-10.52	-71.83	12.31
ISO2249	22-139	2022-08-02, 14:30	RWe	23.	5	-9.69	-63.81	13.71
ISO2250	22-139	2022-08-02, 13:10	sPFt	0.0	96	-11.91	-82.25	13.07
ISO2251	22-136	2022-08-02, 12:35	sPFc	0.0	123	-11.69	-81.09	12.46
ISO2252	22-139	2022-08-25, 10:30	SE	4.0	131	-12.19	-85.32	12.20
ISO2253	22-136	2022-08-25, 11:00	SD	0.2	170	-11.25	-77.75	12.26
ISO2254	22-136	2022-08-25, 11:30	RWe	19.5	6	-8.09	-51.45	13.23
ISO2255	22-139	2022-08-25, 11:30	RWi	19.5	6	-8.37	-53.81	13.17
ISO2256	22-136	2022-08-25, 13:00	sPFc	0.8	120	-11.96	-81.87	13.84
ISO2257	22-139	2022-08-23, 14:00	sPFc			-11.52	-78.75	13.44
ISO2258	22-139	2022-09-08, 11:10	SEE	1.7	51	-9.32	-60.85	13.71
ISO2259	22-136	2022-09-08, 11:15	SE	0.1	104	-10.19	-68.04	13.49
ISO2260	22-136	2022-09-08, 11:20	SW	0.3	164	-9.59	-61.65	15.11
ISO2261	22-139	2022-09-08, 11:25	SWW	-0.1	131	-9.62	-61.90	15.06
ISO2262	22-139	2022-09-08, 12:45	RWe	12.0	6	-9.65	-61.78	15.40
ISO2263	22-136	2022-09-08, 12:45	RWi	12.0	6	-9.60	-61.41	15.40
ISO2264	22-136	2022-09-08, 12:20	sPFc	0.2	112	-9.37	-59.68	15.29
ISO2265	22-136	2022-09-08, 15:30	SE	-0.0	111	-10.61	-70.46	14.44
ISO2266	22-136	2022-09-08, 15:35	SW	0.0	163	-9.50	-61.04	14.99

Cf. Table B1 for abbreviations of sample locations.

Table B5. Isotope data (5/5). Water temperature and EC measured in the field with WTW probe.

ID	Job	Sampling date	Location	T_w [°C]	EC [µS cm^{-1}]	δ^{18}O [‰]	δ^{2}H [‰]	d_{excess} [‰]
ISO2267	22-136	2022-09-18, 12:35	SD	0.1	230	-10.50	-69.63	14.38
ISO2268	22-136	2022-09-28, 12:00	SD	-0.1	330	-10.85	-72.99	13.80
ISO2269	22-139	2022-09-28, 11:30	RWe	0.0	10	-11.70	-75.69	17.90
ISO2270	22-136	2022-09-28, 11:30	RWi	0.0	6	-11.14	-71.83	17.30
ISO2271	22-136	2022-10-05, 11:50	SD	-0.1	301	-10.91	-72.96	14.31
ISO2272	22-139	2022-10-05, 11:30	RWe		5	-15.56	-112.59	11.91
ISO2273	22-136	2022-10-05, 12:00	SS	0.0	5	-14.03	-101.22	11.05
ISO2274	22-136	2022-10-14, 14:05	SEE	1.8	92	-10.78	-71.31	14.90
ISO2275	22-136	2022-10-14, 12:30	SD	0.0	295	-10.82	-72.25	14.29
ISO2276	22-139	2022-10-14, 13:40	RWe		5	-12.49	-85.05	14.89
ISO2277	22-136	2022-10-14, 14:55	sPFc	0.0	183	-10.83	-70.54	16.09
ISO2278	22-136	2022-10-14, 14:55	SS	0.0	5	-10.54	-72.99	11.33
ISO2279	22-136	2022-10-19, 13:15	SD	0.0	280	-10.85	-72.44	14.32
ISO2280	22-136	2022-10-19, 12:25	sPFc	0.0	192	-10.99	-71.50	16.43
ISO2281	22-139	2022-10-19, 12:25	SS	0.0	6	-11.33	-81.14	9.52

Cf. Table B1 for abbreviations of sample locations.

Author contributions. DA performed the fieldwork, model development and analyses for the study and wrote the manuscript. MS, MH and BK supervised the study, provided financial and field support and contributed to the manuscript preparation. AH and CK provided logistical support and editorial suggestions on the manuscript. HG designed the novel sensor array, regularly checked data quality, contributed to the analyses and provided editorial suggestions on the manuscript.

Competing interests. The authors declare that they have no conflict of interest.

Acknowledgements. This work is a collaboration between the University of Fribourg and GEOTEST and was funded by the Swiss Innovation Agency Innosuisse (project 36242.1 IP-EE 'Permafrost Meltwater Assessment eXpert Tool PERMA-XT'). The authors wish to thank Walter Jäger (Waljag GmbH, Malans) and Thomas Sarbach (Sarbach Mechanik, St. Niklaus) for the technical support, Stephan Bolay (GEOTEST) for the field assistance (dilution gaugings), and the Corvatsch cable car company for logistical support~~, and~~. Insightful discussions with Theo Jenk (Paul Scherrer Institute PSI), Isabelle Gärtner-Roer and Andreas Vieli (University of Zurich)~~for the insightful discussions~~, Landon Halloran and Clément Roques (University of Neuchâtel) contributed to the manuscript.

References

Aldrich, H. P. and Paynter, H. M.: First Interim Report: Analytical Studies of Freezing and Thawing of Soils (ACFEL Technical Report No. 42), Tech. rep., US Corps of Engineers, Boston (MA), http://hdl.handle.net/11681/6526, Arctic Construction and Frost Effects Laboratory (ACFEL), 1953.

Amschwand, D., Ivy-Ochs, S., Frehner, M., Steinemann, O., Christl, M., and Vockenhuber, C.: Deciphering the evolution of the Bleis Marscha rock glacier (Val d'Err, eastern Switzerland) with cosmogenic nuclide exposure dating, aerial image correlation, and finite element modeling, The Cryosphere, 15, 2057–2081, https://doi.org/10.5194/tc-15-2057-2021, 2021.

Amschwand, D., Scherler, M., Hoelzle, M., Krummenacher, B., Haberkorn, A., Kienholz, C., and Gubler, H.: Surface heat fluxes at coarse blocky Murtèl rock glacier (Engadine, eastern Swiss Alps), The Cryosphere, 18, 2103–2139, https://doi.org/10.5194/tc-18-2103-2024, 2024a.

Amschwand, D., Wicky, J., Scherler, M., Hoelzle, M., Krummenacher, B., Haberkorn, A., Kienholz, C., and Gubler, H.: Sub-surface processes and heat fluxes at coarse-blocky Murtèl rock glacier (Engadine, eastern Swiss Alps), Preprint submitted to Earth Surface Dynamics, https://doi.org/10.5194/egusphere-2024-172, 2024b.

Arenson, L., Hoelzle, M., and Springman, S.: Borehole deformation measurements and internal structure of some rock glaciers in Switzerland, Permafrost and Periglacial Processes, 13, 117–135, https://doi.org/10.1002/ppp.414, 2002.

Arenson, L. U., Hauck, C., Hilbich, C., Seward, L., Yamamoto, Y., and Springman, S. M.: Sub-surface heterogeneities in the Murtèl-Corvatsch rock glacier, Switzerland, in: Proceedings of the joint 63rd Canadian Geotechnical Conference and the 6th Canadian Permafrost Conference (GEO2010), September 12–15 2010, Calgary (Alberta), Canada, pp. 1494–1500, Canadian Geotechnical Society, CNC-IPA/NRCan, Calgary, AB, Canada, 2010.

Arenson, L. U., Harrington, J. S., Koenig, C. E. M., and Wainstein, P. A.: Mountain Permafrost Hydrology—A Practical Review Following Studies from the Andes, Geosciences, 12, https://doi.org/10.3390/geosciences12020048, 2022.

Arnoux, M., Halloran, L. J. S., Berdat, E., and Hunkeler, D.: Characterizing seasonal groundwater storage in alpine catchments using time-lapse gravimetry, water stable isotopes and water balance methods, Hydrological Processes, 34, 4319–4333, https://doi.org/10.1002/hyp.13884, 2020.

Azócar, G. F. and Brenning, A.: Hydrological and geomorphological significance of rock glaciers in the dry Andes, Chile (27°–33°S), Permafrost and Periglacial Processes, 21, 42–53, https://doi.org/10.1002/ppp.669, 2010.

Barandun, M., Fiddes, J., Scherler, M., Mathys, T., Saks, T., Petrakov, D., and Hoelzle, M.: The state and future of the cryosphere in Central Asia, Water Security, 11, 100 072, https://doi.org/10.1016/j.wasec.2020.100072, 2020.

Barsch, D.: Rockglaciers. Indicators for the Present and Former Geoecology in High Mountain Environments, vol. 16 of *Springer Series in Physical Environment*, Springer Berlin, Heidelberg, https://doi.org/10.1007/978-3-642-80093-1, 1996.

Barsch, D. and Hell, G.: Photogrammetrische Bewegungsmessungen am Blockgletscher Murtèl I, Oberengadin, Schweizer Alpen, Zeitschrift für Gletscherkunde und Glazialgeologie, 11, 111–142, 1975.

Bast, A., Kenner, R., and Phillips, M.: Short-term cooling, drying, and deceleration of an ice-rich rock glacier, The Cryosphere, 18, 3141–3158, https://doi.org/10.5194/tc-18-3141-2024, 2024.

Bearzot, F., Colombo, N., Cremonese, E., di Cella, U. M., Drigo, E., Caschetto, M., Basiricò, S., Crosta, G., Frattini, P., Freppaz, M., Pogliotti, P., Salerno, F., Brunier, A., and Rossini, M.: Hydrological, thermal and chemical influence of an intact rock glacier discharge on mountain stream water, Science of The Total Environment, 876, 162 777, https://doi.org/https://doi.org/10.1016/j.scitotenv.2023.162777, 2023.

Beniston, M., Farinotti, D., Stoffel, M., Andreassen, L. M., Coppola, E., Eckert, N., Fantini, A., Giacona, F., Hauck, C., Huss, M., Huwald, H., Lehning, M., López-Moreno, J.-I., Magnusson, J., Marty, C., Morán-Tejéda, E., Morin, S., Naaim, M., Provenzale, A., Rabatel, A., Six, D., Stötter, J., Strasser, U., Terzago, S., and Vincent, C.: The European mountain cryosphere: a review of its current state, trends, and future challenges, The Cryosphere, 12, 759–794, https://doi.org/10.5194/tc-12-759-2018, 2018.

Beria, H., Larsen, J. R., Ceperley, N. C., Michelon, A., Vennemann, T., and Schaefli, B.: Understanding snow hydrological processes through the lens of stable water isotopes, WIREs Water, 5, e1311, https://doi.org/10.1002/wat2.1311, 2018.

Biskaborn, B. K., Smith, S. L., Noetzli, J., Matthes, H., Vieira, G., Streletskiy, D. A., Schoeneich, P., Romanovsky, V. E., Lewkowicz, A. G., Abramov, A., Allard, M., Boike, J., Cable, W. L., Christiansen, H. H., Delaloye, R., Diekmann, B., Drozdov, D., Etzelmüller, B., Grosse, G., Guglielmin, M., Ingeman-Nielsen, T., Isaksen, K., Ishikawa, M., Johansson, M., Johannsson, H., Joo, A., Kaverin, D., Kholodov, A., Konstantinov, P., Kröger, T., Lambiel, C., Lanckman, J.-P., Luo, D., Malkova, G., Meiklejohn, I., Moskalenko, N., Oliva, M., Phillips, M., Ramos, M., Sannel, A. B. K., Sergeev, D., Seybold, C., Skryabin, P., Vasiliev, A., Wu, Q., Yoshikawa, K., Zheleznyak, M., and Lantuit, H.: Permafrost is warming at a global scale, Nature Communications, 10, https://doi.org/10.1038/s41467-018-08240-4, 2019.

Blumstengel, W. and Harris, S.: Observations on an active lobate rock glacier, Slims River valley, St. Elias Range, Canada, in: Proceedings of the 5th International Conference on Permafrost, August 2–5 1988, Trondheim, Norway, vol. 1, pp. 689–695, 1988.

Bodin, X., Rojas, F., and Brenning, A.: Status and evolution of the cryosphere in the Andes of Santiago (Chile, 33.5°S.), Geomorphology, 118, 453–464, https://doi.org/https://doi.org/10.1016/j.geomorph.2010.02.016, 2010.

Boike, J., Roth, K., and Ippisch, O.: Seasonal snow cover on frozen ground: Energy balance calculations of a permafrost site near Ny-Ålesund, Spitsbergen, Journal of Geophysical Research: Atmospheres, 108, ALT 4–1–ALT 4–11, https://doi.org/10.1029/2001JD000939, 2003.

Bonnaventure, P. P. and Lamoureux, S. F.: The active layer: A conceptual review of monitoring, modelling techniques and changes in a warming climate, Progress in Physical Geography: Earth and Environment, 37, 352–376, https://doi.org/10.1177/0309133313478314, 2013.

Bowen, G. J.: The Online Isotopes in Precipitation Calculator, version 3.1., http://www.waterisotopes.org, https://wateriso.utah.edu/waterisotopes/pages/data_access/oipc.html, 2017.

Brenning, A.: Geomorphological, hydrological and climatic significance of rock glaciers in the Andes of Central Chile (33–35°S), Permafrost and Periglacial Processes, 16, 231–240, https://doi.org/10.1002/ppp.528, 2005.

Brenning, A. and Azócar, G. F.: Statistical analysis of topographic and climatic controls and multispectral signatures of rock glaciers in the dry Andes, Chile (27°–33°S), Permafrost and Periglacial Processes, 21, 54–66, https://doi.org/10.1002/ppp.670, 2010.

Brighenti, S., Tolotti, M., Bruno, M. C., Engel, M., Wharton, G., Cerasino, L., Mair, V., and Bertoldi, W.: After the peak water: the increasing influence of rock glaciers on alpine river systems, Hydrological Processes, 33, 2804–2823, https://doi.org/10.1002/hyp.13533, 2019a.

Brighenti, S., Tolotti, M., Bruno, M. C., Wharton, G., Pusch, M. T., and Bertoldi, W.: Ecosystem shifts in Alpine streams under glacier retreat and rock glacier thaw: A review, Science of The Total Environment, 675, 542–559, https://doi.org/10.1016/j.scitotenv.2019.04.221, 2019b.

Brighenti, S., Hotaling, S., Finn, D. S., Fountain, A. G., Hayashi, M., Herbst, D., Saros, J. E., Tronstad, L. M., and Millar, C. I.: Rock glaciers and related cold rocky landforms: Overlooked climate refugia for mountain biodiversity, Global Change Biology, 27, 1504–1517, https://doi.org/10.1111/gcb.15510, 2021.

Burger, K., Degenhardt, J., and Giardino, J.: Engineering geomorphology of rock glaciers, Geomorphology, 31, 93–132, https://doi.org/10.1016/S0169-555X(99)00074-4, 1999.

Cecil, L. D., Green, J., Vogt, S., Michel, R., and Cottrell, G.: Isotopic composition of ice cores and meltwater from Upper Fremont Glacier and Galena Creek rock glacier, Wyoming, Geografiska Annaler: Series A, Physical Geography, 80, 287–292, https://doi.org/10.1111/j.0435-3676.1998.00044.x, 1998.

Cheng, G. and Jin, H.: Permafrost and groundwater on the Qinghai-Tibet Plateau and in northeast China, Hydrogeology Journal, 21, 5–23, https://doi.org/10.1007/s10040-012-0927-2, 2012.

Chinellato, G., Tonidandel, D., Lang, K., and Krainer, K.: Analysis of the contribution of permafrost ice to the hydrological water regime (PermaNET WP 7.3), in: PermaNET project WP7 Water resources, University of Innsbruck, http://www.permanet-alpinespace.eu/products.html, 2011.

Cicoira, A., Beutel, J., Faillettaz, J., and Vieli, A.: Water controls the seasonal rhythm of rock glacier flow, Earth and Planetary Science Letters, 528, 115 844, https://doi.org/10.1016/j.epsl.2019.115844, 2019.

Cicoira, A., Marcer, M., Gärtner-Roer, I., Bodin, X., Arenson, L. U., and Vieli, A.: A general theory of rock glacier creep based on in-situ and remote sensing observations, Permafrost and Periglacial Processes, 32, 139–153, https://doi.org/10.1002/ppp.2090, 2021.

Colombo, N., Gruber, S., Martin, M., Malandrino, M., Magnani, A., Godone, D., Freppaz, M., Fratianni, S., and Salerno, F.: Rainfall as primary driver of discharge and solute export from rock glaciers: The Col d'Olen Rock Glacier in the NW Italian Alps, Science of The Total Environment, 639, 316–330, https://doi.org/10.1016/j.scitotenv.2018.05.098, 2018a.

Colombo, N., Salerno, F., Gruber, S., Freppaz, M., Williams, M., Fratianni, S., and Giardino, M.: Review: Impacts of permafrost degradation on inorganic chemistry of surface fresh water, Global and Planetary Change, 162, 69–83, https://doi.org/10.1016/j.gloplacha.2017.11.017, 2018b.

Corte, A.: The Hydrological Significance of Rock Glaciers, Journal of Glaciology, 17, 157–158, https://doi.org/10.3189/S0022143000030859, 1976.

Cusicanqui, D., Rabatel, A., Vincent, C., Bodin, X., Thibert, E., and Francou, B.: Interpretation of Volume and Flux Changes of the Laurichard Rock Glacier Between 1952 and 2019, French Alps, Journal of Geophysical Research: Earth Surface, 126, e2021JF006 161, https://doi.org/10.1029/2021JF006161, e2021JF006161 2021JF006161, 2021.

Del Siro, C., Scapozza, C., Perga, M.-E., and Lambiel, C.: Investigating the origin of solutes in rock glacier springs in the Swiss Alps: A conceptual model, Frontiers in Earth Science, 11, https://doi.org/10.3389/feart.2023.1056305, 2023.

Delaloye, R. and Lambiel, C.: Evidence of winter ascending air circulation throughout talus slopes and rock glaciers situated in the lower belt of alpine discontinuous permafrost (Swiss Alps), Norsk Geografisk Tidsskrift – Norwegian Journal of Geography, 59, 194–203, https://doi.org/10.1080/00291950510020673, 2005.

Duguay, M. A., Edmunds, A., Arenson, L. U., and Wainstein, P. A.: Quantifying the significance of the hydrological contribution of a rock glacier–A review, in: GEOQuébec 2015: Challenges From North to South, Québec, Canada, Canadian Geotechnical Society (CGS), https://www.researchgate.net/profile/Lukas_Arenson/publication/282402787_Quantifying_the_significance_of_the_hydrological_contribution_of_a_rock_glacier_-_A_review/links/560f651708aec422d1131a30/Quantifying-the-significance-of-the-hydrological-contribution-of-a-rock-glacier-A-review.pdf, 2015.

Endrizzi, S., Gruber, S., Dall'Amico, M., and Rigon, R.: GEOtop 2.0: simulating the combined energy and water balance at and below the land surface accounting for soil freezing, snow cover and terrain effects, Geoscientific Model Development, 7, 2831–2857, https://doi.org/10.5194/gmd-7-2831-2014, 2014.

Fugger, S., Shaw, T. E., Jouberton, A., Miles, E. S., Buri, P., McCarthy, M., Fyffe, C., Fatichi, S., Kneib, M., Molnar, P., and Pellicciotti, F.: Hydrological regimes and evaporative flux partitioning at the climatic ends of high mountain Asia, Environmental Research Letters, 19, 044 057, https://doi.org/10.1088/1748-9326/ad25a0, 2024.

Geiger, S. T., Daniels, J. M., Miller, S. N., and Nicholas, J. W.: Influence of Rock Glaciers on Stream Hydrology in the La Sal Mountains, Utah, Arctic, Antarctic, and Alpine Research, 46, 645–658, https://doi.org/10.1657/1938-4246-46.3.645, 2014.

Gleick, P. H. and Palaniappan, M.: Peak water limits to freshwater withdrawal and use, Proceedings of the National Academy of Sciences, 107, 11 155–11 162, https://doi.org/10.1073/pnas.1004812107, 2010.

Guodong, C., Yuanming, L., Zhizhong, S., and Fan, J.: The 'thermal semi-conductor' effect of crushed rocks, Permafrost and Periglacial Processes, 18, 151–160, https://doi.org/10.1002/ppp.575, 2007.

Haeberli, W.: Die Basis-Temperatur der winterlichen Schneedecke als moglicher Indikator fur die Verbreitung von Permafrost in den Alpen, Zeitschrift für Gletscherkunde und Glazialgeologie, 9, 221–227, 1973.

Haeberli, W.: Untersuchungen zur Verbreitung von Permafrost zwischen Flüelapassund Piz Grialetsch (Graubünden), Mitteilungen der VAW/ETH Zürich 17, VAW/ETH Zürich, 1975.

Haeberli, W., ed.: Pilot analysis of permafrost cores from the active rock glacier Murtèl I, Piz Corvatsch, Eastern Swiss Alps. A workshop report., no. 9 in Arbeitsheft, VAW/ETH Zürich, 1990.

Haeberli, W. and Patzelt, G.: Permafrostkartierung im Gebiet der Hochebenkar-Blockgletscher, Obergurgl, Ötztaler Alpen, Zeitschrift für Gletscherkunde und Glazialgeologie, 18, 127–150, 1982.

Haeberli, W. and Vonder Mühll, D.: On the characteristics and possible origins of ice in rock glacier permafrost, Zeitschrift für Geomorphologie N.F., Supplement-Band, 104, 43–57, 1996.

Haeberli, W., Huder, J., Keusen, H., Pika, J., and Röthlisberger, H.: Core drilling through rock glacier-permafrost, in: Proceedings of the 5th International Conference on Permafrost, August 2–5 1988, Trondheim, Norway, vol. 2, pp. 937–942, by Senneset-Kaare, 1988.

Haeberli, W., Brandova, D., Burga, C., Egli, M., Frauenfelder, R., Kääb, A., Maisch, M., Mauz, B., and Dikau, R.: Methods for absolute and relative age dating of rock-glacier surfaces in alpine permafrost, in: Proceedings of the 8th International Conference on Permafrost, 21–25 July 2003, Zurich, Switzerland, edited by Phillips, M., Springman, S. M., and Arenson, L. U., vol. 1, pp. 343–348, Swets & Zeitlinger, Lisse, Zürich, iSBN 90 5809 582 7, 2003.

Haeberli, W., Hallet, B., Arenson, L., Elconin, R., Humlum, O., Kääb, A., Kaufmann, V., Ladanyi, B., Matsuoka, N., Springman, S., and Mühll, D. V.: Permafrost creep and rock glacier dynamics, Permafrost and Periglacial Processes, 17, 189–214, https://doi.org/10.1002/ppp.561, 2006.

Haeberli, W., Schaub, Y., and Huggel, C.: Increasing risks related to landslides from degrading permafrost into new lakes in de-glaciating mountain ranges, Geomorphology, 293, 405–417, https://doi.org/10.1016/j.geomorph.2016.02.009, permafrost and periglacial research from coasts to mountains, 2017.

Haeberli, W., Arenson, L. U., Wee, J., Hauck, C., and Mölg, N.: Discriminating viscous-creep features (rock glaciers) in mountain permafrost from debris-covered glaciers – a commented test at the Gruben and Yerba Loca sites, Swiss Alps and Chilean Andes, The Cryosphere, 18, 1669–1683, https://doi.org/10.5194/tc-18-1669-2024, 2024.

Halla, C., Blöthe, J. H., Tapia Baldis, C., Trombotto Liaudat, D., Hilbich, C., Hauck, C., and Schrott, L.: Ice content and interannual water storage changes of an active rock glacier in the dry Andes of Argentina, The Cryosphere, 15, 1187–1213, https://doi.org/10.5194/tc-15-1187-2021, 2021.

Hanson, S. and Hoelzle, M.: The thermal regime of the coarse blocky active layer at the Murtèl rock glacier in the Swiss Alps, in: Proceedings of the 8th International Conference on Permafrost, 21–25 July 2003, Zurich, Switzerland, edited by Phillips, M., Springman, S. M., and Arenson, L. U., pp. 51–52, Swets & Zeitlinger, Lisse, Zürich, iSBN 90 5809 582 7, 2003.

Hanson, S. and Hoelzle, M.: The thermal regime of the active layer at the Murtèl rock glacier based on data from 2002, Permafrost and Periglacial Processes, 15, 273–282, https://doi.org/10.1002/ppp.499, 2004.

Harrington, J. S., Mozil, A., Hayashi, M., and Bentley, L. R.: Groundwater flow and storage processes in an inactive rock glacier, Hydrological Processes, 32, 3070–3088, https://doi.org/10.1002/hyp.13248, 2018.

Harris, S. A. and Pedersen, D. E.: Thermal regimes beneath coarse blocky materials, Permafrost and Periglacial Processes, 9, 107–120, https://doi.org/10.1002/(SICI)1099-1530(199804/06)9:2<107::AID-PPP277>3.0.CO;2-G, 1998.

Harris, S. A., Blumstengel, W. K., Cook, D., Krouse, H. R., and Whitley, G.: Comparison of the Water Drainage from an Active Near-Slope Rock Glacier and a Glacier, St. Elias Mountains, Yukon Territory (Vergleich der Entwässerung eines aktiven Hangfuß-Blockgletschers und eines Gletschers, St. Elias Mountains, Yukon-Territorium), Erdkunde, 48, 81–91, http://www.jstor.org/stable/25646552, 1994.

Hauck, C.: New concepts in geophysical surveying and data interpretation for permafrost terrain, Permafrost and Periglacial Processes, 24, 131–137, https://doi.org/10.1002/ppp.1774, 2013.

Hauck, C. and Hilbich, C.: Preconditioning of mountain permafrost towards degradation detected by electrical resistivity, Environmental Research Letters, 19, 064 010, https://doi.org/10.1088/1748-9326/ad3c55, 2024.

Hauck, C., Böttcher, M., and Maurer, H.: A new model for estimating subsurface ice content based on combined electrical and seismic data sets, The Cryosphere, 5, 453–468, https://doi.org/10.5194/tc-5-453-2011, 2011.

Hayashi, M.: Temperature-electrical conductivity relation of water for environmental monitoring and geophysical data inversion, Environmental Monitoring and Assessment, 96, 119–128, https://doi.org/10.1023/B:EMAS.0000031719.83065.68, 2004.

Hayashi, M.: Alpine hydrogeology: The critical role of groundwater in sourcing the headwaters of the world, Groundwater, 58, 498–510, https://doi.org/10.1111/gwat.12965, 2020.

Hayashi, M., Goeller, N., Quinton, W. L., and Wright, N.: A simple heat-conduction method for simulating the frost-table depth in hydrological models, Hydrological Processes, 21, 2610–2622, https://doi.org/10.1002/hyp.6792, 2007.

Herz, T.: Das Mikroklima grobblockiger Schutthalden der alpinen Periglazialstufe und seine Auswirkungen auf Energieaustauschprozesse zwischen Atmosphäre und Lithosphäre [The microclimate of coarse debris covers in the periglacial belt of high mountains and its effects on the energy exchange between atmosphere and lithosphere], PhD thesis, Justus-Liebig-Universität Gießen, https://doi.org/10.22029/jlupub-9548, 2006.

Hilbich, C., Hauck, C., Hoelzle, M., Scherler, M., Schudel, L., Völksch, I., Vonder Mühll, D., and Mäusbacher, R.: Monitoring mountain permafrost evolution using electrical resistivity tomography: A 7-year study of seasonal, annual, and long-term variations at Schilthorn, Swiss Alps, Journal of Geophysical Research: Earth Surface, 113, https://doi.org/10.1029/2007JF000799, 2008.

Hilbich, C., Marescot, L., Hauck, C., Loke, M. H., and Mäusbacher, R.: Applicability of electrical resistivity tomography monitoring to coarse blocky and ice-rich permafrost landforms, Permafrost and Periglacial Processes, 20, 269–284, https://doi.org/10.1002/ppp.652, 2009.

Hinkel, K. M. and Outcalt, S. I.: Identification of heat-transfer processes during soil cooling, freezing, and thaw in central alaska, Permafrost and Periglacial Processes, 5, 217–235, https://doi.org/10.1002/ppp.3430050403, 1994.

Hock, R., Rasul, G., Adler, C., Cáceres, B., Gruber, S., Hirabayashi, Y., Jackson, M., Kääb, A., Kang, S., Kutuzov, S., Milner, A., Molau, U., Morin, S., Orlove, B., and Steltzer, H.: IPCC Special Report on the Ocean and Cryosphere in a Changing Climate [H.–O. Pörtner,

D.C. Roberts, V. Masson-Delmotte, P. Zhai, M. Tignor, E. Poloczanska, K. Mintenbeck, A. Alegrìa, M. Nicolai, A.Okem, J. Petzold, B. Rama, N.M. Weyer (eds.)], chap. 4: High Mountain Areas, pp. 131–202, Cambridge University Press (Cambridge, UK and New York, NY, USA), https://doi.org/10.1017/9781009157964.004, 2022.

Hoelzle, M., Mittaz, C., Etzelmüller, B., and Haeberli, W.: Surface energy fluxes and distribution models of permafrost in European mountain areas: an overview of current developments, Permafrost and Periglacial Processes, 12, 53–68, https://doi.org/10.1002/ppp.385, 2001.

Hoelzle, M., Barandun, M., Bolch, T., Fiddes, J., Gafurov, A., Muccione, V., Saks, T., and Shahgedanova, M.: The status and role of the alpine cryosphere in Central Asia, in: The Aral Sea Basin: Water for Sustainable Development in Central Asia, edited by Xenarios, S., Schmidt-Vogt, D., Qadir, M., Janusz-Pawletta, B., and Abdullaev, I., Earthscan Series on Major River Basins of the World, chap. 8, pp. 100–121, Routledge, London and New York, 2020.

Hoelzle, M., Hauck, C., Mathys, T., Noetzli, J., Pellet, C., and Scherler, M.: Long-term energy balance measurements at three different mountain permafrost sites in the Swiss Alps, Earth System Science Data, 14, 1531–1547, https://doi.org/10.5194/essd-14-1531-2022, 2022.

Hotaling, S., Foley, M. E., Zeglin, L. H., Finn, D. S., Tronstad, L. M., Giersch, J. J., Muhlfeld, C. C., and Weisrock, D. W.: Microbial assemblages reflect environmental heterogeneity in alpine streams, Global Change Biology, 25, 2576–2590, https://doi.org/10.1111/gcb.14683, 2019.

Hrbáček, F. and Uxa, T.: The evolution of a near-surface ground thermal regime and modeled active-layer thickness on James Ross Island, Eastern Antarctic Peninsula, in 2006–2016, Permafrost and Periglacial Processes, 31, 141–155, https://doi.org/10.1002/ppp.2018, 2019.

Humlum, O.: Active layer thermal regime at three rock glaciers in Greenland, Permafrost and Periglacial Processes, 8, 383–408, https://doi.org/10.1002/(SICI)1099-1530(199710/12)8:4<383::AID-PPP265>3.0.CO;2-V, 1997.

Humlum, O., Christiansen, H. H., and Juliussen, H.: Avalanche-derived rock glaciers in Svalbard, Permafrost and Periglacial Processes, 18, 75–88, https://doi.org/10.1002/ppp.580, 2007.

IAEA/WMO: Global Network of Isotopes in Precipitation. The GNIP Database., https://nucleus.iaea.org/wiser, https://nucleus.iaea.org/wiser, 2015.

IAEA/WMO: Global Network of Isotopes in Precipitation, https://nucleus.iaea.org/wiser/, 2023.

Janke, J. R., Ng, S., and Bellisario, A.: An inventory and estimate of water stored in firn fields, glaciers, debris-covered glaciers, and rock glaciers in the Aconcagua River Basin, Chile, Geomorphology, 296, 142–152, https://doi.org/10.1016/j.geomorph.2017.09.002, 2017.

Jones, D., Harrison, S., Anderson, K., and Betts, R. A.: Mountain rock glaciers contain globally significant water stores, Nature Scientific Reports, 8, https://doi.org/10.1038/s41598-018-21244-w, 2018a.

Jones, D., Harrison, S., Anderson, K., Selley, H., Wood, J., and Betts, R.: The distribution and hydrological significance of rock glaciers in the Nepalese Himalaya, Global and Planetary Change, 160, 123–142, https://doi.org/10.1016/j.gloplacha.2017.11.005, 2018b.

Jones, D. B., Harrison, S., Anderson, K., and Whalley, W. B.: Rock glaciers and mountain hydrology: A review, Earth-Science Reviews, 193, 66–90, https://doi.org/10.1016/j.earscirev.2019.04.001, 2019.

Juliussen, H. and Humlum, O.: Thermal regime of openwork block fields on the mountains Elgåhogna and Sølen, central-eastern Norway, Permafrost and Periglacial Processes, 19, 1–18, https://doi.org/10.1002/ppp.607, 2008.

Kääb, A., Gudmundsson, G. H., and Hoelzle, M.: Surface deformation of creeping mountain permafrost. Photogrammetric investigations on Murtèl rock glacier, Swiss Alps, in: Proceedings of the 7th International Conference on Permafrost, 23–27 June 1998, Yellowknife, Northwest Territories, Canada, edited by A.G., L. and M., A., pp. 531–537, Centre d'Études Nordiques, Université Laval (Québec), Canada, 1998.

Kane, D. L., Hinkel, K. M., Goering, D. J., Hinzman, L. D., and Outcalt, S. I.: Non-conductive heat transfer associated with frozen soils, Global and Planetary Change, 29, 275–292, https://doi.org/10.1016/S0921-8181(01)00095-9, 2001.

Kenner, R., Noetzli, J., Hoelzle, M., Raetzo, H., and Phillips, M.: Distinguishing ice-rich and ice-poor permafrost to map ground temperatures and ground ice occurrence in the Swiss Alps, The Cryosphere, 13, 1925–1941, https://doi.org/10.5194/tc-13-1925-2019, 2019.

Kenner, R., Pruessner, L., Beutel, J., Limpach, P., and Phillips, M.: How rock glacier hydrology, deformation velocities and ground temperatures interact: Examples from the Swiss Alps, Permafrost and Periglacial Processes, 31, 3–14, https://doi.org/10.1002/ppp.2023, 2020.

Kern, Z., Kohán, B., and Leuenberger, M.: Precipitation isoscape of high reliefs: interpolation scheme designed and tested for monthly resolved precipitation oxygen isotope records of an Alpine domain, Atmospheric Chemistry and Physics, 14, 1897–1907, https://doi.org/10.5194/acp-14-1897-2014, 2014.

Krainer, K. and Mostler, W.: Hydrology of Active Rock Glaciers: Examples from the Austrian Alps, Arctic, Antarctic, and Alpine Research, 34, 142–149, https://doi.org/10.1080/15230430.2002.12003478, 2002.

Krainer, K., Mostler, W., and Spötl, C.: Discharge from active rock glaciers, Austrian Alps: a stable isotope approach, Austrian Journal of Earth Sciences, 100, https://www.zobodat.at/pdf/MittGeolGes_100_0102-0112.pdf, 2007.

Krainer, K., Bressan, D., Dietre, B., Haas, J. N., Hajdas, I., Lang, K., Mair, V., Nickus, U., Reidl, D., Thies, H., and Tonidandel, D.: A 10,300-year-old permafrost core from the active rock glacier Lazaun, southern Ötztal Alps (South Tyrol, northern Italy), Quaternary Research, 83, 324–335, https://doi.org/10.1016/j.yqres.2014.12.005, 2015.

Kurylyk, B. L.: Discussion of 'A simple thaw-freeze algorithm for a multi-layered soil using the Stefan equation' by Xie and Gough (2013), Permafrost and Periglacial Processes, 26, 200–206, https://doi.org/10.1002/ppp.1834, 2015.

Kurylyk, B. L. and Hayashi, M.: Improved Stefan equation correction factors to accommodate sensible heat storage during soil freezing or thawing, Permafrost and Periglacial Processes, 27, 189–203, https://doi.org/10.1002/ppp.1865, 2016.

Lehmann, B., Anderson, R. S., Bodin, X., Cusicanqui, D., Valla, P. G., and Carcaillet, J.: Alpine rock glacier activity over Holocene to modern timescales (western French Alps), Earth Surface Dynamics, 10, 605–633, https://doi.org/10.5194/esurf-10-605-2022, 2022.

Liaudat Trombotto, D., Sileo, N., and Dapeña, C.: Periglacial water paths within a rock glacier-dominated catchment in the Stepanek area, Central Andes, Mendoza, Argentina, Permafrost and Periglacial Processes, 31, 311–323, https://doi.org/10.1002/ppp.2044, 2020.

Louis, C., Halloran, L. J. S., and Roques, C.: Seasonal and diurnal freeze-thaw dynamics of a rock glacier and their impacts on mixing and solute transport, EGUsphere, 2024, 1–26, https://doi.org/10.5194/egusphere-2024-927, 2024.

Luethi, R., Phillips, M., and Lehning, M.: Estimating Non-Conductive Heat Flow Leading to Intra-Permafrost Talik Formation at the Ritigraben Rock Glacier (Western Swiss Alps), Permafrost and Periglacial Processes, 28, 183–194, https://doi.org/10.1002/ppp.1911, 2017.

Luetschg, M., Lehning, M., and Haeberli, W.: A sensitivity study of factors influencing warm/thin permafrost in the Swiss Alps, Journal of Glaciology, 54, 696–704, https://doi.org/10.3189/002214308786570881, 2008.

Maierhofer, T., Flores Orozco, A., Roser, N., Limbrock, J. K., Hilbich, C., Moser, C., Kemna, A., Drigo, E., Morra di Cella, U., and Hauck, C.: Spectral induced polarization imaging to monitor seasonal and annual dynamics of frozen ground at a mountain permafrost site in the Italian Alps, The Cryosphere, 18, 3383–3414, https://doi.org/10.5194/tc-18-3383-2024, 2024.

Marchenko, S., Romanovsky, V., and Gorbunov, A.: Hydrologic and thermal regimes of coarse blocky materials in Tien Shan Mountains, Central Asia, in: Extended abstracts of the 10th International Conference on Permafrost, 25–29 June 2012, Salekhard (Yamal-Nenets Autonomous District), Russia, edited by Hinkel, K. M. and Melnikov, V. P., vol. 4, pp. 361–362, Fort Dialog-Iset: Ekaterinburg, Russia, 2012.

Marchenko, S., Jin, H., Hoelzle, M., Lentschke, J., Kasatkin, N., and Saks, T.: Thermal and hydrologic regimes of blocky materials in Tianshan Mountains, Central Asia, in: Proceedings vol. II (Extendend Abstracts) of the 12th International Conference on Permafrost, 16–20 June 2024, Whitehorse (Yukon), Canada, edited by Beddoe, R. and Karunaratne, K., pp. 455–456, International Permafrost Association, 2024.

Mari, S., Scapozza, C., Pera, S., and Delaloye, R.: Prove di multitracciamento di ghiacciai rocciosi e ambienti periglaciali nel Vallon de Réchy (VS) e nella Valle di Sceru (TI) [Multiple water tracing of rockglaciers and periglacial environments in the Vallon de Réchy (VS) and in the Valle di Sceru (TI)], Bollettino della Società ticinese di scienze naturali, 101, 13–20, https://repository.supsi.ch/3625/, 2013.

McCleskey, R. B., Kirk Nordstrom, D., and Ryan, J. N.: Electrical conductivity method for natural waters, Applied Geochemistry, 26, S227–S229, https://doi.org/10.1016/j.apgeochem.2011.03.110, ninth International Symposium on the Geochemistry of the Earth's Surface (GES-9), 2011.

Mendoza López, M., Tapia Baldis, C., Trombotto Liaudat, D., and Pastore, S.: Water content and ground temperature variations in the active layer of a rock glacier in the Central Andes of San Juan, Argentina, Earth Surface Processes and Landforms, https://doi.org/10.1002/esp.5926, 2024.

Millar, C. I., Westfall, R. D., and Delany, D. L.: Thermal and hydrologic attributes of rock glaciers and periglacial talus landforms: Sierra Nevada, California, USA, Quaternary International, 310, 169 – 180, https://doi.org/10.1016/j.quaint.2012.07.019, pACLIM: Proceedings of the 25th Pacific Climate Workshop, 2011, 2013.

Mittaz, C., Hoelzle, M., and Haeberli, W.: First results and interpretation of energy-flux measurements over Alpine permafrost, Annals of Glaciology, 31, 275–280, https://doi.org/10.3189/172756400781820363, 2000.

Mollaret, C., Hilbich, C., Pellet, C., Flores-Orozco, A., Delaloye, R., and Hauck, C.: Mountain permafrost degradation documented through a network of permanent electrical resistivity tomography sites, The Cryosphere, 13, 2557–2578, https://doi.org/10.5194/tc-13-2557-2019, 2019.

Mollaret, C., Wagner, F. M., Hilbich, C., Scapozza, C., and Hauck, C.: Petrophysical Joint Inversion Applied to Alpine Permafrost Field Sites to Image Subsurface Ice, Water, Air, and Rock Contents, Frontiers in Earth Science, 8, https://doi.org/10.3389/feart.2020.00085, 2020.

Morard, S., Hilbich, C., Mollaret, C., Pellet, C., and Hauck, C.: 20-year permafrost evolution documented through petrophysical joint inversion, thermal and soil moisture data, Environmental Research Letters, 19, 074 074, https://doi.org/10.1088/1748-9326/ad5571, 2024.

Müller, J., Vieli, A., and Gärtner-Roer, I.: Rock glaciers on the run – understanding rock glacier landform evolution and recent changes from numerical flow modeling, The Cryosphere, 10, 2865–2886, https://doi.org/10.5194/tc-10-2865-2016, 2016.

Munroe, J. S.: Distribution, evidence for internal ice, and possible hydrologic significance of rock glaciers in the Uinta Mountains, Utah, USA, Quaternary Research, 90, 50–65, https://doi.org/10.1017/qua.2018.24, 2018.

Munroe, J. S. and Handwerger, A. L.: Contribution of rock glacier discharge to late summer and fall streamflow in the Uinta Mountains, Utah, USA, Hydrology and Earth System Sciences, 27, 543–557, https://doi.org/10.5194/hess-27-543-2023, 2023a.

Munroe, J. S. and Handwerger, A. L.: Examining the variability of rock glacier meltwater in space and time in high-elevation environments of Utah, United States, Frontiers in Earth Science, 11, https://doi.org/10.3389/feart.2023.1129314, 2023b.

Müller, J., Gärtner-Roer, I., Kenner, R., Thee, P., and Morche, D.: Sediment storage and transfer on a periglacial mountain slope (Corvatsch, Switzerland), Geomorphology, 218, 35–44, https://doi.org/10.1016/j.geomorph.2013.12.002, 2014.

Navarro, G., MacDonell, S., and Valois, R.: A conceptual hydrological model of semiarid Andean headwater systems in Chile, Progress in Physical Geography: Earth and Environment, 47, 668–686, https://doi.org/10.1177/03091333221147649, 2023.

Nickus, U., Thies, H., Krainer, K., Lang, K., Mair, V., and Tonidandel, D.: A multi-millennial record of rock glacier ice chemistry (Lazaun, Italy), Frontiers in Earth Science, 11, https://doi.org/10.3389/feart.2023.1141379, 2023.

Noetzli, J., Pellet, C., and Staub, B., eds.: Permafrost in Switzerland 2014/2015 to 2017/2018, Glaciological Report Permafrost No. 16–19 (PERMOS Report 2019), Fribourg: Cryospheric Commission of the Swiss Academy of Sciences, https://doi.org/10.13093/permos-rep-2019-16-19, 2019.

Pavoni, M., Boaga, J., Wagner, F., Bast, A., and Phillips, M.: Characterization of rock glaciers environments combining structurally-coupled and petrophysically-coupled joint inversions of electrical resistivity and seismic refraction datasets, Journal of Applied Geophysics, 215, 105 097, https://doi.org/10.1016/j.jappgeo.2023.105097, 2023.

Phillips, M., Haberkorn, A., and Rhyner, H.: Snowpack characteristics on steep frozen rock slopes, Cold Regions Science and Technology, 141, 54–65, https://doi.org/10.1016/j.coldregions.2017.05.010, 2017.

Pomeroy, J., Brown, T., Fang, X., Shook, K., Pradhananga, D., Armstrong, R., Harder, P., Marsh, C., Costa, D., Krogh, S., Aubry-Wake, C., Annand, H., Lawford, P., He, Z., Kompanizare, M., and Lopez Moreno, J.: The cold regions hydrological modelling platform for hydrological diagnosis and prediction based on process understanding, Journal of Hydrology, 615, 128 711, https://doi.org/https://doi.org/10.1016/j.jhydrol.2022.128711, 2022.

Pruessner, L., Phillips, M., Farinotti, D., Hoelzle, M., and Lehning, M.: Near-surface ventilation as a key for modeling the thermal regime of coarse blocky rock glaciers, Permafrost and Periglacial Processes, 29, 152–163, https://doi.org/10.1002/ppp.1978, 2018.

Pruessner, L., Huss, M., Phillips, M., and Farinotti, D.: A framework for modeling rock glaciers and permafrost at the basin-scale in high Alpine catchments, Journal of Advances in Modeling Earth Systems, 13, e2020MS002 361, https://doi.org/10.1029/2020MS002361, e2020MS002361 2020MS002361, 2021.

Pruessner, L., Huss, M., and Farinotti, D.: Temperature evolution and runoff contribution of three rock glaciers in Switzerland under future climate forcing, Permafrost and Periglacial Processes, 33, 310–322, https://doi.org/10.1002/ppp.2149, 2022.

Pérez, F. L.: Conservation of soil moisture by different stone covers on alpine talus slopes (Lassen, California), CATENA, 33, 155–177, https://doi.org/10.1016/S0341-8162(98)00091-5, 1998.

Rangecroft, S., Harrison, S., and Anderson, K.: Rock Glaciers as Water Stores in the Bolivian Andes: An Assessment of Their Hydrological Importance, Arctic, Antarctic, and Alpine Research, 47, 89–98, https://doi.org/10.1657/AAAR0014-029, 2015.

Reato, A., Silvina Carol, E., Cottescu, A., and Alfredo Martínez, O.: Hydrological significance of rock glaciers and other periglacial landforms as sustenance of wet meadows in the Patagonian Andes, Journal of South American Earth Sciences, 111, 103 471, https://doi.org/10.1016/j.jsames.2021.103471, 2021.

Reato, A., Borzi, G., Martínez, O. A., and Carol, E.: Role of rock glaciers and other high-altitude depositional units in the hydrology of the mountain watersheds of the Northern Patagonian Andes, Science of The Total Environment, 824, 153 968, https://doi.org/10.1016/j.scitotenv.2022.153968, 2022.

Reid, T. D. and Brock, B. W.: An energy-balance model for debris-covered glaciers including heat conduction through the debris layer, Journal of Glaciology, 56, 903–916, https://doi.org/10.3189/002214310794457218, 2010.

Renette, C., Aalstad, K., Aga, J., Zweigel, R. B., Etzelmüller, B., Lilleøren, K. S., Isaksen, K., and Westermann, S.: Simulating the effect of subsurface drainage on the thermal regime and ground ice in blocky terrain in Norway, Earth Surface Dynamics, 11, 33–50, https://doi.org/10.5194/esurf-11-33-2023, 2023.

Reznichenko, N., Davies, T., Shulmeister, J., and McSaveney, M.: Effects of debris on ice-surface melting rates: an experimental study, Journal of Glaciology, 56, 384–394, https://doi.org/10.3189/002214310792447725, 2010.

Rigon, R., Bertoldi, G., and Over, T. M.: GEOtop: a distributed hydrological model with coupled water and energy budgets, Journal of Hydrometeorology, 7, 371 – 388, https://doi.org/10.1175/JHM497.1, 2006.

Riseborough, D., Shiklomanov, N., Etzelmüller, B., Gruber, S., and Marchenko, S.: Recent advances in permafrost modelling, Permafrost and Periglacial Processes, 19, 137–156, https://doi.org/10.1002/ppp.615, 2008.

Rist, A.: Hydrothermal processes within the active layer above alpine permafrost in steep scree slopes and their influence on slope stability, PhD thesis, University of Zurich, Zürich, https://doi.org/10.5167/uzh-163579, 2007.

Rist, A. and Phillips, M.: First results of investigations on hydrothermal processes within the active layer above alpine permafrost in steep terrain, Norsk Geografisk Tidsskrift – Norwegian Journal of Geography, 59, 177–183, https://doi.org/10.1080/00291950510020574, 2005.

Rogger, M., Chirico, G. B., Hausmann, H., Krainer, K., Brückl, E., Stadler, P., and Blöschl, G.: Impact of mountain permafrost on flow path and runoff response in a high alpine catchment, Water Resources Research, 53, 1288–1308, https://doi.org/10.1002/2016WR019341, 2017.

Sakai, A., Fujita, K., and Kubota, J.: Evaporation and percolation effect on melting at debris-covered Lirung Glacier, Nepal Himalayas, 1996, Bulletin of Glaciological Research, 21, 9–15, 2004.

Sawada, Y., Ishikawa, M., and Ono, Y.: Thermal regime of sporadic permafrost in a block slope on Mt. Nishi-Nupukaushinupuri, Hokkaido Island, Northern Japan, Geomorphology, 52, 121–130, https://doi.org/10.1016/S0169-555X(02)00252-0, 2003.

Scapozza, C., Deluigi, N., Bulgheroni, M., Ibarguren, S. P., Pozzoni, M., Colombo, L., and Lepori, F.: Assessing the impact of ground ice degradation on high mountain lake environments (Lago Nero catchment, Swiss Alps), Aquatic Sciences, 82, https://doi.org/10.1007/s00027-019-0675-7, 2020.

Schaffer, N. and MacDonell, S.: Brief communication: A framework to classify glaciers for water resource evaluation and management in the Southern Andes, The Cryosphere, 16, 1779–1791, https://doi.org/10.5194/tc-16-1779-2022, 2022.

Schaffer, N., MacDonell, S., Réveillet, M., Yáñez, E., and Valois, R.: Rock glaciers as a water resource in a changing climate in the semiarid Chilean Andes, Regional Environmental Change, 19, 1263–1279, https://doi.org/10.1007/s10113-018-01459-3, 2019.

Scherler, M., Hauck, C., Hoelzle, M., Stähli, M., and Völksch, I.: Meltwater infiltration into the frozen active layer at an alpine permafrost site, Permafrost and Periglacial Processes, 21, 325–334, https://doi.org/10.1002/ppp.694, 2010.

Scherler, M., Hauck, C., Hoelzle, M., and Salzmann, N.: Modeled sensitivity of two alpine permafrost sites to RCM-based climate scenarios, Journal of Geophysical Research: Earth Surface, 118, 780–794, https://doi.org/10.1002/jgrf.20069, 2013.

Scherler, M., Schneider, S., Hoelzle, M., and Hauck, C.: A two-sided approach to estimate heat transfer processes within the active layer of the Murtèl–Corvatsch rock glacier, Earth Surface Dynamics, 2, 141–154, https://doi.org/10.5194/esurf-2-141-2014, 2014.

Schneider, S.: The heterogeneity of mountain permafrost – A field-based analysis of different periglacial materials, PhD thesis, University of Fribourg (Switzerland), 2014.

Schneider, S., Daengeli, S., Hauck, C., and Hoelzle, M.: A spatial and temporal analysis of different periglacial materials by using geo-electrical, seismic and borehole temperature data at Murtèl–Corvatsch, Upper Engadin, Swiss Alps, Geographica Helvetica, 68, 265–280, https://doi.org/10.5194/gh-68-265-2013, 2013.

Speck, C. K.: Änderung des Grundwasserregimes unter dem Einfluss von Gletschern und Permafrost, PhD thesis, VAW/ETH, Mitteilungen der Versuchsanstalt für Wasserbau, Hydrologie und Glaziologie (VAW), Nr. 134, 1994.

Springman, S. M., Arenson, L. U., Yamamoto, Y., Maurer, H., Kos, A., Buchli, T., and Derungs, G.: Multidisciplinary investigations on three rock glaciers in the swiss alps: legacies and future perspectives, Geografiska Annaler: Series A, Physical Geography, 94, 215–243, https://doi.org/10.1111/j.1468-0459.2012.00464.x, 2012.

Steig, E. J., Fitzpatrick, J. J., Noel Potter, j., and Clark, D. H.: The geochemical record in rock glaciers, Geografiska Annaler: Series A, Physical Geography, 80, 277–286, https://doi.org/10.1111/j.0435-3676.1998.00043.x, 1998.

Steiner, M., Wagner, F. M., Maierhofer, T., Schöner, W., and Flores Orozco, A.: Improved estimation of ice and water contents in alpine permafrost through constrained petrophysical joint inversion: The Hoher Sonnblick case study, GEOPHYSICS, 86, WB61–WB75, https://doi.org/10.1190/geo2020-0592.1, 2021.

Stocker-Mittaz, C., Hoelzle, M., and Haeberli, W.: Modelling alpine permafrost distribution based on energy-balance data: a first step, Permafrost and Periglacial Processes, 13, 271–282, https://doi.org/10.1002/ppp.426, 2002.

Stucki, T.: Permafrosttemperaturen im Oberengadin. Eine Auswertung der Bohrlochtemperaturen im alpinen Permafrost des Oberengadins im Hinblick auf einen Erwärmungstrend und Schmelzwasserabfluss aus dem Permafrost., Master's thesis, Abteilung Erdwissenschaften der ETH Zürich, 1995.

Tenthorey, G. and Gerber, E.: Hydrologie du glacier rocheux de Murtèl (Grisons). Description et interprétation de traçages d'eau, in: Modèles en Géomorphologie – exemples Suisses. Session scientfique de la Société suisse de Géomorphologie. Fribourg, 22/23 juin 1990., edited by Monbaron, M. and Haeberli, W., vol. 3 of *Rapport et recherches, Institut de Géographie Fribourg*, 1991.

Trombotto, D. and Borzotta, E.: Indicators of present global warming through changes in active layer-thickness, estimation of thermal diffusivity and geomorphological observations in the Morenas Coloradas rockglacier, Central Andes of Mendoza, Argentina, Cold Regions Science and Technology, 55, 321–330, https://doi.org/10.1016/j.coldregions.2008.08.009, 2009.

Trombotto-Liaudat, D. and Bottegal, E.: Recent evolution of the active layer in the Morenas Coloradas rock glacier, Central Andes, Mendoza, Argentina and its relation with kinematics, Cuadernos de Investigación Geográfica, 46, 159–185, https://doi.org/10.18172/cig.3946, 2020.

Tronstad, L. M., Hotaling, S., Giersch, J. J., Wilmot, O. J., and Finn, D. S.: Headwaters Fed by Subterranean Ice: Potential Climate Refugia for Mountain Stream Communities?, Western North American Naturalist, 80, 395 – 407, https://doi.org/10.3398/064.080.0311, 2020.

van Tiel, M., Aubry-Wake, C., Somers, L., Andermann, C., Avanzi, F., Baraer, M., Chiogna, G., Daigre, C., Das, S., Drenkhan, F., Farinotti, D., Fyffe, C. L., de Graaf, I., Hanus, S., Immerzeel, W., Koch, F., McKenzie, J. M., Müller, T., Popp, A. L., Saidaliyeva, Z., Schaefli, B., Schilling, O. S., Teagai, K., Thornton, J. M., and Yapiyev, V.: Cryosphere–groundwater connectivity is a missing link in the mountain water cycle, Nature Water, https://doi.org/10.1038/s44221-024-00277-8, 2024.

Villarroel, C. D., Ortiz, D. A., Forte, A. P., Tamburini Beliveau, G., Ponce, D., Imhof, A., and López, A.: Internal structure of a large, complex rock glacier and its significance in hydrological and dynamic behavior: A case study in the semi-arid Andes of Argentina, Permafrost and Periglacial Processes, 33, 78–95, https://doi.org/https://doi.org/10.1002/ppp.2132, 2022.

Vonder Mühll, D. and Haeberli, W.: Thermal characteristics of the permafrost within an active rock glacier (Murtèl/Corvatsch, Grisons, Swiss Alps), Journal of Glaciology, 36, 151–158, https://doi.org/10.3189/S0022143000009382, 1990.

Vonder Mühll, D. S.: Evidence of intrapermafrost groundwater flow beneath an active rock glacier in the Swiss Alps, Permafrost and Periglacial Processes, 3, 169–173, https://doi.org/10.1002/ppp.3430030216, 1992.

Vonder Mühll, D. S.: Geophysikalische Untersuchungen im Permafrost des Oberengadins, PhD thesis, Versuchsanstalt für Wasserbau, Hydrologie und Glaziologie (VAW), ETH Zürich, https://era.library.ualberta.ca/items/ba365b39-a006-497f-b263-669748322635, 1993.

Vonder Mühll, D. S. and Holub, P.: Borehole logging in alpine permafrost, upper Engadin, Swiss Alps, Permafrost and Periglacial Processes, 3, 125–132, https://doi.org/10.1002/ppp.3430030209, 1992.

Vonder Mühll, D. S. and Klingelé, E. E.: Gravimetrical investigation of ice-rich permafrost within the rock glacier Murtèl-Corvatsch (upper Engadin, swiss alps), Permafrost and Periglacial Processes, 5, 13–24, https://doi.org/10.1002/ppp.3430050103, 1994.

Vonder Mühll, D. S., Hauck, C., and Lehmann, F.: Verification of geophysical models in Alpine permafrost using borehole information, Annals of Glaciology, 31, 300–306, https://doi.org/10.3189/172756400781820057, 2000.

Wagner, T., Pauritsch, M., and Winkler, G.: Impact of relict rock glaciers on spring and stream flow of alpine watersheds: Examples of the Niedere Tauern Range, Eastern Alps (Austria), Austrian Journal of Earth Sciences, 109, https://doi.org/10.17738/ajes.2016.0006, 2016.

Wagner, T., Pauritsch, M., Mayaud, C., Kellerer-Pirklbauer, A., Thalheim, F., and Winkler, G.: Controlling factors of microclimate in blocky surface layers of two nearby relict rock glaciers (Niedere Tauern Range, Austria), Geografiska Annaler: Series A, Physical Geography, 101, 310–333, https://doi.org/10.1080/04353676.2019.1670950, 2019.

Wagner, T., Brodacz, A., Krainer, K., and Winkler, G.: Active rock glaciers as shallow groundwater reservoirs, Austrian Alps, Grundwasser – Zeitschrift der Fachsektion Hydrogeologie, 25, 215–230, https://doi.org/10.1007/s00767-020-00455-x, 2020.

Wagner, T., Kainz, S., Helfricht, K., Fischer, A., Avian, M., Krainer, K., and Winkler, G.: Assessment of liquid and solid water storage in rock glaciers versus glacier ice in the Austrian Alps, Science of The Total Environment, 800, 149 593, https://doi.org/https://doi.org/10.1016/j.scitotenv.2021.149593, 2021a.

Wagner, T., Kainz, S., Krainer, K., and Winkler, G.: Storage-discharge characteristics of an active rock glacier catchment in the Innere Ölgrube, Austrian Alps, Hydrological Processes, 35, e14 210, https://doi.org/https://doi.org/10.1002/hyp.14210, 2021b.

Wakonigg, H.: Unterkühlte Schutthalden [Undercooled talus], Arbeiten aus dem Institut für Geographie der Karl-Franzens Universität Graz, 33, 209–223, 1996.

Wanner, C., Moradi, H., Ingold, P., Cardenas Bocanegra, M. A., Mercurio, R., and Furrer, G.: Rock glaciers in the Central Eastern Alps – How permafrost degradation can cause acid rock drainage, mobilization of toxic elements and formation of basaluminite, Global and Planetary Change, 227, 104 180, https://doi.org/10.1016/j.gloplacha.2023.104180, 2023.

Wicky, J. and Hauck, C.: Air convection in the active layer of rock glaciers, Frontiers in Earth Science, 8, 335, https://doi.org/10.3389/feart.2020.00335, 2020.

Wicky, J., Hilbich, C., Delaloye, R., and Hauck, C.: Modeling the link between air convection and the occurrence of short-term permafrost in a low-altitude cold talus slope, Permafrost and Periglacial Processes, 35, 202–217, https://doi.org/10.1002/ppp.2224, 2024.

Williams, M. W., Knauf, M., Caine, N., Liu, F., and Verplanck, P. L.: Geochemistry and source waters of rock glacier outflow, Colorado Front Range, Permafrost and Periglacial Processes, 17, 13–33, https://doi.org/10.1002/ppp.535, 2006.

Williams, M. W., Hood, E., Molotch, N. P., Caine, N., Cowie, R., and Liu, F.: The 'teflon basin' myth: hydrology and hydrochemistry of a seasonally snow-covered catchment, Plant Ecology & Diversity, 8, 639–661, https://doi.org/10.1080/17550874.2015.1123318, 2015.

Winkler, G., Pauritsch, M., Wagner, T., and Kellerer-Pirklbauer, A.: Reliktische Blockgletscher als Grundwasserspeicher in Alpinen Einzugsgebieten der Niederen Tauern, Berichte der Wasserwirtschaftlichen Planung Steiermark. Bandolier, 87, 134, 2016a.

Winkler, G., Wagner, T., Pauritsch, M., Birk, S., Kellerer-Pirklbauer, A., Benischke, R., Leis, A., Morawetz, R., Schreilechner, M. G., and Hergarten, S.: Identification and assessment of groundwater flow and storage components of the relict Schöneben Rock Glacier, Niedere Tauern Range, Eastern Alps (Austria), Hydrogeology Journal, 24, 937–953, https://doi.org/10.1007/s10040-015-1348-9, 2016b.

Winkler, G., Wagner, T., and Krainer, K.: Wasserwirtschaftliche Aspekte von Blockgletschern in Kristallingebieten der Ostalpen – Speicherverhalten, Abflussdynamik und Hydrochemie mit Schwerpunkt Schwermetallbelastungen [Water resources management issues of rock glaciers in alpine catchments of the Eastern Alps – storage capacity, flow dynamics and hydrochemistry in particular heavy metal pollution], Beiträge zur Hydrogeologie, 63, 65–98, 2021a.

Winkler, M., Schellander, H., and Gruber, S.: Snow water equivalents exclusively from snow depths and their temporal changes: the ΔSNOW model, Hydrology and Earth System Sciences, 25, 1165–1187, https://doi.org/10.5194/hess-25-1165-2021, 2021b.

Woo, M.-K.: Sustaining Groundwater Resources: A Critical Element in the Global Water Crisis, chap. Linking Runoff to Groundwater in Permafrost Terrain, pp. 119–129, Springer Netherlands, Dordrecht, https://doi.org/10.1007/978-90-481-3426-7_8, 2011.

Woo, M.-k.: Permafrost Hydrology, Springer Berlin Heidelberg, ISBN 9783642234620, https://doi.org/10.1007/978-3-642-23462-0, 2012.

Woo, M.-k. and Xia, Z.: Effects of Hydrology on the Thermal Conditions of the Active Layer: Paper presented at the 10th Northern Res. Basin Symposium (Svalbard, Norway — 28 Aug./3 Sept. 1994), Hydrology Research, 27, 129–142, https://doi.org/10.2166/nh.1996.0024, 1996.

Yoshikawa, K., Schorghofer, N., and Klasner, F.: Permafrost and seasonal frost thermal dynamics over fifty years on tropical Maunakea volcano, Hawai'i, Arctic, Antarctic, and Alpine Research, 55, 2186 485, https://doi.org/10.1080/15230430.2023.2186485, 2023.

Zhu, M., Wang, J., Ivanov, V., Sheshukov, A., Zhou, W., Zhang, L., Mazepa, V., Sokolov, A., and Valdayskikh, V.: An analytical model of active layer depth under changing ground heat flux, Journal of Geophysical Research: Atmospheres, 129, https://doi.org/10.1029/2023JD039453, 2024.